

Chapter 2

Semiconductor-Based Photocatalytic Systems for the Solar-Light-Driven Water Splitting and Hydrogen Evolution

The research and development of new technologies for the conversion and storage of inexhaustible solar light energy were boosted several decades ago by the 1970th fuel crisis and a strategic need for sustainable power sources that can serve as alternatives to the fossil fuels. The basic idea was to accumulate the solar light energy as the electricity as well as to store it in the form of highly endothermic and eco-friendly fuels, in particular, molecular hydrogen produced by the photochemical splitting of water.

Direct photochemical water splitting to gaseous hydrogen and oxygen can occur only under the illumination with highly energetic quanta at the wavelength λ shorter than 240 nm [1]. However, such irradiation is completely absorbed by the atmosphere and does not reach the Earth surface. To overcome this obstacle, the water splitting is realized in the presence of *photocatalysts*—the substances capable of absorbing longer-wavelength light quanta ($\lambda > 300$ nm) and inducing chemical transformations of water molecules.

Inorganic semiconductors are probably the most broadly studied photocatalysts of water splitting. The semiconductor photocatalysts combine a high photosensitivity with a photochemical activity, stability, availability and relative simplicity of practical implementation. It should be noted that the photocatalytic and electro-photocatalytic (photoelectrochemical) processes with the participation of semiconductor nanomaterials are very similar by the nature and start with the same primary act of light quantum absorption resulting in the generation of an electron-hole couple. Differences between photocatalytic and photoelectrochemical/photoelectrocatalytic processes arise mainly on the secondary steps of the charge carrier migration to the reaction participants. By this reason, both types of processes can be regarded as photocatalytic ones occurring in “usual” and electrochemical regimes and discussed together.

Molecular hydrogen can be produced in photocatalytic systems of two types: (a) *water splitting* systems where stoichiometric amounts of H_2 and O_2 are produced simultaneously, and (b) systems with a so-called “*sacrificial*” donor which is consumed irreversibly supplying electrons for the water reduction.

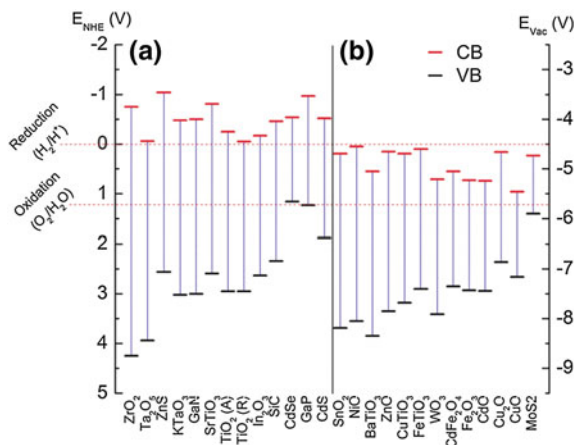
Stoichiometric (total) water splitting is accompanied by the energy accumulation and a free energy increment $\Delta G = 238$ kJ/mole [2, 3]. Such process requires a semiconductor photocatalyst with a valence band (VB) potential more positive than the water oxidation potential (1.23 V vs. normal hydrogen electrode (NHE) at pH 0) and a conduction band (CB) potential more negative than the NHE potential ($E = 0.0$ V at pH 0). Therefore, a minimal light quantum energy required for the semiconductor-driven water splitting is 1.23 eV. Invariable losses accompanying interfacial charge transfers as well as over-voltages of the H_2 and O_2 formation increase this minimal energy to 1.7–1.9 eV [2, 3]. Therefore, the photocatalytic conversion of solar light energy should be the most favorable from the energetic viewpoints for semiconductors with a band gap (E_g) around 1.7–1.9 eV and a corresponding fundamental absorption band edge at $\lambda_{be} = 650$ –730 nm.

The wider-band-gap semiconductors with $\lambda_{be} < 400$ nm can also be used for the water splitting. However, due to a relatively small fraction of the UV light in the solar flux at the Earth surface, the conversion efficiency in such systems is typically not higher than 1–2%. Therefore, successful application of wide-band-gap semiconductors for the water splitting can be achieved only by expansion of their light sensitivity range to the visible domain of the spectrum. This effect can be achieved either by doping with metal/non-metal additives during the semiconductor synthesis or by various post-synthesis modifications.

It should be noted that the semiconductors-based systems for the total water splitting have not yet showed reasonably high conversion efficiency as a result of a fast recombination of the oppositely charge photogenerated charge carriers as well as of primary intermediates—hydrogen atoms and hydroxyl radicals. A much higher conversion efficiency was achieved in the photo-catalytic systems with sacrificial donors. The range of sacrificial donors is very broad including inorganic sulfur compounds (H_2S and alkali metal sulfides, sulfites, thiosulfates, thionates, etc.), hydrazine and aliphatic amines (triethylamine, triethanolamine (TEA), etc.), aliphatic alcohols (methanol, ethanol, 2-propanol), carboxylic acids (formic acid, ethylenediaminetetraacetic (EDTA) acid, etc.), carbohydrates and other organic substances, in particular those abundant in the broadly available and sustainable source—the fermented bio-mass.

In the donor-based systems the photocatalytic process includes following typical stages: (i) excitation of a semiconductor photocatalyst by a light quantum with a proper (typically above-band-gap) energy, (ii) the interfacial transfer of a CB electron to an adsorbed water molecule followed by its reduction ($e^- + H_2O \rightarrow H^\bullet + OH^\bullet$), (iii) filling of a VB hole with an electron from a sacrificial donor ($h^+ + D \rightarrow D^{+\bullet}$). This cycle requires the CB potential of a semiconductor photocatalyst to be more negative than the water reduction potential in given conditions and the VB potential—to be more positive than the oxidation potential of a sacrificial donor (or water molecules). Figure 2.1 provides a graphic review of band edge positions for a series of semiconductor materials relative to the standard potentials of water reduction and oxidation. The figure shows separately the semiconductors suitable (a) and unsuitable (b) for the evolution of the solar hydrogen from water.

Fig. 2.1 CB and VB energy levels for some semiconducting photocatalysts with respect to NHE (E_{NHE}) and vacuum (E_{vac}). Reprinted with permission from Ref. [4]. Copyright (2015) The Royal Society of Chemistry



Typically, the semiconductor-based photocatalytic systems for the hydrogen production include a *co-catalyst*, that has no inherent photochemical activity but is capable of increasing dramatically the efficiency of semiconductor photocatalysts. Metal particles (Pt, Pd, Rh) deposited either on the semiconductor surface or on the surface of an inert carrier are typical co-catalysts for the semiconductor-based photocatalytic systems. The co-catalyst accepts and accumulates the charge carriers photogenerated in the semiconductor crystals inhibiting their recombination as well as contributes to a lowering of the water reduction overvoltage.

In recent years the studies of new light energy conversion systems based on semiconductor photocatalysts and photoelectrodes have bloomed in leading research centers [5–34]. The research focused also on the photosynthetic microorganisms and other photoactive bio-systems capable of the molecular hydrogen evolution [35–37]. The present chapter obviously cannot encompass the whole variety of papers reporting on the photochemical water splitting. It aims mainly to highlight typical and most important directions of the recent research as well as to give the reader a notion of the current state of the area and its future development.

2.1 Photocatalytic Systems Based on the Wide-Band-Gap Semiconductors and Sensitizers

The wide-band-gap semiconductors, mostly metal oxides, belong to a large group of light-sensitive materials broadly studied as photocatalysts of the water reduction. The spectral sensitivity range of such materials can be expanded to longer wavelengths by combining them with dyes-sensitizers that absorb strongly UV and near IR light.

Upon absorption of the visible and near IR light a sensitizer gets excited from the ground singlet state S^0 into the first (or a higher) singlet excited state S^1 (S^n). The S^1 state can either return to S^0 via emitting fluorescence or via the radiationless internal conversion. It can also convert into the first triplet excited state T^1 or inject an electron into the conduction band (CB) of a semiconductor. After that, the water reduction occurs either on the semiconductor surface or (most often) on the surface of a metal co-catalysts (Fig. 2.2). The role of spectral sensitizers is typically played by organic dyes or metal complexes (Fig. 2.3). The basic operation principles and the state-of-the-art of the photocatalytic H_2 evolution with the dye-sensitized semiconductors are comprehensively outlined in a recent review [38].

The most studied sensitized systems are based on titanium(IV) dioxide. For example, the hydrogen evolution under the illumination with the visible light (Vis-illumination) was observed in the presence of TiO_2/Pt heterostructures modified by eosin [39, 40], derivatives of phenothiazine [41, 42], triphenylamine [43] and perylene [44], by various complexes of Pt^{IV} [45], Zn^{II} [46] and Ni^{II} [47], copper phthalocyanine and ruthenium bipyridyl complexes [39]. Eosins adsorbed on the surface of $Na_2Ti_2O_4(OH)_2$ nanotubes (NTs) or MCM-41 zeolite modified by TiO_2 nanoparticles (NPs) in the presence of the photodeposited Pt NPs act as spectral sensitizers of the hydrogen evolution from aqueous TEA solutions [48, 49]. A sensitization effect was also observed in a similar system based on eosin Y and N-doped TiO_2 NPs [50].

Hydrogen generation from water/acetonitrile/KI occurs at the expense of I^- oxidation under the Vis-illumination of the platinized titania and layered $K_4Nb_6O_{17}$ sensitized by adsorbed coumarin and merocyanine dyes [51]. In the latter case, an effect of Pt NP localization on the photocatalyst activity was observed. The hydrogen formation rate over the $K_4Nb_6O_{17}/Pt$ composites with Pt NPs formed inside the interlayer space was found to be much higher than in similar systems where the metal NPs were distributed evenly between the inner and outer surface of the semiconductor or deposited only onto the outer semiconductor surface. The effect is caused by a side reaction of I_3^- complex with the CB electrons.

The eosin Y acts as a “universal” sensitizer for a series of layered wide-band-gap magnesium, calcium and strontium titanates [52]. The highest photocatalytic activity in the hydrogen evolution from aqueous diethanolamine solutions was

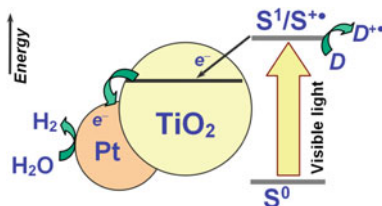


Fig. 2.2 Scheme of a photocatalytic system for the hydrogen evolution based on a TiO_2/Pt heterostructure and a sensitizer (S). S^0 , S^1 , S^{+} —sensitizer in the ground state, excited state and oxidized state, respectively, D—sacrificial donor

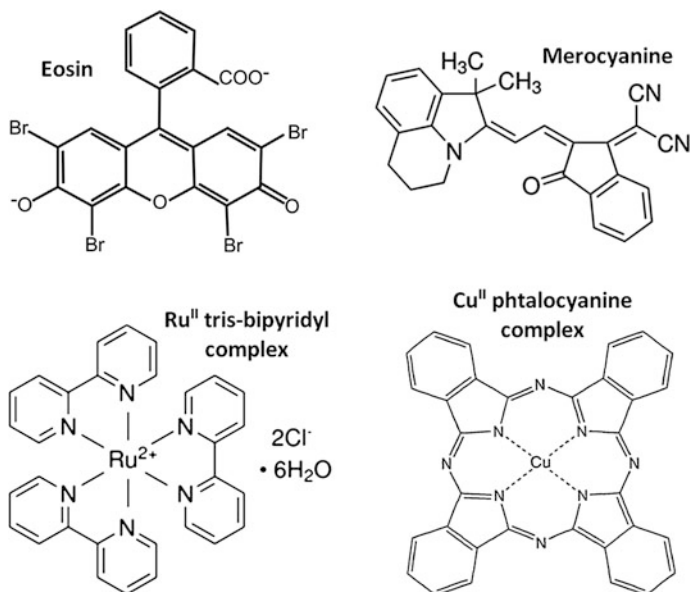


Fig. 2.3 Structure of some molecular sensitizers used in the semiconductor-based photocatalytic systems for hydrogen evolution

observed for SrTiO₃ modified by 0.5 wt.% Pt. Co₃O₄ NPs sensitized by eosin Y showed a high activity in the water reduction under the Vis-illumination in the absence of any additional co-catalysts [53].

Adsorption of 1,1'-dinaphthyl-2,2'-diol on the surface of TiO₂ NPs results in the formation of a charge-transfer complex with an intense absorption band centered at 550–600 nm. The photoexcitation of the complex into a charge-transfer absorption band leads to the hydrogen evolution from aqueous TEA solutions with a quantum yield (QY) of 0.02% [54]. The photocatalytic hydrogen evolution from aqueous glycerol solutions was observed for TiO₂/Pt nanoheterostructures sensitized by inorganic tungsten-containing heteropolyacids [55, 56].

Molecular and metal complex dyes were successfully used to sensitize not only metal oxide photocatalysts but also semiconductors of other types, such as cadmium sulfide [57] and graphitic carbon nitride (g-C₃N₄, GCN) [58]. The Vis-illumination of aqueous GCN suspensions in the presence of eosin Y, TEA, and Pt NPs resulted in the hydrogen evolution with a QY of around 19% [58]. In similar photocatalytic systems, g-C₃N₄ was sensitized by erythrosin [59, 60] and copper phthalocyanine [61]. GCN sensitized by Zn^{II} phthalocyanines revealed a comparatively high quantum yield of H₂ evolution reaching 3.05% and a spectral sensitivity of up to 750 nm [62].

Starting from 1980th, various Ru^{III/II} complexes with bipyridyl ligands were broadly studied as sensitizers of the hydrogen production and the studies in this direction are still advancing. For example, a photocatalytic system for the hydrogen

production comprising Ru^{2+} tris-bipyridyl complexes, TiO_2 NPs and hydrogenase as a co-catalyst was reported [63]. The hydrogen evolution under the Vis-illumination of aqueous solutions of sacrificial donors (methanol [64, 65] or TEA [66]) was observed in the presence of mesoporous TiO_2 modified by Pt NPs and mono- and bidentate Ru^{2+} bipyridyl complexes.

A strong electrostatic interaction between $\text{Ru}(\text{bpy})_3^{2+}$ cation and the negatively charged surface of $\text{K}_4\text{Nb}_6\text{O}_{17}$ nanoscrolls produced by the exfoliation of the bulk potassium niobate results in efficient electron phototransfer from the excited sensitizer to the semiconductor CB. The rate of photocatalytic hydrogen evolution from aqueous EDTA solutions is by an order of magnitude higher in the case of $\text{K}_4\text{Nb}_6\text{O}_{17}$ nanoscrolls than for the bulk semiconductor [67]. The H_2 evolution QY from EDTA solutions in the presence of $\text{H}_4\text{Nb}_6\text{O}_{17}$ and $\text{HCa}_2\text{Nb}_3\text{O}_{10}$ nanoscrolls modified by platinum NPs and $\text{Ru}(\text{bpy})_3^{2+}$ and $\text{Ru}(\text{bpy})_2(4,4'-(\text{PO}_3\text{H}_2)_2\text{bpy})^{2+}$ complexes reached 20–25% [68].

New sensitizers of titanium dioxide—binuclear Ru^{III} complexes with separate fragments connected by an azobenzene “bridge” were reported in [69]. As opposite to “classical” sensitizers of such type that typically adsorb strongly on the semiconductor surface, the bonding between the sensitizer and the photocatalyst is weak in this case. The weak coupling allows for the photooxidized sensitizer to desorb from the semiconductor surface inhibiting a reverse electron transfer and accelerating the photocatalytic hydrogen evolution from aqueous solutions of methanol or TEA.

A recent extensive review of the sensitized H_2 evolution in the semiconductor-based systems [38] outlined principal challenges that still need to be met in this area. Most dyes have relatively narrow absorption bands, typically in the Vis range and an expansion of the light-harvesting range into the near IR is a vital challenge to be addressed. Some strategies aimed at resolving this problem include co-sensitization of semiconductor nanomaterials with combinations of dyes having complementary absorption spectra; fabrication of heterostructures with dyes, narrow-band-gap semiconductors, and conductive polymers; search for ligands capable of bonding to the semiconductor surface and forming intense ligand-to-metal charge transfer absorption bands, etc.

The second challenge lies in a typically low stability of the molecular sensitizers. The organic dyes suffer from the photodegradation as a result of alternative reactions involving the singlet and triplet excited dyes, while the metal complexes are prone to photoinduced ligand exchange and photosolvation reactions resulting in the deterioration of their light-harvesting ability. Attempts of abating this problem include a proper modification of the semiconductor surface to mitigate secondary reactions as well as a rational design of the dye structure to reduce the possibility of the excited state relaxation pathways competing with the charge injection.

In recent years, a new research direction formed focusing on the visible-light-induced photocatalytic activity of heterostructures of wide-bandgap semiconductors with noble metal NPs, the latter exhibiting a surface plasmon resonance in the visible spectral range. This effect was christened as “plasmonic photocatalysis” [16, 70, 71] and was first accepted sceptically, but a number of reports on various photocatalytic transformations and photoelectrochemical

processes that can be performed by illuminating the semiconductor/metal NPs with the visible light was growing steadily, showing good perspectives of this phenomenon for the solar light harvesting [16, 34, 70–73].

The NPs of noble metals—gold, and silver reveal intense absorption bands in the visible spectral range as a result of electron gas oscillations in a surface layer of the metal NPs that is referred to as surface plasmon resonance (SPR). The SPR effect can be observed only for NPs (roughly smaller than 100 nm) and not for the corresponding bulk metals. The spectral parameters of SPR absorption band depend on the metal type, NP size and shape, dielectric parameters of the dispersive medium (solvent), nature of species adsorbed on the NP surface, on the proximity of neighboring metal NPs and many other factors [70–72]. For spherical non-aggregated silver and gold NPs the SPR maxima can be found around 390–400 and 530–550 nm, respectively.

The SPR absorption of gold NPs, though being quite intense and fitting to the solar spectrum, does not result in an interband electron transition and generation of additional free charge carriers, as it happens at the above-bandgap photoexcitation of semiconductors. Therefore, the Au NPs cannot act similarly to conventional molecular spectral sensitizers that inject an electron into the wide-bandgap semiconductor after the photoexcitation. The fact fed the skepticism concerning the reality of the “plasmon photocatalysis” phenomenon when it was only emerging in the field of solar light harvesting. Meanwhile, more and more reports on the photocatalytic transformations occurring under excitation into the SPR band of various gold/semiconductor heterostructures were steadily accumulated, some reports providing photoaction spectra (dependences of the QY of a photoreaction on the excitation wavelength) coinciding with the absorption spectra of Au NPs [74–79]. In attempts to interpret these processes, several alternative mechanisms were proposed including the heat transfer from Au NPs to the semiconductor resulting in the interband electron transition, ionization of the surface states of semiconductor NPs under the influence of the electromagnetic field of SPR-excited Au NPs, and others. However, a number of recently reported scrupulous and sophisticated studies showed that Au NPs excited into the SPR band can indeed inject “hot” electrons into the CB of wide-bandgap semiconductors, such as titania, in the cases when the Fermi level of photoexcited metal NPs shifts higher than the Schottky barrier on the semiconductor-metal interface (Fig. 2.4) [13, 34, 70–73].

For the plasmonic NPs smaller than 20 nm the hot electrons exhibit a broad spectrum of energies falling within the range from $E_{F,M}$ to $E_{F,M} + h\nu$, while larger particles exhibit much smaller hot electron energies close to $E_{F,M}$ and therefore for the larger metal NPs the probability of the hot electron injection is much lower.

The electrons with an energy lower than the Schottky barrier relax through the electron-electron and electron-phonon interactions. After the hot electron injection, a metal NP recompenses via a hole transfer to a water molecule (resulting in the O_2 evolution) or to another sacrificial donor, similarly as it happens with the photoexcited molecules of dye sensitizers or the photoexcited semiconductor NPs. The hot electron injection probability depends also on the distance to the semiconductor surface that should be covered by a hot electron before the internal relaxation

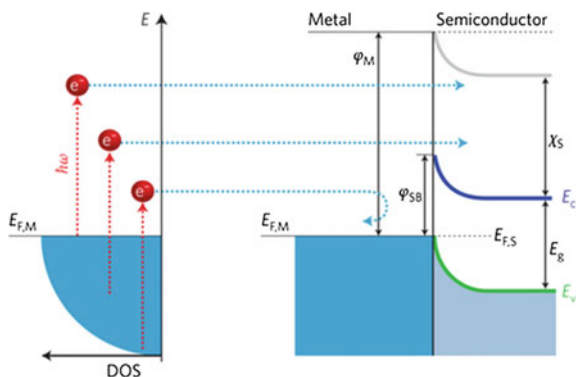


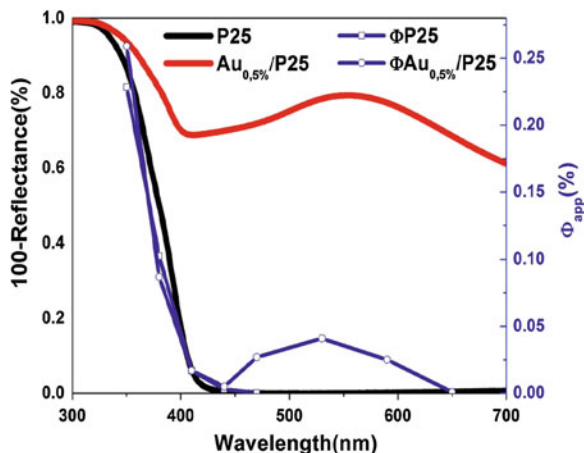
Fig. 2.4 Plasmonic energy conversion: electrons from occupied energy levels are excited above the Fermi energy. Hot electrons with energies high enough to overcome the Schottky barrier $\varphi_{SB} = \varphi_M - \chi_S$ are injected into the conduction band E_c of the neighboring semiconductor, where φ_M is the work function of the metal and χ_S is the electron affinity of the semiconductor. DOS is the density of states, $E_{F,M}$ and $E_{F,S}$ —Fermi level of the metal and metal/semiconductor heterojunction, E_v —valence band of semiconductor. Reprinted with permissions from Ref. [72]. Copyright (2014) Macmillan Publishers Limited

occurs, as well as on the density of states on the semiconductor surface that can accommodate a hot electron [71]. In this chapter, the effect of plasmonic light absorption in the semiconductor-based photocatalytic for the hydrogen evolution will be discussed only concisely. A series of recent reviews covers the issue of plasmonic photocatalysis much more extensively and can serve as a perfect guide for further development of this area [13, 16, 34, 70–73, 80].

The most popular plasmonic photocatalyst for hydrogen production is probably a TiO_2/Au combination. The SPR-enhanced H_2 evolution under illumination with the visible light (typically with $\lambda > 420\text{--}450\text{ nm}$) was observed in the presence of nanocrystalline TiO_2/Au heterostructures [74, 81–84], N-doped TiO_2 decorated with Au NPs [78], mesoporous TiO_2/Au composites [75] and aerogels [77], porous flat TiO_2/Au electrodes [85], TiO_2/Au photonic crystals [86]. Mixed Au/Pt NPs deposited onto the surface of TiO_2 nanosheets can play a double role, the gold providing SPR for the visible light harvesting, while Pt acting as a co-catalyst of hydrogen evolution [87]. The photoaction spectrum of TiO_2/Au composite as a photocatalyst of H_2 evolution was found to be very similar to the absorption spectrum (Fig. 2.5) indicating unambiguously on the participation of SPR-excited gold NPs in the photochemical transformations.

Direct participation of Au NPs in the photocatalytic reaction was clearly demonstrated for a mesoporous TiO_2/Au heterostructure evolving hydrogen from aqueous solutions of ascorbic acid when excited into narrow spectral windows of 500 ± 20 and $550 \pm 20\text{ nm}$ [75]. No H_2 was detected in such conditions for the pure titania. It is notable that the excitation into the $500 \pm 20\text{ nm}$ window results in a higher rate of hydrogen evolution because the energy of hot electrons depends on

Fig. 2.5 Absorption and photoaction spectra of TiO₂ Evonik P25 and a P25/Au heterostructure. Reprinted with permissions from Ref. [74]. Copyright (2016) American Chemical Society



the excitation energy and the probability of injection is higher for the shorter-wavelength light.

The effect of SPR-induced enhancement of the photocatalytic/photoelectrochemical H₂ evolution is of general nature and can be observed for other photoactive semiconductors, such as nanocrystalline CdS [88] and Ta₂O₅/Ta₃N₅ [89], ZnO nanorods (NRs) [76, 90], La₂Ti₂O₇ nanosheets [77]. The CdS/Au heterostructures exhibited not only an enhanced activity in the photocatalytic water reduction but also a much higher photostability in aqueous Na₂S/Na₂SO₃ solutions as compared to the individual CdS [88].

A spectacular plasmon enhancement of the photocatalytic/photoelectrochemical H₂ evolution was also observed for branched ZnO nanowires (NWs) decorated with gold NPs [76]. The deposition of Au NPs onto a highly developed surface of branched ZnO NWs resulted in a much broader spectral response extending to 700–750 nm. The incident-photon-to-current-efficiency (IPCE) spectra (analogs of photoaction spectra) of ZnO and ZnO/Au NWs excited by UV light (Fig. 2.6, panel 1) are roughly the same revealing no appreciable spectral differences and corresponding to the direct interband electron excitation of the semiconductor photocatalyst. However, the ZnO/Au heterostructures, as opposite to bare ZnO NWs, revealed a spectral response in the visible range with the band shape mimicking closely the SPR band shape of gold NPs (Fig. 2.6, panel 2).

Recently, the family of “plasmonic” photocatalysts was joined by GCN/Au nanoheterostructures. Graphitic carbon nitride absorbs only a limited portion of the visible light up to 460–470 nm and can be sensitized to longer-wavelength irradiation by the deposition of Au NPs [91, 92].

Similarly to gold, Ag NPs exhibit an intense SPR band in the visible spectral range and can induce the effect of spectral sensitization when excited into the SPR band, however, in this case the sensitization effect is not so obvious, as for gold, because the SPR band maximum of Ag NPs is closer or even overlapped with the absorption spectra of the most photoactive semiconductors. The effect of

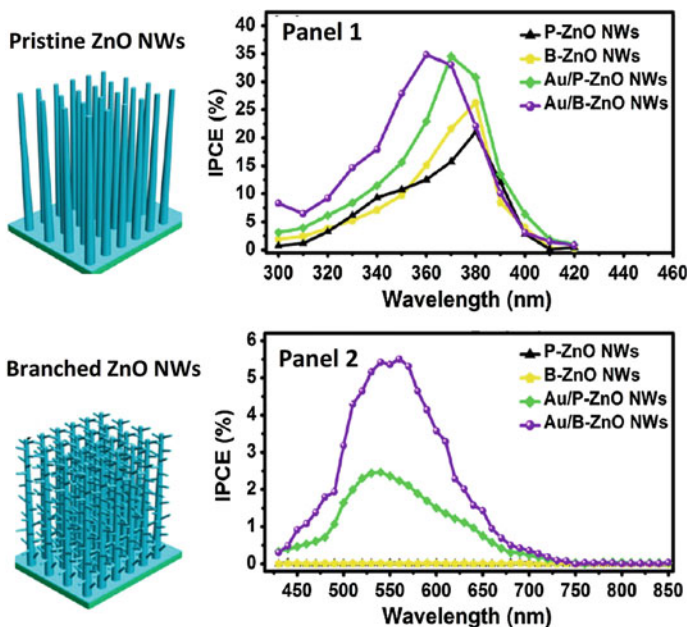


Fig. 2.6 IPCE spectra of P-ZnO, B-ZnO, Au/P-ZnO, and Au/B-ZnO NW photoanodes collected at 1.23 V versus NHE in a wavelength window of 300–420 nm (panel 1) and 420–850 nm (panel 2). Reprinted and adapted with permissions from Ref. [76]. Copyright (2014) American Chemical Society

plasmon-enhanced H_2 evolution was reported for N-doped TiO_2/Ag heterostructures [78], ZnO/Ag [93], GCN/Ag [94]. The ZnO NRs decorated with triangular Ag nanoprisms revealed a higher plasmon-activated photoactivity as compared with similar heterostructures based on regular spherical Ag NPs as a result of a strong electromagnetic field generated on the prism edges [94].

2.2 Photocatalytic Systems Based on the Binary and More Complex Semiconductor Heterostructures

Absorption of the visible light by a narrow-band-gap component of binary semiconductor composites also results in the electron injection to the CB of a wide-band-gap component, where, with the participation of a co-catalyst, hydrogen formation occurs. The photogenerated hole remains separated from the electron and reacts with a donor. Such spatial separation of the charge carriers is a reason for typically high rates of the photocatalytic hydrogen evolution over binary hetero-structures composed of narrow-band-gap metal sulfides and wide-band-gap metal oxides [95–100]. Figure 2.7 shows a scheme of charge transfers in a

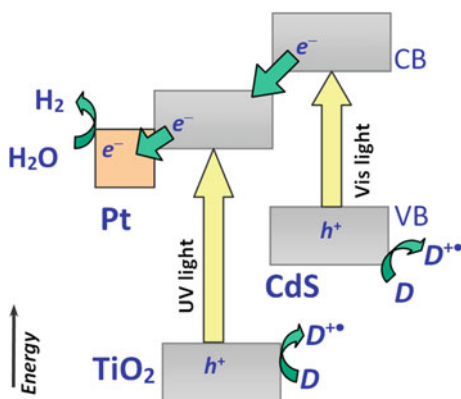
photocatalytic system based on a very popular TiO_2/CdS composite. In the further discussion we will define binary and more complex heterostructures by listing their components one after other separated by a “/” symbol. Typically we will put to the left of the slash a “basic” component of the heterostructure, for example, a wide-bandgap semiconductor (TiO_2) onto which another component, such as a narrow-bandgap sensitizer (CdS) is deposited or attached.

One of the most broadly studied semiconductor sensitizers for the hydrogen evolution is cadmium sulfide as well as related solid solutions, such as cadmium zinc sulfide. For example, Vis-sensitive photocatalysts of the hydrogen evolution from aqueous solutions of 2-propanol or Na_2S – Na_2SO_3 were formed by the deposition of CdS NPs on the surface of nanocrystalline titania [101, 102]. The photoactivity of the heterostructures increases remarkably with a decrease of the CdS NP size as a result of a size-dependent increase of the CB energy of CdS NPs [103, 104]. The photocatalytic activity of such systems can be further boosted by modification with fullerenes acting as photoelectron acceptors [105].

Ternary $\text{TiO}_2/\text{CdS}/\text{Pt}$ heterostructures can be used for the photocatalytic H_2 evolution directly from the sea water after addition of sacrificial donors (Na_2S and Na_2SO_3) [106]. An important factor governing the photocatalytic properties of ternary $\text{TiO}_2/\text{CdS}/\text{Pt}$ composites in the water reduction is a “correct” spatial organization of components [107–109]. A photocatalyst produced by the Pt NP photodeposition on the surface of preliminarily formed binary TiO_2/CdS heterostructure showed by an order of magnitude lower photoactivity than similar composites prepared by the CdS NP deposition onto pre-formed TiO_2/Pt heterostructure [107]. The same photocatalytic behavior is typical for a broad range of ternary $\text{TiO}_2/\text{CdS}/\text{M}$ composites, where $\text{M} = \text{Au}, \text{Ag}, \text{Pd}, \text{Pt}$ [110].

$\text{TiO}_2/\text{CdS}/\text{Pt}$ heterostructures produced by the impregnation of TiO_2/CdS composites with chloroplatinic acid followed by the thermal Pt(IV) reduction exhibited a higher photoactivity in the H_2 evolution than similar composites produced via the photocatalytic Pt(IV) reduction [108]. In this case, the difference in photoactivity also owes to the fact that the thermally deposited Pt NPs are attached mostly to the

Fig. 2.7 Scheme of spatial separation of the photogenerated charge carriers in a CdS/ TiO_2 heterostructure and the H_2 formation under the Vis-illumination



TiO₂ surface, where the water reduction takes place, while the photo-deposited metal NPs are distributed randomly between the CdS and TiO₂ NPs.

Ternary WO₃/CdS/Au heterostructures built on the basis of inverted WO₃ opals are more active photocatalysts of the water splitting than their analogs produced from randomly structured tungsten oxide. An advanced photoactivity of the opal-based photocatalysts stems from a more efficient light absorption due to the multiple scattering and refraction of light in the regular pores of the opals [111].

A shape anisotropy of zinc oxide NRs [112] and nanobelts [113] favors to the spatial charge carrier separation in ZnO/CdS heterostructures reflecting in a high photocatalytic activity in the H₂ evolution from water/methanol mixtures.

The ion exchange capability of a Ti(IV)-modified MCM-41 zeolite was used to form 2.5-nm CdS NPs in the zeolite pores [114]. After the Pt NP photodeposition such heterostructure exhibits a high photocatalytic activity in the hydrogen evolution from aqueous sodium sulfite solutions exceeding strongly that of bulk cadmium sulfide. The photocatalytic H₂ evolution from aqueous TEA solutions was also observed in the presence of CdS NPs immobilized on MCM-41 with a fraction of Si atoms replaced with Zr and Ti [115].

The heterostructures of CdS NPs [116–118] and Cd_{0.5}Zn_{0.5}S NPs [119] with TiO₂ NTs are efficient Vis-sensitive photocatalysts of the hydrogen evolution from aqueous Na₂S/Na₂SO₃ solutions. The CdS NP deposition the surface of TiO₂ nanoplates [120] and meso-porous microspheres [121] with prevalingly exposed {001} facets yields efficient photocatalysts of the water reduction by lactic acid [120]. The photoactivity of such heterostructures exceeds that of similar composites produced from conventional titania crystals because the {001} lattice face of titania exhibits a relatively higher efficiency of the interfacial electron transfer [120, 121].

Spatial separation of the photogenerated charge carriers between the host titanasilicate matrices ETS-4 and ETS-10 comprising ultra-thin (–O–Ti–O–Ti–O–)_x “quantum wires” and CdS NPs deposited into the host pores results in a high photoactivity of such heterostructures in the H₂ evolution from aqueous Na₂S/Na₂SO₃ solutions [122]. Similar approaches were used to introduce CdS NPs into the interlayer galleries of layered titanates [123–127], niobates [128–130] and tantalates [129, 131, 132], as well as layered mixed Zn^{II} and Cr^{III} hydroxides [133]. In such composites, the water reduction to H₂ occurs on co-catalyst NPs (Pt, Ni or RuO₂) deposited on the outer photocatalyst surface, while the oxidation of a sacrificial donor (Na₂S or Na₂SO₃) involves CdS NPs attached to the inner surface of the layered host material. Due to the spatial separation of the charge carriers the photocatalytic activity of the composites exceeds strongly that of individual cadmium sulfide or a mechanical mixture of CdS and a layered metallate [123, 124, 128].

To achieve favorable conditions for the formation of CdS NP-based heterostructures and to promote photocatalytic processes with their participation, a preliminary treatment of layered host materials is often performed aimed at an expansion of the interlayer galleries. For example, the intercalation of propylamine and [Pt(NH₃)₄]Cl₂ complex into the interlayer space of HNbWO₆ expands considerably the inner voids between the layers favoring to the secondary intercalation with Cd^{II} and Zn^{II} [134]. The annealing and sulfurization of such material resulted

in a $\text{HNbWO}_6/\text{Cd}_{0.8}\text{Zn}_{0.2}\text{S}/\text{Pt}$ heterostructure exhibiting a Vis-light-driven photocatalytic activity in the hydrogen evolution from aqueous solutions of sodium sulfite.

A treatment of co-deposited CdS and TiO_2 NPs with titanium(IV) chloride followed by the annealing [135] assures the formation of TiO_2/CdS heterostructures with a good mechanical and electronic contact between the CdS and TiO_2 NPs favoring to the charge transfers between the components. The highest photocurrent and photocatalytic activity in the hydrogen generation were observed at 80 wt.% titania content [135].

Directed migration of the photogenerated charge carriers—from a layer of cadmium selenide to TiO_2 NTs through an intermediary CdS layer in ternary $\text{TiO}_2/\text{CdS}/\text{CdSe}$ heterostructures contributes to their high photoelectrochemical activity in the hydrogen evolution from aqueous solutions of $\text{Na}_2\text{S}/\text{Na}_2\text{SO}_3$ or ethylene glycol with QY reaching $\sim 9.5\%$ [136]. A similar effect was observed for nanoheterostructures formed by CdS “nanoflowers” grown on the surface of TiO_2 NT arrays (Fig. 2.8a) [137].

A very efficient charge transport from the visible-light-sensitive CdSe NPs to the thin (~ 5 nm thick) titania NSs results in a strong non-additive enhancement of the photocatalytic hydrogen evolution from aqueous $\text{Na}_2\text{S}/\text{Na}_2\text{SO}_3$ solutions [138]. Coupling of the TiO_2 NSs to CdS NPs via a molecular bridge—bifunctional mercaptopropionic acid (MPA) anion allows to double the H_2 evolution efficiency as compared to the bare CdSe NPs, while direct (without linkers) deposition of the sensitizer NPs onto the TiO_2 NSs increases the efficiency by another $\sim 100\%$ (Fig. 2.8b). An electron paramagnetic resonance (EPR) study showed that Ti^{4+} ions can be converted into Ti^{3+} by the photogenerated CB electrons and act as charge transfer mediators to the CdSe NPs. Due to the fact, the annealing of TiO_2 NSs that

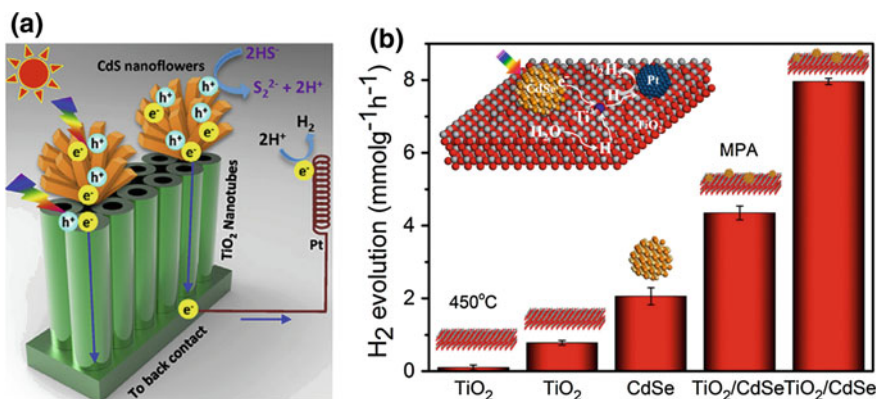


Fig. 2.8 **a** A scheme of the photoelectrochemical H_2 evolution with “ TiO_2 nanotube/ CdS nanoflower” heterostructures; **b** The rate of photocatalytic hydrogen evolution in the presence of TiO_2 nanosheets and NS/ CdSe heterostructures. Reprinted with permissions from Ref. [137] (a) and [138] (b). Copyright (2015, 2016) Elsevier (a) and American Chemical Society (b)

caused their aggregation and a loss of the surface area had a detrimental effect on the photocatalytic activity of both bare TiO_2 NSs and TiO_2 NS/CdSe nanocomposites [138].

The sol-gel deposition of 10–20-nm titania NPs on the surface of microcrystalline cadmium sulfide followed by the photodeposition of Pt NPs results in a ternary $\text{CdS}/\text{TiO}_2/\text{Pt}$ composite that reveals photocatalytic properties in the hydrogen evolution from aqueous $\text{Na}_2\text{S}/\text{Na}_2\text{SO}_3$ solutions [139]. Other platinum group metals can also act as co-catalysts of this process forming the following activity sequence: $\text{Pt} > \text{Rh} > \text{Pd} > \text{Ru}$. Isotopic studies in a similar system, where H_2S was used as a sacrificial electron donor, showed that H_2 is evolved at the expense of the decomposition of both H_2O and H_2S [140].

CdS/TiO_2 heterostructures based on cadmium sulfide NWs [141] exhibited a much higher photocatalytic activity in the H_2 evolution from aqueous $\text{Na}_2\text{S}/\text{Na}_2\text{SO}_3$ solutions than non-modified CdS NWs. Spatial separation of the photogenerated charge carriers between the heterostructure components results in the separation of oxidative and reductive steps of the process—the water reduction to H_2 occurs on the TiO_2 NPs, while the sacrificial donors are oxidized on the surface of CdS NWs.

Despite the fact that sacrificial donors, especially sodium sulfide and sulfite can efficiently quench the oxidative photocorrosion of cadmium sulfide, some inevitable release of inherently toxic Cd^{II} ions can be expected for the CdS-based photocatalysts. This hazard stimulates a constant search for other less toxic narrow-bandgap sensitizers capable of competing with cadmium sulfide in the hydrogen evolution efficiency.

A particular attention in this search is paid to ternary and quaternary metal-chalcogenide NPs, such as indium-based chalcopyrite CuInS_2 and AgInS_2 (AgIn_5S_8) NPs and quaternary kesterite $\text{Cu}_2\text{ZnSnS}_4$ NPs. These compounds have relatively narrow bandgaps of around 1.4–1.8 eV and reveal strong absorption bands covering the entire visible spectral range thus making such NPs ideal light harvesters for the photocatalytic hydrogen evolution systems.

The $\text{CuInS}_2/\text{TiO}_2$ [142, 143] and $\text{TiO}_2/\text{AgIn}_5\text{S}_8$ [144] heterostructures revealed a photocatalytic activity under the photoexcitation over almost the whole visible spectral range. The sensitization of Ag NP-decorated ZnO NW arrays with CuInS_2 NPs results in ~ 100 -fold enhancement of the photoelectrochemical hydrogen production efficiency under the Vis-illumination as compared to the original NWs [145].

The quaternary kesterite NPs were successfully employed as a light harvester for the photoelectrochemical hydrogen production over a $\text{ZnO}/\text{CdS}/\text{Cu}_2\text{ZnSnS}_4$ heterostructure based on ZnO NWs [146]. The mutual positions of the CB and VB levels of the components are ideally suitable for a cascade transfer of the photogenerated electrons from the outer kesterite layer to the CdS buffer layer to the ZnO NW layer (Fig. 2.9a). After the cascade the electrons are collected into the electric circuit and transferred to a Pt counter electrode, where the H_2 evolution occurs, while the $\text{CdS}/\text{Cu}_2\text{ZnSnS}_4$ (CZTS) light-harvesting layer is regenerated via the oxidation of a sacrificial donor ($\text{Na}_2\text{S}/\text{Na}_2\text{SO}_3$) [146]. The photocurrent (and correspondingly, H_2 on the counter electrode) is generated under the illumination in the

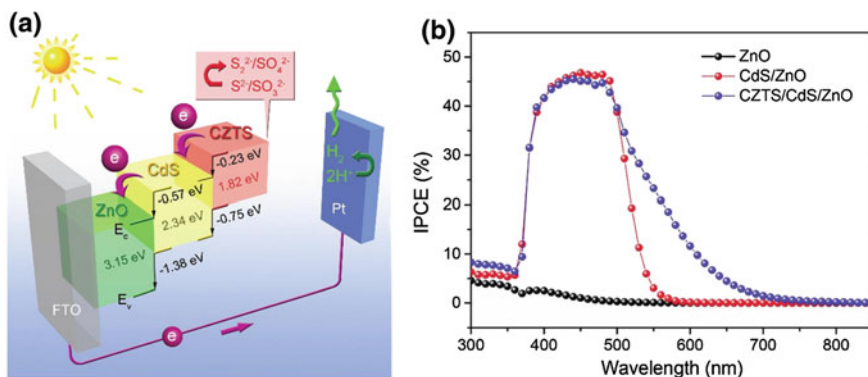


Fig. 2.9 **a** A scheme of charge transfers in ZnO NW/CdS/Cu₂ZnSnS₄ (CZTS) system; **b** IPCE spectra of ZnO NW-based heterostructures with CdS and CZTS NPs. Reprinted with permissions from Ref. [146]. Copyright (2015) The Royal Society of Chemistry

entire visible range (400–700 nm) with the light-to-current conversion efficiency reaching $\sim 45\%$ (Fig. 2.9b).

Quaternary NPs of other types, such as Cu–Ga–In–S NPs [147], are also currently probed as spectral sensitizers with the aim of combining a high absorptivity in the visible spectral range and a “suitable” band positions for the efficient charge transfer to TiO₂.

Among the binary non-toxic semiconductor sensitizers, a special attention is focused on bismuth and antimony chalcogenides that combine a high sensitivity to the visible light, a relative stability and band positions favorable for the charge injection into TiO₂, ZnO, and other wide-bandgap semiconductor materials. Thermal hydrolysis of thiourea in the presence of Bi(NO₃)₃ and nanocrystalline TiO₂ yields TiO₂/Bi₂S₃ heterostructures manifesting a photocatalytic activity in the Vis-light-driven H₂ production from aqueous Na₂S/Na₂SO₃ solutions [148]. The photoactivity of the composite was found to be much higher than that of bismuth sulfide alone and maximal—at the equimolar content of the components [148]. The TiO₂/Bi₂S₃ composites produced by a solvothermal method from 10 to 15-nm titania NPs exhibited photocatalytic properties in the hydrogen evolution from water/methanol mixtures [149].

Spatial separation of negative and positive charge carriers in the nanoheterostructures of titania and copper(I,II) oxides as well as the capability of copper oxides of accumulating electrons and decreasing the water reduction over-voltage allowed to carry out the photocatalytic H₂ evolution under the illumination with the visible light [138, 150–160]. A p/n heterojunction also forms on the interface between TiO₂ and copper phosphide Cu₃P NPs enabling efficient separation of the photogenerated charge carriers and the water reduction with an apparent QY (measured at a certain wavelength) of 4.6%, which is by an order of magnitude higher than for sole titania NPs [161].

The photocatalytic Vis-light-driven formation of hydrogen was observed also in the presence of $\text{In}_2\text{O}_3/\text{In}_2\text{S}_3$ [162], CuO/ZnO [163], $\text{In}_{1-x}\text{Ga}_x\text{N}/\text{ZnO}$ [164], $\text{CuFeO}_2/\text{SnO}_2$ [165], $\text{RuO}_2/\text{TiO}_2$ [166], and $\text{CuAlO}_2/\text{TiO}_2$ [167] nanoheterostructures.

Along with the development of photocatalytic systems based on traditional semiconductors, a search is also performed for new photosensitive semiconducting materials combining the visible light sensitivity with a capacity to act as spectral sensitizers for wide-band-gap semiconductors. At that, a special attention is paid to carbon materials—fullerenes, carbon NTs, etc. For example, a composite of multiwall carbon NTs with titania modified by Ni NPs exhibited a photocatalytic activity in the water reduction when excited by the visible light [113, 168]. It was assumed that the photoexcitation of carbon NTs results in the electron injection into the TiO_2 CB followed by the electron transfer to the Ni NPs where the final act of the water reduction occurs. The oxidized NTs are then regenerated at the expense of methanol oxidation.

Recently, good perspectives were shown for the sensitization of wide-bandgap semiconductor materials with carbonaceous nanostructured species, such as carbon NPs and nanodispersed carbon nitride. The carbon NPs can be produced by thermal/electrochemical decomposition of a variety of organic precursors and contain a partially aromatic carbon core and an outer shell abundant with various functional groups [169, 170]. They absorb light in broad and intense bands extending throughout the visible range and can strongly bind to the most of the photoactive wide-bandgap semiconductors typically used for the photocatalytic processes. A comprehensive account of recent successes and challenges associated with the utilization of carbon NPs in the photocatalysis can be found in [169]. For example, the nanocrystalline titania can be sensitized to the visible light by the carbon NPs [171, 172] produced via hydrothermal treatment of vitamin C [171] or by the electrochemical destruction of graphite [172, 173]. Such heterostructures exhibited almost by an order of magnitude higher photocatalytic activity in the H_2 evolution from water/methanol mixtures under the illumination with the “white” light ($\lambda > 400$ nm) as compared to the bare titania.

Graphitic carbon nitride is often called a “rising star” of the semiconductor photocatalysis as it combines a unique set of properties including chemical stability, sensitivity to the visible light, “appropriate” positions of CB and VB energies allowing both for the water reduction and oxidation to occur simultaneously. This material will be discussed in details later in the section devoted to new photoactive materials. Here, we only mention the role of GCN as a component of composite H_2 evolution photocatalysts. It was found that spatial separation of the photogenerated charge carriers imparts TiO_2/GCN heterostructures with a photocatalytic activity in the Vis-light-driven hydrogen evolution from water with no sacrificial donors [174–176] as well as from aqueous solutions of methanol [177] or TEA [178].

The exfoliation of GCN into a-few-layer or even single-layer CN sheets increases strongly its activity as a hydrogen evolution photocatalyst, both in the individual state and when incorporated into complex nanoheterostructures. It is reported that the photocatalytic activity of composites of titania NRs with the GCN

nanosheets produced by an ultrasound treatment of the bulk GCN is by far higher than the photoactivity of a mixture of TiO_2 NRs and the unexfoliated GCN [179].

As GCN has a bulk bandgap of 2.7 eV it can also be a subject to the spectral sensitization. Such effect was achieved for CdS/GCN [180] and $\text{ZnIn}_2\text{S}_4/\text{GCN}$ [181] composites, as well as for CdSe NP-decorated hollow GCN spheres [182].

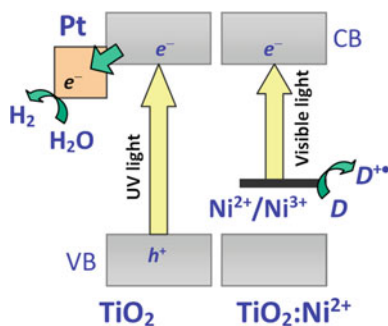
The GCN NSs can be used as a “mat” to accommodate wide-bandgap semiconductor NPs. For example, GCN/TiO_2 heterostructures produced by the solvothermal deposition of titania NPs onto GCN NSs demonstrated the rates of photocatalytic hydrogen evolution by ~ 10 and ~ 20 times higher than those observed in the presence of sole TiO_2 and the bulk GCN [183]. A similar effect was also achieved for ~ 20 -nm InVO_4 nanocrystals grown on the GCN sheets [184].

2.3 Photocatalytic Systems Based on the Metal-Doped Wide-Band-Gap Semiconductors

Doping of the wide-band-gap semiconductors with metal ions introduces new occupied local states in the band gap that can be excited by the visible light and supply electrons to CB (Fig. 2.10). The CB electrons participate then in the water reduction while the holes localized on the dopant states get filled by electrons from a sacrificial donor or water [137, 185–189].

Visible-light-sensitive photocatalysts of the hydrogen evolution from aqueous solutions of sodium sulfite were prepared by doping ZnS with Pb^{II} [190], Ni^{II} [191] and Cu^{II} [192]. Such photocatalysts can function without additional co-catalysts. The visible-light absorption by these compounds originates from the photoinduced electron transition from the local dopant states in the CB of zinc sulfide. The photocatalytic activity of $\text{ZnS}:\text{Pb}^{\text{II}}$ is maximal at 1.4 wt.% lead content and decreases considerably at a higher dopant concentration (more than 2%) as a result of the formation of a separate PbS phase. Additional co-doping of the photocatalyst with halogen anions results in a 3-fold increase of the photoactivity, the effect originating from a relaxation of the lattice strain and a decrease of the number of non-radiative recombination sites [192]. At an optimal dopant concentration of 4.3 wt.% the

Fig. 2.10 A photocatalytic system for the hydrogen production based on Ni^{II} -doped titania



ZnS:Cu^{II}-based photocatalytic system exhibits an apparent hydrogen production QY of 3.7% [192]. A maximal increment of the photocatalytic H₂ evolution rate after doping of zinc sulfide with Cu(II)—by a factor of 11 is observed after the introduction of ~5 mol% copper [193]. At the same time, for ZnS:Ni^{II} the peak photocatalytic activity in the water reduction was achieved already at 0.1 mol% Ni content [191].

Doping of titania with Bi^{III} imparts this semiconductor with a photocatalytic activity in the H₂ evolution from water/ethanol mixture under the Vis-illumination [194]. In a similar way, doping of SrTiO₃ with Cr [195, 196] and Rh ions [197, 198] yields Vis-light-sensitive photocatalysts of the hydrogen evolution from aqueous methanol [195, 196] and pure water splitting [197, 198].

The substitution of Ti⁴⁺ with Cr³⁺ or Fe³⁺ in titania crystals requires a compensation of the excessive negative lattice charge and induces self-oxidation of Cr^{III} to Cr^{VI} and the release of molecular oxygen [199–202]. The recombination of charge carriers at anion vacancies forming after the O₂ subtraction decreases the photocatalytic activity. To balance the charge and to increase the stability and activity of Cr-doped titania an equimolar amount of Ta⁵⁺ or Nb⁵⁺ should additionally be introduced into the lattice. An increase of the photocatalytic activity of a doped semiconductor as a result of the charge compensation was also observed for the co-doping of TiO₂ and SrTiO₃ with combinations of Ni²⁺/Ta⁵⁺ [199] and Cr³⁺/Sb⁵⁺ [200].

A strong doping-induced photoactivity enhancement of a semiconductor host in the water reduction was observed after the introduction of Bi³⁺ into NaTaO₃ [203], Zn²⁺ into SrTiO₃ and BaTiO₃ [204], Ag⁺ into BiVO₄ [205], cations of Y, La, Ce or Yb into NaTaO₃ [206], and Zn²⁺ into Ga₂O₃ [207].

The photocatalytic water reduction to H₂ under Vis illumination was reported for ZnS and SrTiO₃ doped with La³⁺ [208], Ni²⁺-doped InTaO₄ and InNbO₄ [209]. After the deposition of a co-catalyst (Pt, RuO₂, NiO_x) the latter two systems demonstrated an apparent QY of up to 0.66% (at $\lambda = 400$ nm). Besides doping with Ni²⁺, InTaO₄ can be turned into a Vis-sensitive photocatalyst of the H₂ evolution by introducing Mn, Fe, Co, and Cu cations [210]. Doping with chromium turns a Ba₂In₂O₅/In₂O₃ heterostructure into a “universal” photocatalyst capable of the hydrogen evolution from water and water/methanol mixtures in the presence of Pt or Ni as well as of the O₂ evolution from aqueous AgNO₃ (electron acceptor) solutions [211].

A broad range of dopants—Cr^{VI}, Fe^{III}, Co^{II}, Ni^{II}, Ru^{II}, and Pd^{II} was used to convert nanocrystalline Bi₂O₃ ($E_g = 2.8$ eV) into a Vis-sensitive photocatalyst of the water reduction [212]. Doping with palladium(II) resulted in the best characteristics, the fact apparently originating from in situ Pd(II) photoreduction Pd⁰ which can act as a co-catalyst.

Almost in each system based on doped semiconductors there exists an optimal dopant concentration range where the maximal photoactivity is observed, while a higher dopant amount deteriorates the semiconductor activity in the water reduction. For TiO₂ doped with Ni²⁺ [213, 214] or Bi³⁺ [194], the maximal rate of the photocatalytic hydrogen evolution from water/alcohol mixtures was observed at a

1% mol. dopant content [213]. This effect is typically associated with a hindrance of the free migration of photogenerated charge carriers in the bulk of highly-doped semiconductor crystals because of an abundance of the local dopant states acting as charge traps.

In some cases doping results in a fusion of the dopant states and a “top” of the host VB. The effect narrows the band gap (and increases the Vis-light sensitivity of a semiconductor) without the emergence of additional local states in the forbidden band. For example, doping of indium titanate with a mixture of nickel and chromium cations results in a fusion of Ni3d, Cr3d, Ti3d/In5sp, and O2p orbitals yielding a Vis-light-sensitive $\text{In}_{12}\text{NiCr}_2\text{Ti}_{10}\text{O}_{42}$ photocatalyst ($E_g = 2.14$ eV) of the H_2 evolution from water/methanol mixtures [215, 216], more efficient than “mono-doped” $\text{In}_6\text{NiTi}_6\text{O}_{22}$ ($E_g = 2.48$ eV) and $\text{In}_3\text{CrTi}_2\text{O}_{10}$ ($E_g = 2.00$ eV) [215].

Sometimes a variation in the metal dopant nature allows switching the semiconductor activity between the water reduction and the water oxidation. For example, doping of SrTiO_3 with Mn^{2+} or Ru^{3+} impart this semiconductor with a photocatalytic activity for the Vis-light-driven oxygen evolution from aqueous AgNO_3 solutions [217]. At the same time, doping of strontium titanate with Ru, Rh, or Ir (1 wt.%) cations and the deposition of 0.1 wt.% Pt converts this wide-band-gap semiconductor into a Vis-light-sensitive photocatalyst of the water reduction by methanol demonstrating an apparent H_2 evolution QY of 5.2% at 420 nm [217].

The radio-frequency magnetron sputtering technique is typically used [218–224] to produce titania films that exhibit a visible light sensitivity originating from a stoichiometry deviation, that is a gradient of the O/Ti atomic ratio from the surface to the bulk of the films. A post-synthesis hydrothermal treatment of the films enhances considerably their photocatalytic activity in the water reduction as a result of an increase of the film crystallinity and the specific surface area [222]. This method was also applied to produce Ti foils decorated with titania nano-columns oriented normally to the film surface [225] with an O/Ti ratio changing from 2.00 on the column top to 1.93 at the site of the column contact with the substrate. After the modification of an opposite side of a Ti/TiO₂ foil with Pt NPs, it was used as a Vis-light-sensitive photocatalyst of the total water splitting in a combined reactor with membrane-separated compartments for the water reduction to H_2 and the water oxidation to O_2 (Fig. 2.11a) [218, 225]. Such design allows avoiding the recombination between primary products of the reduction (H atoms) and the oxidation (OH radicals), which is one of the main factors limiting the H_2 evolution efficiency.

Recently, a so-called “black” titania emerged as a new visible-light-sensitive photocatalyst of the water reduction [29]. The “black” TiO₂ is typically produced by treating titania with hydrogen or aluminium resulting in a massive reduction of Ti^{4+} to Ti^{3+} , the latter imparting the material with a characteristic blackish-gray to black color (Fig. 2.11b, insert).

According to [226], reduction with Al yields much deeper reduced TiO_{2-x} samples with the absorbance extending to longer wavelengths as compared to the hydrogen-processed titania (HP-TiO₂), the absorption band encompassing the entire visible and near IR ranges (Fig. 2.11b). A strong light-harvesting capability of the “black” TiO₂ results in much higher photocurrents/ H_2 evolution rates in the

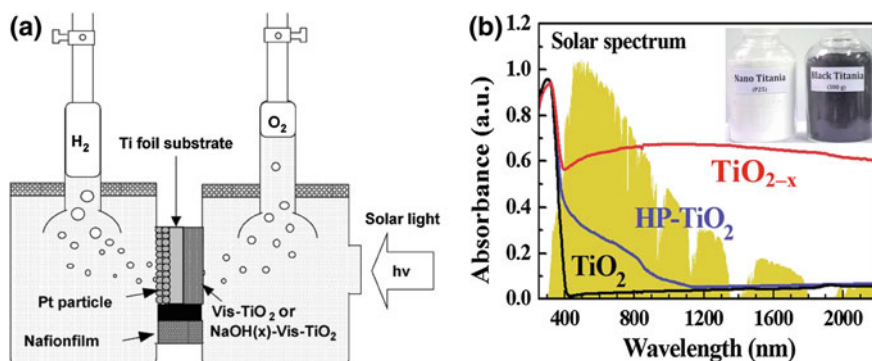


Fig. 2.11 **a** A combined photocatalytic reactor for simultaneous evolution of H_2 and O_2 from water in the presence of a “Pt/Ti foil/Ti NTs” heterostructure; **b** absorption spectra of original TiO_2 and products of titania reduction with hydrogen (HP-TiO_2) and aluminium (TiO_{2-x}). Yellow background—solar AM1.5 irradiation spectrum. Insert: photographs of conventional nanocrystalline titania (Evonik P25) and black TiO_{2-x} produced by the reduction with Al. Reprinted with permissions from Refs. [222] (a) and [226] (b). Copyright (2008, 2015) Elsevier (a) and American Chemical Society (b)

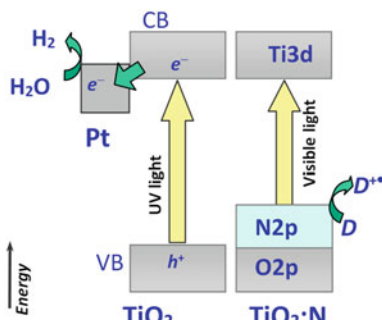
photoelectrochemical/photocatalytic systems as compared to those with conventional nanocrystalline TiO_2 powders [226], NTs [227] or mesoporous TiO_2 [228].

2.4 Photocatalytic Systems Based on the Nonmetal-Doped Wide-Band-Gap Semiconductors

A partial oxygen substitution in a metal oxide semiconductor lattice by other non-metals—nitrogen, carbon, sulfur, etc., was found to be one of the most versatile methods of tailoring the band gap of semiconductor photocatalysts. The p-orbitals of a dopant typically have a higher energy than the p-orbitals of oxygen, so the dopant introduction results in a narrowing of the band gap without appreciable shifts of the CB edge (Fig. 2.12). The effect is explored by a so-called “band design” concept, that is, tailoring of the band gap and the VB position of semiconductor photocatalysts by non-metal dopings [2, 137, 185, 187–189].

The introduction of nitrogen into the lattice of titanium dioxide NPs achieved by TiO_2 synthesis in the presence of ammonia [50], results in a retardation of the NPs growth during the calcination, a decrease of the average NP size from 20 to 14 nm, and a shift of the light sensitivity threshold of titania to longer wavelengths. Also, the doping generates oxygen vacancies on the TiO_2 NP surface that promote adsorption of a sensitizer—eosin [50]. Such sensitized $\text{TiO}_2\text{:N}$ NPs showed a 3-times higher photocatalytic activity in the hydrogen evolution from aqueous TEA solutions as compared to undoped TiO_2 NPs.

Fig. 2.12 A scheme of a photocatalytic system for the hydrogen production based on N-doped titania



N-doped TiO_2 produced by the titania calcination with urea [229, 230] absorbs the visible light with $\lambda < 600$ nm and exhibits a photocatalytic activity in the Vis-light-driven H_2 production from aqueous solutions of Na_2SO_3 [229] and methanol [230]. Of two forms of surface nitrogen—the chemisorbed N and the nitrogen substituting O atoms in the oxide lattice, it is the latter that imparts titania with a Vis-sensitivity and the enhanced photocatalytic activity. Among N-doped titania materials a higher photocatalytic activity in the Vis-light-induced water splitting is typically observed for the mesoporous TiO_2 [231–233]. The photocatalytic activity of $\text{TiO}_2\text{:N}$ in the water reduction can be further enhanced by combining it with Pt NPs [234] or other electron acceptors such as graphene derivatives [235, 236].

Annealing of tantalum oxide in a stream of ammonia and water vapors (to prevent the formation of tantalum nitride) yields tantalum oxynitride TaON absorbing visible light in a range of $\lambda < 500$ nm (Fig. 2.13a) [236–239]. The material demonstrates a high photocatalytic activity in the water oxidation to O_2 (with an apparent QY of 30% at 420–500 nm excitation), but possesses a negligible photoactivity in the water reduction, even in the presence of Pt (QY of 0.2% at 420–500 nm). Oppositely to pure oxide semiconductors, for which platinum is typically the best co-catalyst of hydrogen evolution, for the N-doped semiconductors a much higher activity is observed for a ruthenium co-catalyst (QY of 0.8% and 2.1% in the presence of methanol and ethanol, respectively). The photocatalytic deposition of Ru NPs produces 2–4-nm particles exhibiting a higher catalytic activity than 20–50-nm Ru NPs formed by the conventional impregnation/annealing [237]. Complete substitution of O with nitrogen yields tantalum nitride Ta_3N_5 with $E_g = 2.1$ eV (Fig. 2.13a) that is also an active photocatalyst of the water splitting [238].

The annealing in ammonia stream was used to produce zirconium oxynitride Zr_2ON_2 from ZrO_2 [240]. The fusion of N2p-orbitals and O2p-orbitals in the VB of zirconium oxynitride results in the bandgap shrinking to 2.6 eV. After the photodeposition of 5 wt.% Pt, Zr_2ON_2 crystals exhibited a photocatalytic activity in the H_2 evolution from aqueous solutions of methanol as well as the O_2 evolution from silver nitrate solutions under the Vis-illumination. Solar-light-sensitive photocatalysts of the water reduction/oxidation were prepared by a partial nitridation of $\text{ZrO}_2/\text{Ta}_2\text{O}_5$ composite [241]. In a similar way, layered LaTaON_2 and $\text{Y}_2\text{Ta}_2\text{O}_5\text{N}_2$

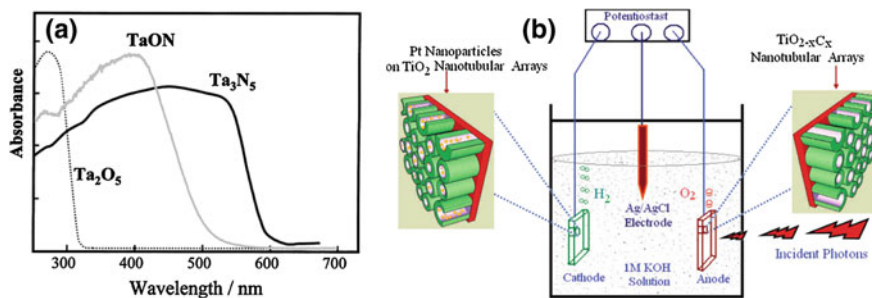


Fig. 2.13 Diffuse reflectance spectra of Ta_2O_5 , TaON , and Ta_3N_5 ; **b** a layout of the photoelectrocatalytic system for water splitting based on C-doped and Pt-decorated TiO_2 NTs. Reprinted with permissions from Refs. [238] (a) and [251] (b). Copyright (2003, 2007) Elsevier (a) and American Chemical Society (b)

perovskites were produced [242] exhibiting a photocatalytic activity in the hydrogen evolution from water/ethanol mixtures in the presence of Pt and Ru NPs.

The introduction of a nitrogen dopant into the $\text{Sr}_2\text{Nb}_2\text{O}_7$ perovskite yields a series of $\text{Sr}_2\text{Nb}_2\text{O}_{7-x}\text{N}_x$ compounds that preserve the layered structure and, due to a contribution of the N2p-orbitals into the VB, exhibit a photocatalytic activity in the hydrogen evolution from water/methanol mixtures under the Vis-illumination [243].

A nitrogen-doped solid solution of gallium and zinc oxides $(\text{Ga}_{1-x}\text{Zn}_x)(\text{N}_{1-x}\text{O}_x)$ with $x = 0.18$ was used as a photocatalyst of the water reduction that, in a combination with a mixed co-catalyst $\text{Rh}_{2-y}\text{Cr}_y\text{O}_3$, exhibited a QY of 6% at 420–440 nm [244]. The co-catalyst was produced in situ via the photocatalytic reduction of KCrO_4 over a $(\text{Ga}_{1-x}\text{Zn}_x)(\text{N}_{1-x}\text{O}_x)/\text{Rh}$ composite that, in turn, was synthesized by the photocatalytic deposition of Rh NPs [245]. A layer of chromium oxide on the metal surface prevents reverse reactions between H_2 and O_2 allowing the $(\text{Ga}_{1-x}\text{Zn}_x)(\text{N}_{1-x}\text{O}_x)/\text{Rh}_{2-y}\text{Cr}_y\text{O}_3$ heterostructure to function as a photocatalyst of the total water splitting. Active co-catalysts for this system were also produced by the semiconductor impregnation with a mixture of rhodium salts and ruthenium carbonyl $\text{Ru}_3(\text{CO})_{12}$ followed by annealing [246–248]. The nitridation of a mixture of germanium and zinc oxides yields a compound $(\text{Zn}_{1+x}\text{Ge})(\text{N}_2\text{O}_x)$ that exhibits a photocatalytic activity in the water reduction under illumination with the visible light [249].

N-doping of indium oxide narrows its band gap from 3.5 to 2.0 eV and imparts the semiconductor with a sensitivity to the visible light [250]. The photocurrent (proportional to the water reduction rate) generated under the Vis-illumination by the $\text{In}_2\text{O}_3:\text{N}$ electrode is by a factor of 2 higher than that for the undoped indium oxide, and by a factor of almost 50—than the photocurrent generated by a $\text{TiO}_2:\text{N}$ reference photoelectrode [250].

The photoelectrochemical hydrogen generation was realized in a system, where a TiO_2 NT array incorporated with Pt NPs acted as a cathode, while a photoanode

was formed by the carbon-doped TiO₂ NTs (Fig. 2.13b) [251]. The photoanode was produced by the sonoelectrochemical anodization of titanium foil in a mixture of NH₄F with ethylene glycol followed by the annealing in the H₂ atmosphere. The cell demonstrated a photocurrent QY of 8.5% [251].

By the calcination of titanate NTs at 600 °C in a CO stream, 8–42 mol% carbon can be introduced without the formation of a separate titanium carbide phase [252]. The fusion of O2p- and C2p-orbitals in the VB results in the bandgap shrinking to 2.2 eV and a corresponding expansion of the spectral sensitivity range. By combining the carbon-doped TiO₂ NTs (a photoanode) with Pt (a cathode) the Vis-light-driven water splitting to H₂ and O₂ was achieved [252, 253].

An alternative approach to the C-doped TiO₂ consists in the burning of Ti foils in the carbon-enriched flame [254, 255]. The carbon doping results in a bandgap reduction from 3.20 to 2.65 eV as well as in the formation of a filled sub-band 1.6 eV above the VB top. This material was tested as a photoanode for the photoelectrochemical water splitting and showed a QY of 13% under the illumination with “white” light in aqueous 5.0 M NaOH solution. The C-doping increases electrode surface porosity favoring additionally to the photoelectrochemical reaction [254, 255].

Sulfur-doped TiO₂ nanocrystals produced by a mechanochemical treatment of a mixture of titania with S₈ were used for the photoelectrochemical water splitting under the Vis-illumination [256]. The photocatalytic water reduction or oxidation (depending on the type of co-catalyst—Pt or IrO₂) under the Vis-illumination (420–480 nm) with the participation of indium-lanthanum oxysulfides was observed in [257].

2.5 Photocatalytic Systems Based on the Metal-Sulfide Semiconductors

Among the “solar” hydrogen production systems based on narrow-band-gap semiconductors a leading role is evidently played by metal-sulfide photocatalysts, mainly CdS, that is, however, photochemically unstable and liable to the photocorrosion. By this reason, a further development of the photocatalytic systems for the hydrogen production based on metal-sulfide semiconductors requires new methods of the photocorrosion mitigation. Also, a search is performed for new metal-sulfide materials that do not contain cadmium, lead, and other acutely toxic metals. Among the challenges in this field is also a search for new co-catalysts that do not contain precious platinum group/noble metals. New ways of photoactivity enhancement of the metal-sulfide semiconductors are constantly probed via a careful design of composite materials and harnessing of the quantum size effects inherent in the nanocrystalline metal-chalcogenide semiconductors.

The anti-corrosion stability can be achieved via a combination of metal-sulfide NPs with various photochemically passive carriers. For example, CdS NPs formed in the pores of zeolites were found to be photochemically stable when used as a

photocatalyst of the hydrogen evolution from water/alcohol mixtures [128, 258–263]. The photoactivity of such heterostructures depends considerably on the carrier structure and increases from zeolite L to SBA-15 to zeolite Y [258].

A combination of a high photocatalytic activity and photostability was observed for CdS NPs stabilized by the colloidal silica [264] and organic polymers [265, 266], as well as for CdS NPs deposited on the surface of carbon nanofibers [267], aluminium oxide [268], silica gels [269–271], and glasses [272, 273]. The glass-incorporated CdS NPs revealed a high photostability and can be used as visible-light-sensitive photocatalysts for the hydrogen evolution from aqueous H₂S solutions with a QY of 17–18% [272].

Interaction between cadmium(II) salts and polyvinylidene sulfide yields 5–30-nm CdS NPs regularly dispersed over the polymer surface [274]. Such composite exhibits photochemical stability and a high (up to 20%) QY of the hydrogen evolution from aqueous H₂S solutions.

The interest to nanocrystalline cadmium sulfide is greatly stimulated by a strong dependence of the electron properties of CdS NPs on the crystal size (d) at $d < 5$ –6 nm. A variation of the CdS NP size in this range is accompanied by pronounced changes of the optical and photochemical NP properties allowing for a tuning of the spectral sensitivity range and efficiency of the NP-based photocatalytic systems. This feature is excellently exemplified by the photocatalytic systems for the hydrogen production based on size-selected CdS NPs decorated with Pt NP co-catalyst [275]. The H₂ evolution QY decreases from around 17 to ~11%, as the CdS NP size increases from 2.8 to 4.6 nm. The dependence was interpreted in terms of a size-dependent driving force of photoinduced charge transfer from CdS to vacant states of Pt NPs (Fig. 2.14a). However, the photoactivity increase is counter-weighted by a “blue” shift of the absorption band edge of CdS NPs as their size is reduced (Fig. 2.14b), resulting in a partial loss of the solar light harvesting ability. To compensate for this detrimental effect, a double-chamber photocatalytic reactor was proposed [275], where shorter-wavelength light is absorbed selectively by smaller and more active 2.8-nm CdS NPs, while a longer-wavelength portion of the light passes through the first chamber and is absorbed in the second chamber by larger CdS NPs. In this way, a 50% increment of the H₂ evolution efficiency can be achieved for the double-chamber systems as compared with a single photocatalytic reactor with a mixture of smaller and larger CdS NPs [275].

Similarly to cadmium sulfide, a reduction in the size of MoS₂ NPs from 15–25 to ~5 nm was found to result in almost doubled photocatalytic activity in the H₂ evolution, both types of NPs being much active than bulk molybdenum sulfide [276].

Alternatively to CdS, bismuth, indium, iron, ruthenium, zirconium and silver sulfides, as well as related solid solutions can be used as water reduction photocatalysts. For example, RuS₂ NPs immobilized on thiol-modified polystyrene beads exhibited a photocatalytic activity in the hydrogen evolution from water/2-propanol [277].

The earth abundant pyrite FeS₂ was shown to be a suitable candidate for the Vis-light photo-electrochemical H₂ generation [278].

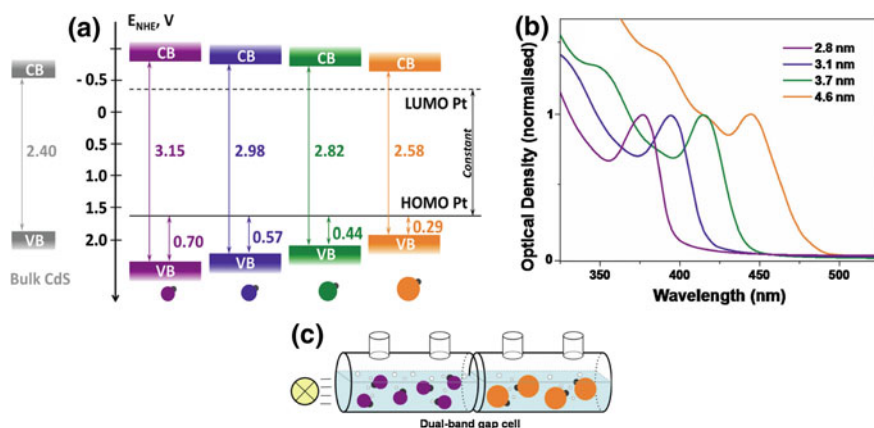


Fig. 2.14 Band diagram (a) and absorption spectra (b) of 2.8–4.6-nm CdS NPs; c a scheme of a dual photocatalytic reactor for the H_2 evolution. Reprinted with permissions from Ref. [275]. Copyright (2015) The Royal Society of Chemistry

A solvothermal synthesis of tin sulfide starting from Sn(II) salts yields a mixed SnS_2/SnS nanostructure with the intertwined tin(IV) and tin(II) sulfide layers. A lattice mismatch between the layers generates inherent sulfur vacancies resulting in a E_g narrowing by around 0.3 eV (to ~ 2 eV) as compared with pure SnS_2 [279]. Such composite showed an excellent activity in the H_2 evolution under illumination with a “blue” LED source (400–500 nm).

Layered zinc indium sulfide and its composites with metal NPs exhibited a photocatalytic activity in the Vis-light-driven H_2 evolution from aqueous $\text{Na}_2\text{S}/\text{Na}_2\text{SO}_3$ solutions [280–292]. The photoactivity of ZnIn_2S_4 was found to increase proportionally to the post-synthesis hydrothermal treatment duration as well as to the concentration of cetyltrimethyl ammonium bromide acting as a template. The dependence was assumed to originate from a deformation of the ZnIn_2S_4 crystal lattice resulting in a dipole moment in the semiconductor interlayer space that favors to the photogenerated charge carriers separation. The copper(II) doping of ZnIn_2S_4 expands its spectral sensitivity to around 800 nm, the maximal rate of photocatalytic hydrogen production registered at 0.5 wt.% copper content [293].

Good perspectives as Vis-sensitive photocatalysts of the water reduction could be envisaged for a number of ternary/multinary metal sulfides with a narrow band gap that suit perfectly as visible light harvesters and can potentially induce the water photodecomposition— CaIn_2S_4 with a band gap of 1.76 eV [294, 295], AgGaS_2 ($E_g = 2.48$ eV) [296], CuGaS_2 [297], $\text{CuIn}_{1-x}\text{Ga}_x\text{S}$ [298], $(\text{CuGa})_{1-x}\text{Zn}_{2x}\text{S}_2$ [299, 300], $\text{Zn}_{1-2x}(\text{CuGa})_x\text{Ga}_2\text{S}_4$ [301], Cu_3SnS_4 (1.38 eV) [302], and $\text{Cu}_2\text{ZnSnS}_4$ ($E_g = 1.75$ eV) [303–307]. Some of these materials were studied as nanocrystalline materials, while for others the effects of nano-scaling are still to be explored.

A photocatalytic activity in the hydrogen evolution from aqueous $\text{Na}_2\text{S}/\text{Na}_2\text{SO}_3$ solutions under the Vis-illumination was observed for mesoporous agglomerates of

CuInS₂ NPs ($E_g = 1.53$ eV) modified by Pt NPs [308], for CuIn₅S₈ [309] and CuIn_{0.7}Ga_{0.3}S₂ films [310], CuInS₂/NaInS₂ nanoheterostructures [311], (CuIn)_xZn_{2(1-x)}S₂ ($x = 0.01$ – 0.50) microspheres [312–317], non-stoichiometric Cu–In–Zn–S NPs attached to reduced graphene oxide (RGO) sheets [318], as well as for the nanocrystalline (CuAg)_xIn_{2x}Zn_{2(1-2x)}S₂ solid solutions [319–322]. The Vis-light sensitivity of these materials originates from a contribution of Cu3d- and S3p-orbitals into the VB and In5s5p- and Zn4s4p-orbitals—into the CB of mixed sulfide semiconductor.

Nanoporous ZnS–In₂S₃–Ag₂S solid solutions demonstrated a photocatalytic activity in the water reduction without additional co-catalysts [323]. Similarly, ternary sulfide AgInZn₇S₉ ($E_g = 2.3$ eV) is capable of the photocatalytic hydrogen evolution from water with no co-catalysts and electron donors present in the system [324]. When used together with Pt NPs and a sacrificial donor (Na₂S/Na₂SO₃), this quaternary photocatalyst showed an H₂ production QY of ~15%. CdIn₂S₄ NTs revealed the photocatalytic properties in the water reduction with no additional sacrificial donors with a QY of up to 17% [325]. A high photocatalytic activity in this process was also observed for ZnIn₂S₄/CdIn₂S₄ [326, 327], In₂S₃/ZnIn₂S₄ [328], and CdS/ZnIn₂S₄/RGO heterostructures [329]. A mixed sulfide AgIn₅S₈ ($E_g = 1.77$ eV) modified by Pt NPs was used as a Vis-sensitive photocatalyst of the hydrogen evolution from aqueous sulfide/sulfite solutions with a QY of 5.3% [330].

Various layered metal-sulfide nanomaterials, both in the form of nanometer grains and especially as a few-layer (single-layer) NSs are of a great potential for the solar H₂ production. For example, layered NaInS₂ ($E_g = 2.3$ eV) was found to be an efficient photocatalyst of the water reduction with a QY of 6% [331], while bulk indium sulfide remains inactive in this reaction. The 2.5-nm In₂S₃ NPs produced by ion exchange/sulfidation in the pores of titania-containing Ti-MCM-41 zeolite exhibited pronounced photocatalytic properties in the water reduction [332]. The activity stems from an efficient photoinduced electron transfer from In₂S₃ NPs to the zeolite host and inhibition of the subsequent electron-hole recombination.

First-principles calculations showed perspectives of single-layer and a-few-layer zirconium sulfide as a visible-light-sensitive photocatalyst ($E_g = 1.9$ – 2.0 eV) of the water splitting [333], though these predictions still require an experimental verification.

A comprehensive review of the photochemical water splitting on layered transition metal dichalcogenides (TMDs) can be found in [334]. The exfoliation of some of TMDs into single-layer sheets can result in a dramatic increase of the optical bandgap thus providing an additional driving force for the water splitting processes as illustrated in Fig. 2.15a for MoS₂. A band diagram, shown in Fig. 2.15b for a series of reported single-layer TMDs, provides a notion of possible candidates for the utilization in the photocatalytic/photoelectrochemical systems for the water splitting.

Ultra-thin sheets of MnSb₂S₄ with $E_g = 1.9$ eV and a thickness of 0.76 nm produced by the spontaneous thermal exfoliation of hydrazine-intercalated bulk materials revealed promising properties as a photocatalyst of the water reduction with a peak QY of 0.14% [335].

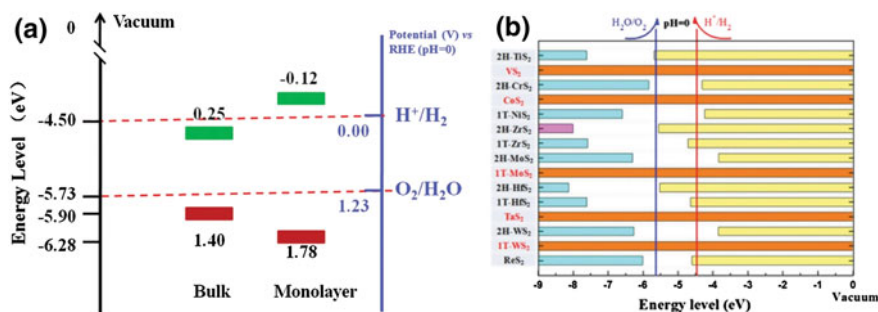


Fig. 2.15 **a** Energy diagram for bulk and single-layer MoS₂; **b** band edge positions of single-layer sulfide TMDs relative to the vacuum level, including the redox potentials for the H⁺/H₂ and O₂/H₂O couples at pH = 0. Reprinted with permissions from Ref. [334]. Copyright (2015) The Royal Society of Chemistry

The films of layered Bi₂S₃ with $E_g = 1.28$ eV produced by the electrodeposition can be used as an efficient and stable photocatalyst of the Vis-light-driven hydrogen evolution from aqueous Na₂S solutions [336]. In a similar photocatalytic system based on a Bi₂S₃/zeolite Y composite the QY of H₂ evolution reached 0.12% [337].

Mixed sulfides Cd_xZn_{1-x}S are typically capable of the photocatalytic water reduction without additional co-catalysts [338–341]. For these semiconductors, as a rule, a dome-shaped relationship between the photocatalyst composition (the parameter x) and the rate of hydrogen evolution is observed. Such dependence is quite non-trivial because both CB and VB potentials of Cd_xZn_{1-x}S solid solutions increase as the Cd is gradually substituted with Zn (Fig. 2.16) and, therefore, a monotonous dependence of the photocatalytic activity of cadmium-zinc sulfide crystals on their composition should be expected.

The exact position of the maximum on this relationship still remains controversial, most probably, due to differences in synthesis methods of Cd_xZn_{1-x}S solid solutions that can affect considerably their photochemical behavior. For example, it was found [338] that a maximal apparent QY of hydrogen evolution from aqueous sulfide/sulfite solutions, 10.2% at 420 nm, corresponds to $x = 0.8$. According to [339], the highest H₂ production QY with the participation of Cd_xZn_{1-x}S crystals can be observed in a range of $x = 0.25$ – 0.30 . Studies of the photocatalytic activity of cadmium-zinc sulfides precipitated on paper revealed two distinct photoactivity maxima corresponding to $x = 0.5$ and 0.2 [342]. The peak activity of Cd_xZn_{1-x}S microspheres produced by hydrothermal synthesis [343] was found at $x = 0.1$.

A detailed transient flash photolysis study [344] showed that a dependence between the capability of Cd_xZn_{1-x}S NPs to accumulate an excessive negative charge (photoinduced polarization of NPs) and the NP composition also has a dome-shaped character. The maximum position on this dependence corresponds to a maximum position on the dependence between the composition of Cd_xZn_{1-x}S NPs and the QY of hydrogen evolution (Fig. 2.17). Therefore, a direct relationship

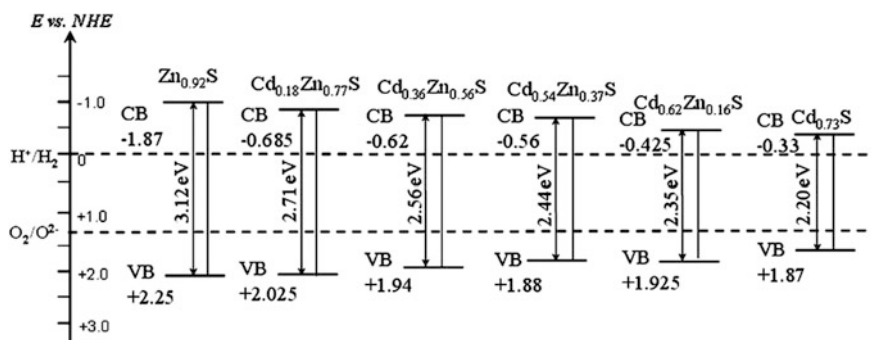


Fig. 2.16 CB and VB potentials of $\text{Cd}_x\text{Zn}_{1-x}\text{S}$ solid solutions with various Cd/Zn ratios. Reprinted with permissions from Ref. [8]. Copyright (2010) Elsevier

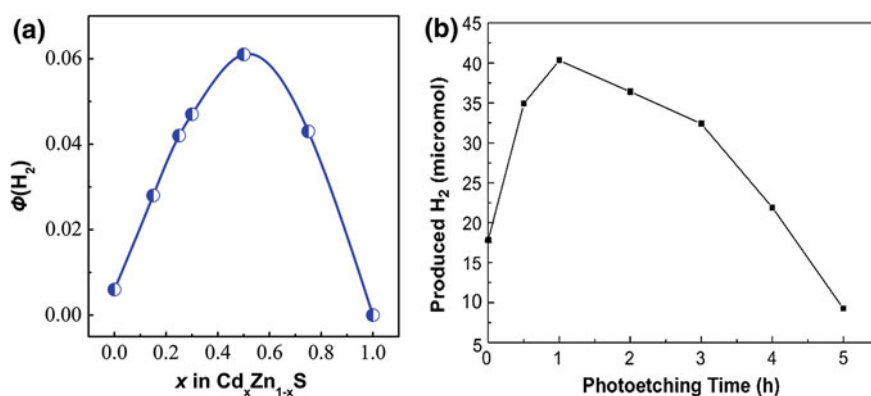


Fig. 2.17 **a** Dependence between the quantum yield $\Phi(\text{H}_2)$ of the photocatalytic H_2 evolution from aqueous Na_2SO_3 solution and the Cd molar fraction x in $\text{Cd}_x\text{Zn}_{1-x}\text{S}$ NPs. **b** Effect of the photoetching time of nanocrystalline Pt/CdS on the photocatalytic H_2 evolution rate. Reprinted and adapted with permission from Ref. [348]. Copyright (2008) Elsevier

between the photocatalytic activity of $\text{Cd}_x\text{Zn}_{1-x}\text{S}$ NPs and their electric capacitance can be concluded from these dependences.

The photocatalytic water reduction by electron donors was reported for more complex semiconductors based on cadmium-zinc sulfide, such as $\text{Cd}_{0.1}\text{Sn}_x\text{Zn}_{0.9-2x}\text{S}$ solid solutions [345]. The compound with $x = 0.01$ exhibited a 1.5-fold higher photocatalytic activity than undoped $\text{Cd}_{0.1}\text{Zn}_{0.9}\text{S}$. Doping of $\text{Cd}_{0.5}\text{Zn}_{0.5}\text{S}$ with Bi^{III} increased considerably the QY of photocatalytic H_2 evolution from aqueous $\text{Na}_2\text{S}/\text{Na}_2\text{SO}_3$ solutions that reached $\sim 10\%$ at 0.1 mol% dopant [346].

Along with the stability issue, various strategies are probed to enhance the photoactivity of metal-sulfide narrow-bandgap semiconductors suitable for the solar water splitting. At that, the most fruitful approaches include using (i) loosely

aggregated nanocrystalline and mesoporous metal sulfides; (ii) biphasic nanocrystalline metal-sulfides and materials with a graded (gradient) composition; (iii) chemical/photochemical treatment of a nanocrystalline metal-sulfide aimed at the elimination of the surface defects/ligands; (iv) metal-sulfide NPs with an anisotropic shape; (v) composites with the water oxidation and reduction processes separated in space.

This list and selected examples given below provide a mere illustration of a variety of the possible ways of influencing/enhancing the photoactivity of metal-sulfide semiconductors. The attractiveness of the metal-sulfide photocatalytic systems for the solar H_2 production can be also enhanced by using broadly available raw materials and contaminants as sacrificial donors.

An ultrasound treatment of reaction mixtures during deposition of cadmium sulfide on the surface of aluminum and magnesium oxides favors to the formation of mesoporous CdS with an average pore diameter of 5.5 nm and a particle size of 4–6 nm [347]. Such materials exhibited a high photocatalytic activity in the hydrogen evolution from Na_2S/Na_2SO_3 solutions in the presence of Pt group metals with the catalytic activity of metals increasing from Rh to Pd to Pt.

The photocatalytic activity of nanocrystalline CdS can be boosted by a photochemical treatment in aqueous air-saturated solutions of formic acid [348]. The treatment decreases the NP size as a result of the oxidative photocorrosion. Simultaneously, the cleavage of a surface NP layer eliminates the surface defects participating in the electron-hole recombination and thus the overall photocatalytic activity of CdS NPs is increased by more than 2 times (Fig. 2.17b) [348].

A ligand shell on the surface of colloidal cadmium sulfide NPs is necessary to ensure the individual character of each NP and prevent their aggregation. However, the ligands even as small as MPA can present an obstacle for the photoinduced electron transfer to water molecules and inhibit the photocatalytic hydrogen evolution. As shown in [349], the CdS NPs “stripped” from the surface ligands and stabilized only by a surface charge reveal a two orders of magnitude higher photoactivity in the H_2 evolution from aqueous Na_2SO_3 solutions as compared to the MPA-capped NPs with the same NP size. The colloidal CdS NPs stabilized electrostatically by an outer shell of sulfide ions revealed a 8–9 times higher efficiency of the photocatalytic H_2 evolution from water/hydrazine mixtures than similar NPs capped with MPA [350].

Typically, different crystalline modifications of a semiconductor differ in the band energies and can be combined to produce heterostructures, where efficient separation of the photogenerated charge carriers becomes possible. The most well-known example of such a heterostructure is the commercially available nanocrystalline titania Evonik P25, consisting of 70–80% anatase and 20–30% rutile, that is extensively used as a benchmark photocatalyst for comparing the photoactivity of different (and not only oxide) semiconductor materials. The anatase and rutile have slightly offset CB potentials enabling a one-way migration of the photogenerated electrons from anatase to rutile.

Similar heterostructures can be composed of different-phase metal sulfide semiconductors. For example, cubic CdS NPs ($E_g = 2.6$ eV) can be deposited on

the surface of hexagonal microcrystalline cadmium sulfide with $E_g = 2.3$ eV [351]. The charge separation occurring in this system due to a difference in the CB positions imparts the composite with a high photocatalytic activity in the hydrogen evolution from aqueous sodium sulfite solutions. Similarly to the above-discussed CdS/TiO₂/Pt system [107], here also the co-catalyst localization plays an important role. The highest activity was observed for a composite produced by the photocatalytic deposition of Pt NPs on the microcrystalline CdS prior to the formation of a layer of cubic CdS NPs.

A dramatic acceleration (by around 500 times) of the photocatalytic H₂ production was observed after the deposition of a thin (~ 2.5 nm) shell of cubic CdS on the surface of hexagonal CdS NRs [352]. The concentric core/shell CdS NRs also exhibited unrivaled photostability and even the possibility of hydrogen evolution in aerobic conditions, indicating a very efficient spatial separation of H₂ and O₂ generation events on different locations of the photocatalyst surface.

Mixed-phase elongated Cd_xZn_{1-x}S NRs with thin hexagonal wurtzite layers “sandwiched” between thicker cubic zinc blend domains were reported to be an efficient hydrogen evolution photocatalyst [341]. The CB and VB edge offsets and an internal electric field existing in such heterostructures result in a directed flow of the photogenerated CB electrons from wurtzite (WZ) to zinc blend (ZB) and the VB holes—in the opposite direction (Fig. 2.18a). In this way, the water reduction and sulfite oxidation occur at different sites and the electron-hole recombination is efficiently suppressed without additional metal co-catalysts [341]. In the case of ZnIn₂S₄, the CB potential of a cubic modification (-1.5 V vs. NHE) is more negative than that of a hexagonal phase (-1.1 V vs. NHE) and thus, a combination of the ZB and WZ NPs results in a flow of the photogenerated electrons from the cubic to the hexagonal zinc indium sulfide phase [291]. As a result, the ZB/WZ ZnIn₂S₄ composite is a highly superior photocatalyst of the water reduction as compared to individual ZB and WZ phases (Fig. 2.18b).

A number of photochemically active metal chalcogenides can form solid solutions with almost ideally mixed components. As discussed above, cadmium and zinc sulfides form solid-solution compounds with the composition varying from pure CdS to pure ZnS via intermediate Cd_xZn_{1-x}S phases with intermixed metal cations and a joint S²⁻ sublattice. As Cd^{II} and Zn^{II} have a different reactivity to sulfide-ions and the sulfides of cadmium and zinc have a different solubility, it is possible, by properly adjusting the synthesis conditions, to form Cd_xZn_{1-x}S crystals with a gradient of cadmium or zinc concentration, for example, the crystals enriched with Cd^{II} on the surface.

The cadmium and zinc sulfide possess quite different bandgaps (2.4 and 3.8 eV for bulk cubic CdS and ZnS, respectively) and differ also in the CB and VB energies, the CB level changing from -0.8 V versus NHE for CdS to -1.8 V versus NHE for ZnS [8]. In a graded Cd_xZn_{1-x}S crystal with a Cd^{II}-enriched outer layer the CB potential on the crystal surface is, therefore, lower (closer to that of pure CdS) than in the bulk of the crystal, where it grows and shifts closer to the CB potential of pure ZnS. The CB level gradient directs the photogenerated electrons to the surface and prevents their recombination with the photogenerated VB holes.

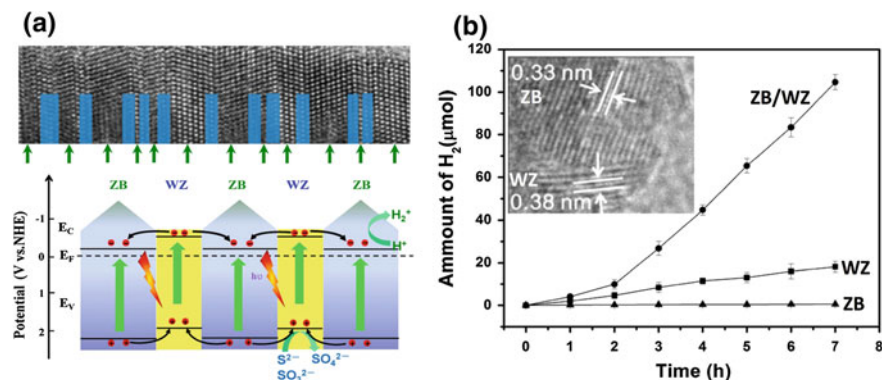


Fig. 2.18 **a** Upper panel: HRTEM image of a typical $\text{Cd}_x\text{Zn}_{1-x}\text{S}$ NR. The blue squares and green arrows index the segments of WZ and ZB structures. Lower panel: migration of charge carriers in $\text{Cd}_x\text{Zn}_{1-x}\text{S}$ ZB/WZ nanojunctions; **b** kinetic curves of the hydrogen evolution in the presence of sole ZB and WZ ZnIn_2S_4 as well as a ZB/WZ nanojunction. Insert: an HRTEM image of the ZB/WZ nanojunction. Reprinted and adapted with permissions from [341] (a) and [291] (b). Copyright (2016) American Chemical Society (a) and Elsevier (b)

This charge separation principle was realized for a $\text{Cd}_x\text{Zn}_{1-x}\text{S}/\text{SiO}_2$ heterostructure produced by the sulfurization of a graded $\text{Cd}_x\text{Zn}_{1-x}\text{O}/\text{SiO}_2$ composite [271]. The surface area of $\text{Cd}_x\text{Zn}_{1-x}\text{S}$ crystals can be cleaved layer by layer via the bombardment with heavy Ar^+ ions thus allowing to reveal with the XPS a graded structure of such crystals, the Cd to Zn molar ratio decreasing from ~ 1 to 2 on the surface to ~ 1 –3 in the bulk of the crystals (Fig. 2.19a).

The graded crystal structure favors to the directed flow of photogenerated CB electrons along a E_{CB} downfall, that is, toward the crystal surface, where they can react with water evolving gaseous hydrogen. Due to this effect, the graded $\text{Cd}_x\text{Zn}_{1-x}\text{S}/\text{SiO}_2$ heterostructure showed a high photocatalytic activity in the water

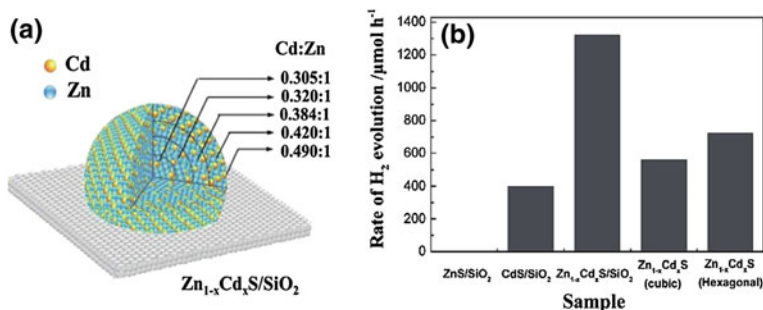


Fig. 2.19 **a** Illustration of a graded structure of $\text{Cd}_x\text{Zn}_{1-x}\text{S}$ crystals; **b** photocatalytic H_2 evolution activity of ZnS/SiO_2 , CdS/SiO_2 , $\text{Cd}_x\text{Zn}_{1-x}\text{S}/\text{SiO}_2$ and $\text{Cd}_x\text{Zn}_{1-x}\text{S}$ with different structures under the visible light irradiation. Reprinted and adapted with permissions from Ref. [271]. Copyright (2016) The Royal Society of Chemistry

reduction leaving behind both the individual sulfides and cubic/hexagonal $\text{Cd}_x\text{Zn}_{1-x}\text{S}$ NPs with a regular non-graded structure (Fig. 2.19b). The electron flow arriving on the crystal surface reduces undercoordinated surface cadmium species to Cd^0 that acts as a metal co-catalyst of the photoprocess and therefore, no additional co-catalyst is necessary [271].

The liability of metal-sulfide semiconductors to the photocorrosion can be used to transform the surface layer of the sulfide crystals into a metal oxide or a mixed oxide/sulfide composition with a tunable band structure. For example, the photolysis of ZnS microcrystals under 254-nm UV light at the ambient air pressure and moisture converts the surface layer of the microcrystals into a graded $\text{ZnS}_x\text{O}_{1-x}$ interface [353]. A combination of the surface etching with Auger spectroscopic probing revealed that the surface layer of such photochemically treated ZnS microcrystals is composed of a zinc oxysulfide solid solution NPs with the oxygen content decreasing from the surface to the crystal bulk (Fig. 2.20a). The graded region extends to 80–100 nm matching the depth of light penetration into the zinc sulfide microcrystals.

As the CB level of pure ZnO (~ -0.5 V vs. NHE at pH 7) is lower than the CB level of ZnS, the CB electrons photogenerated within the graded $\text{ZnS}_x\text{O}_{1-x}$ layer are directed toward the surface, where they can participate in the water reduction. Similarly to the case of $\text{Cd}_x\text{Zn}_{1-x}\text{S}$, this effect results in a drastic enhancement of the hydrogen evolution, that proceeds also without additional co-catalysts due to a partial reduction of surface Zn species to Zn^0 [353]. The photocatalytic activity of the photoproducted $\text{ZnS}_x\text{O}_{1-x}$ layer depends on the duration of photolysis (Fig. 2.20b), most probably, due to a balance between the thickness of oxidized

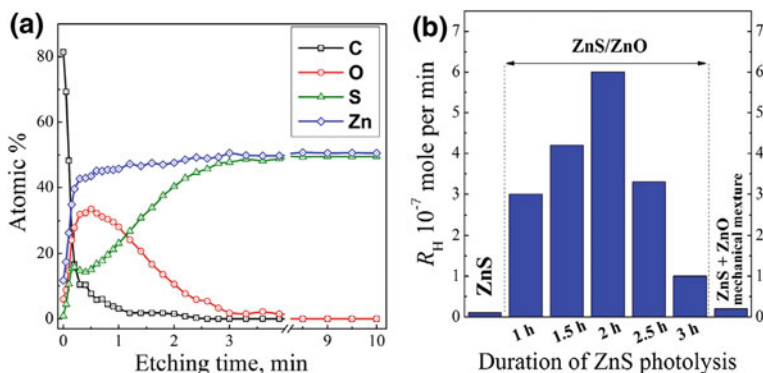


Fig. 2.20 **a** Distribution of Zn, S, C, and O atoms in the photolyzed single ZnS crystal derived from the Auger spectroscopic data. The etching time of 10 min roughly corresponds to a 100-nm etching depth. The signal of adventitious carbon stems from surface contaminations. **b** The rate of the photocatalytic H_2 evolution (R_H) from water/ethanol mixture under UV illumination ($\lambda > 320$ nm) in the presence of microcrystalline ZnS, $\text{ZnS}/\text{ZnS}_x\text{O}_{1-x}$ heterostructures produced by the photolysis and a mechanical mixture of ZnS and ZnO. Reprinted with permissions from Ref. [353]. Copyright (2016) Elsevier

layer and the light penetration depth, and supersedes by an order of magnitude the activity of a mechanical mixture of ZnS and ZnO of the same composition.

A photocatalytic activity increase can be achieved by using semiconductor crystals with an anisotropic (non-spheric) shape, where the charge migration rate is different depending on the crystal axis. For example, CdS NWs with a length of 3–4 μm and a diameter of 50 nm act as a more efficient photocatalyst of H_2 evolution from aqueous $\text{Na}_2\text{S}/\text{Na}_2\text{SO}_3$ solution than isotropic nanocrystalline CdS [354].

The commercial attractiveness of the photocatalytic systems for the hydrogen production based on the narrow-band-gap semiconductors can be enhanced by a cut in the costs of sacrificial donors. For example, a CdS/LaMnO₃ heterostructure can be used as a Vis-sensitive photocatalyst for the hydrogen production either from conventional sulfide/sulfide donors [355] or from the broadly available biomass [356]. The rate of hydrogen evolution from the biomass under the poly-chromatic illumination is comparable to that observed in the sulfide/sulfite/containing systems due to the presence of perfect donors—methanol and formic acid in the partially fermented biomass.

A special interest is evoked by the issue of the utilization of various industrial wastes as sacrificial donors for the water reduction. This approach can be illustrated by the photocatalytic hydrogen evolution from hydrogen sulfide solutions in ethanolamine and other aliphatic amines in the presence of CdS/Pt nanoheterostructures [357]. Such solutions are abundantly produced as wastes of the carbon and natural gas industries as well as in the technologies of crude oil desulfurization. The amines readily dissolve hydrogen sulfide and favor its ionization and proton release that can be reduced to the molecular hydrogen. At the same time, a high solubility of polysulfide anions as products of the S^{2-} oxidation promotes desorption of S_x^{2-} from the photocatalyst surface and prohibits reverse reactions between polysulfide and the photogenerated CB electrons.

The sulfide-capped colloidal CdS NPs were found to be an excellent photocatalyst of H_2 evolution by using aqueous hydrazine as a sacrificial electron donor [350]. The hydrazine contains 12 wt.% of hydrogen and is considered as a promising liquid hydrogen carrier with N_2 as a sole product of the oxidative decomposition.

2.6 Emerging Semiconductor Photocatalysts for the Solar Hydrogen Production

A constant search for new photocatalysts of the water splitting is currently under way. Each new compound emerging within the focus of attention of possible photocatalytic applications is typically tested as a hydrogen evolution photocatalyst. The emerging photocatalysts are of exceedingly broad scope making almost impossible their rigorous classification, the most trend-making of them being new narrow-bandgap semiconductors with a lattice formed by metal ions and oxygen (oxides, metallates,

etc.), metal-chalcogenide semiconductors, carbonaceous species like graphitic carbon nitride and carbon nanoparticles, and metal-organic frameworks.

Some of the new semiconductor photocatalysts can be referred to as “exotic” because they have only recently entered the attention spotlight of the photocatalysis community and only a little is known about the potential and perspectives of such materials. The following subsection provides an account of the photocatalytic hydrogen evolution systems based on the semiconductor materials that can be currently characterized as “emerging” photocatalysts.

Photocatalysts with a chalcogenide lattice. The examples of hydrogen-evolving photocatalysts with a chalcogenide-based lattice are confined mostly to the above-discussed sulfide semiconductors because metal selenide and telluride semiconductors have typically too low bandgaps to induce the water reduction/oxidation reactions and reveal an unacceptably low photostability even in the presence of sacrificial electron donors.

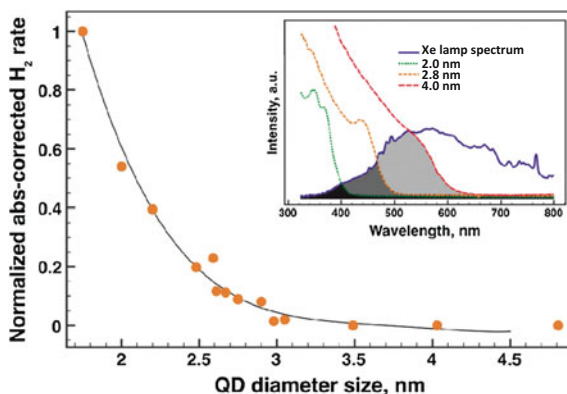
The photocatalytic hydrogen evolution from sulfide/sulfite solutions under the Vis-illumination of CdSe nanobelts [358] was a rare example of the photochemical activity of cadmium selenide and, probably, the first evidence of its capability to induce the water reduction. Later, size dependences of the photocatalytic activity of CdSe NPs in the water reduction were reported [359, 360]. The bandgap of CdSe NPs is broadened considerably as the NP size decreases from 3.1 to ~ 1.8 nm due to the QSEs resulting in a steep growth of the photocatalytic activity with a NP size reduction (Fig. 2.21a). No activity is typically observed for the CdSe NPs larger than 3–4 nm.

As the size of CdSe NPs is reduced, a strong “blue” shift of the NP absorption band edge is observed (Fig. 2.21a, insert) resulting in a drastic loss of visible light harvesting capability. Nevertheless, smaller CdSe NPs still reveal a high photocatalytic activity (when the H_2 evolution rate is normalized to the light absorbance) as a result of a larger driving force of the CB electron transfer to water molecules [361]. This example again illustrates that a reasonable trade-off between the light harvesting capacity and the CB energy should be maintained for the quantum-sized semiconductor NPs to attain the maximal QY of the solar hydrogen production [359, 360]. Also, the control of surface chemistry of the nanocrystalline CdSe plays a crucial role in the photocatalytic water reduction. For example, passivation of the surface defects of CdSe NRs tipped with Pt NPs with an atomically-thick CdS layer increases the H_2 production rate by a factor of 6–7 [362].

Nanocrystalline CdSe was used as a light-harvesting material in a photoanode designed for the water oxidation to O_2 with the hydrogen evolution occurring on a counter electrode [363]. The cadmium selenide was protected against the corrosion/photocorrosion by a sputtered layer of metallic cobalt that was partially converted into a water oxidation co-catalyst— $CoPO_4$ by the oxidative etching in a phosphate buffer [363].

The reported assortment of other (Cd-free) metal selenide photocatalysts of water reduction is apparently limited to the nanocrystalline $\gamma\text{-In}_2\text{Se}_3$ (a Pt NP co-catalyst, TEA as a sacrificial donor, $E_g \sim 1.6$ eV) [364].

Fig. 2.21 a The absorption-corrected rate of the photocatalytic H_2 evolution with the participation of size-selected CdSe NPs. Insert: absorption spectra of 2.0–4.0 nm CdSe NPs overlapped with a typical spectrum of a Xe lamp (used for the simulation of the solar spectrum). Reprinted and adapted with permissions from Ref. [359]. Copyright (2012) The Royal Society of Chemistry



Photocatalysts with oxygen-containing lattice. A broad range of various visible-light-sensitive oxides, both stoichiometric and mixed-valence, as well as numerous metallates (ferrites, aluminates, cuprates, stannates, borates, etc.) can be used as photocatalysts of the solar H_2 production in the bulk and nanocrystalline forms. Among these compounds a special attention was paid to layered perovskites (tantallates, niobates, titanates, ferrites, etc.) used as bulk materials, NPs, NRs, nanofibers, hollow spheres, etc. and exhibiting a lucrative combination of a high stability and activity in the hydrogen evolution.

The $CuGa_2O_4$ and $CuGa_{2-x}Fe_xO_4$ spinels were recently introduced as Vis-sensitive photocatalysts of the H_2 evolution from aqueous H_2S solutions in the presence of a NiO/RuO_2 co-catalyst [365]. A photocatalytic activity in the hydrogen evolution from aqueous sulfide/sulfite solutions was observed for $CuLaO_2$ ($E_g = 2.33$ eV) modified with the photodeposited Pt NPs [366], as well as for $CuLaO_{2.62}$ [367] and $CuAlO_2$ [368].

Ultra-thin (~ 3 nm) tin niobate NSs produced by the hydrothermal exfoliation of thicker 2D $SnNb_2O_6$ particles showed a remarkable photocatalytic activity in the visible-light-driven water reduction, which is 4 and 14 times higher than the activity of the 50-nm thick particles and bulk niobate, respectively [369].

Nanocrystals of $CuFe_2O_4$ and $ZnFe_2O_4$ [370, 371] were successfully tested as photocatalysts of the water reduction under the illumination with the visible light. The photocatalytic properties in similar systems were reported for MnO_2 [372], Ga_2O_3 [373], NiO [374], Sn_3O_4 [375], nanocrystalline $LaFeO_3$ [376, 377] and $LaMg_xTa_{1-x}O_{1+3x}N_{2-3x}$ ($x \geq 1/3$) perovskites [378], nanoparticles of $SrSnO_3$ [379] and $MnCo_2O_4$ [380], copper borate [381], a family of M_2BiSbO_7 ($M = Ga, Fe, Gd$) [382], as well as for $ZnAg_3SbO_4$ [383]. Also, a number of new UV-light-sensitive semiconductor photocatalysts for the water reduction was reported in recent years, such as titanium phosphate [384], gallium borate [385], Zn_2GeO_4 [386, 387], $LaCO_3OH$ [388], Sm_2GaTaO_7 [389], that can potentially be sensitized by molecular dyes and narrow-band-gap semiconductor NPs.

A new family of In-based photocatalysts of the water reduction under the Vis-illumination [370] includes InVO_4 ($E_g = 1.9$ eV), InNbO_4 ($E_g = 2.5$ eV), and InTaO_4 ($E_g = 2.6$ eV). Differences in the band gap among these compounds originate from a contribution of the V3d-, Nb4d- and Ta5d-orbitals in the respective CB positions. Mesoporous InVO_4 produced by a template synthesis exhibited a higher photocatalytic activity in the hydrogen evolution than the non-porous nanocrystalline indium vanadate [390].

A recently reported series of homologous compounds $\text{Zn}_x\text{In}_2\text{O}_{3+x}$ ($x = 4, 5$, or 7) showed a unique combination of a strong light harvesting capability with a high mobility of the photogenerated charge carriers [391]. A layered structure of such compounds comprised of light-absorbing $\text{Zn}(\text{In})\text{O}_{4(5)}$ layers alternated with InO_6 layers provides abundant charge collection sites and transport channels (Fig. 2.22a). An enhanced sensitivity of these compounds to the visible light as compared to individual ZnO and In_2O_3 (Fig. 2.22b) originates from a hybridization between the $\text{O}2p$ and $\text{In}4d$ orbitals in the $\text{Zn}(\text{In})\text{O}_{4(5)}$ layers resulting in an upward shift of the VB edge and a reduced bandgap (2.57–2.67 eV depending on x) [391]. Under the full-spectrum illumination the mixed compounds revealed an almost 5-fold higher photocatalytic activity in the water reduction than the parent zinc and indium(III) oxides (Fig. 2.22c).

Photocathodic production of solar hydrogen. In conventional photoelectrochemical systems for the solar hydrogen production a visible-light-sensitive semiconductor/heterostructure attached to a conductive substrate acts as a photoanode. The light-excited photoanode oxidizes water or a sacrificial donor present in the electrolyte and injects a photogenerated electron into the conductive substrate-collector, that transfers it to an outer electrical circuit. Afterward, the electrons come to a cathode, where the water reduction to molecular hydrogen takes place. In such a system, the reduction and oxidation half-reactions are separated in space and the H_2 evolution efficiency is determined by the catalytic properties of the cathode and the photoactivity of the anode responsible for the donor oxidation.

In recent years, alternative photoelectrochemical systems emerged where the target reaction—the water reduction to H_2 takes place as a direct consequence of the light absorption by a photocathode, while the photogenerated VB holes are transferred into the electric circuit to a counter anode, where the water oxidation and O_2 evolution occur. An account of the current progress in this field can be found in [392].

The assortment of semiconductor materials suitable for the photocathode applications is rather limited, because they should comply with a set of rigorous requirements, in particular, the sensitivity to the visible light (that is, have a relatively narrow enough bandgap) and a high conduction band potential, that is, E_{CB} negative enough to induce the water reduction (Fig. 2.23) [392]. Also, a photocathode should be coupled with an appropriate oxygen-evolving electrocatalyst to ensure the cyclic performance of the photoelectrochemical system and the efficient regeneration of the photocathode.

As compared to the photoanodes comprised typically of n-type semiconductors and prone to the photocorrosion, the photocathodes usually use p-type conducting

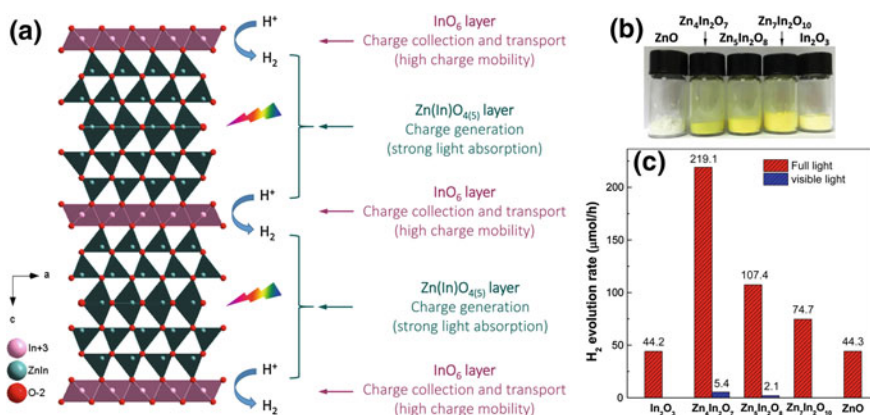
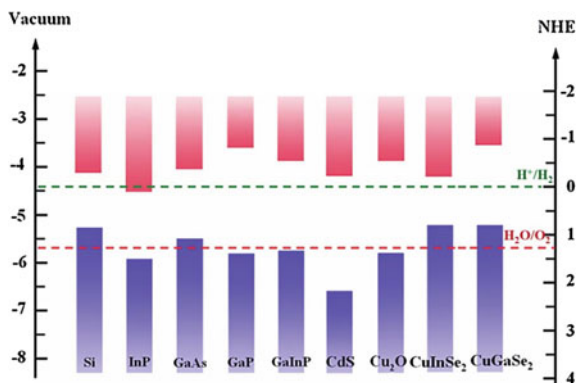


Fig. 2.22 **a** Schematic representation of a $\text{Zn}_4\text{In}_2\text{O}_7$ photocatalyst with different functional parts; **b** photographs of mixed zinc indates and pure zinc and indium oxides; **c** the average photocatalytic hydrogen production rate under the full range irradiation ($\lambda \geq 250 \text{ nm}$) and the visible light irradiation ($\lambda \geq 420 \text{ nm}$). Reprinted with permissions from Ref. [391]. Copyright (2016) Americal Chemical Society

Fig. 2.23 Band edge positions of several typical photocathodic semiconductor materials. Reprinted with permissions from Ref. [392]. Copyright (2015) The Royal Society of Chemistry



semiconductor materials that appear much more stable toward the photocorrosion provided that the photogenerated electrons are efficiently transferred to water molecules.

Copper oxides are very promising visible-light-sensitive materials for the photocathodes of the hydrogen-evolving photoelectrochemical systems [393]. To achieve efficient light harvesting with copper oxides it is suggested to use Cu_2O (CuO) NW arrays rather than conventional planar semiconductor electrodes [393, 394]. A mixed $\text{Cu}_2\text{O}/\text{CuO}$ heterostructure can be easily sensitized with a layer of copper sulfide via the ion exchange reaction and additionally decorated with a Pt NP co-catalyst exhibiting quite spectacular 3.6% efficiency of the solar light conversion [395]. The reduced graphene oxide (RGO) was found to be an efficient

co-catalyst for 1D Cu_2O photocathodes and a promising candidate to replace the conventional noble metal co-catalysts [394].

Another promising and stable photocathode material is nickel oxide. As NiO has a weak absorbance in the visible spectral range it can be coupled with other robust and strongly-absorbing semiconductors, for example, graphitic carbon nitride. Due to a band edge offset in the NiO/GCN heterostructure, the nickel oxide layer accepts the photogenerated VB holes from GCN while the CB electrons of GCN reduce water to H_2 [396]. A similar cascade hole transfer from GCN to a p-type semiconductor is observed in a GCN/ CoSe_2 composite attached to the top of a Si microwire array photocathode [397].

As Fig. 2.23 shows, silicon can also be utilized as a photocathode material for the solar hydrogen production. The Si photocathodes are typically designed as NW arrays [397–400] that can be additionally decorated with other semiconductors [397, 399] and metal co-catalysts (Pt) [399], and covered with a titania layer to protect the photocathode from the photocorrosion [399]. The activity of silicon can be boosted by making porous photocathodes with a highly developed surface area from Si NPs [401]. Amorphous silicon coupled to a triple Ni–Mo–Zn alloy as a hydrogen evolution catalyst and a Co-containing water oxidation catalyst forms a photoelectrochemical cell for the hydrogen evolution with a QY of 4.7% under the 1 Sun illumination [402].

The visible-light-induced H_2 evolution was observed on a photocathode formed by the CuInS_2 nanodisks grown epitaxially on cubic Au NPs (Fig. 2.24a) [403] coupled to a Pt counter-electrode. The water reduction process was assumed to involve both the photogenerated CB electrons of CuInS_2 and the “hot” electrons injected into the semiconductor from the plasmon-excited Au NP seeds. A search into other possible ternary/quaternary narrow-bandgap metal-chalcogenide materials for the H_2 -evolving photocathodes is still performed resulting in ever more complex and highly tunable compositions, like Cu–In–Ga–Se–S [404] and Zn–Cu–In–Ga–Se [405].

A combination of a photocathode and a photoactive anode allows constructing a water splitting system functioning without any externally applied bias. For example, a titania oxygen-evolving photoanode can be combined with a hydrogen-evolving photocathode comprised of the visible-light-sensitive composite of Zn phthalocyanine and fullerene C_{60} decorated with Pt NPs (Fig. 2.24b) [406].

A photoelectrochemical system for the H_2 evolution with no external bias was assembled from a CuGaS_2 /RGO photocathode and a $\text{BiVO}_4/\text{CoO}_x$ photoanode [297]. The RGO layer was deposited by the direct photocatalytic reduction of graphene oxide on the surface of CuGaS_2 photocathode enhancing dramatically its photoresponse to the visible light.

New “exotic” inorganic photocatalysts. Some new photocatalysts for water reduction were recently reported that can be referred to as “exotic” because of their quite rare (or otherwise unreported) photoactivity in the redox-processes. Many of such new compounds were only tested as bulk (microcrystalline) powders to date, but are nevertheless discussed here because a strong enhancement of the

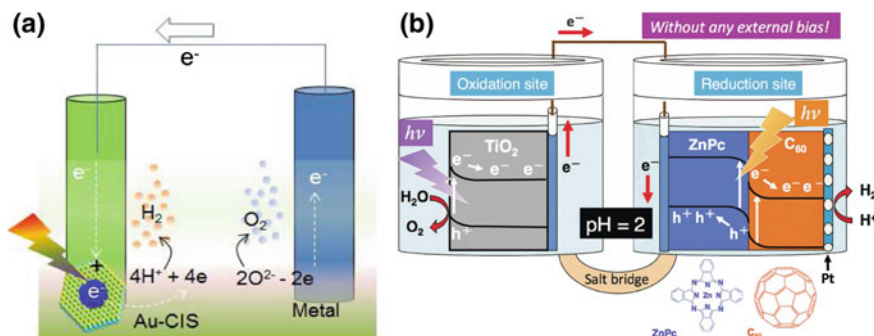


Fig. 2.24 Schemes of the photoelectrochemical water splitting using Au/CuInS₂ (a) and Zn^{II} phthalocyanine (ZnPc)/fullerene C₆₀/Pt (b) heterostructured photocathodes. Reprinted with permissions from Refs. [403] (a) and [406]. Copyright (2016) American Chemical Society (a) and The Royal Society of Chemistry (b)

photocatalytic activity can be anticipated for such compounds in the nanocrystalline state thus posing a challenge for further studies.

For example, a recently discovered fibrous modification of the red phosphorus was reported to have photocatalytic properties in the water reduction [407]. The photoactivity of such materials can be enhanced considerably by decreasing the crystal dimensions via the growth restriction on the silica fibers or by an ultrasound treatment of the bulk material [407]. The red P was reported to have the CB potential around -0.25 V versus NHE at pH 0 which is sufficient for the water reduction, while the VB holes ($E_{\text{VB}} > 1.5$ eV) can oxidize either water or a broad range of sacrificial electron donors [408].

A community of rare photocatalysts of hydrogen evolution was recently joined by silicon carbide [409–414] capable of the water reduction even in the absence of sacrificial donors, as well as by gallium nitride with a CB potential by 0.5 V more negative than the water reduction potential [415]. Such difference appeared to be sufficient to overcome the hydrogen evolution overvoltage and produce H₂ from aqueous solutions of methanol and Na₂S/Na₂SO₃ under the Vis-illumination without additional co-catalysts.

Iron silicide β -FeSi₂ revealed a photocatalytic activity in the hydrogen evolution from aqueous dithionite solutions even under the illumination with the near-IR light [416]. A Vis-sensitive photocatalyst of the H₂ evolution from aqueous solutions of formic acid was prepared via the deposition of Pt NPs on the surface of polycrystalline Si [417]. The photocatalytic water reduction was also observed for macroporous silicon [418], mesoporous Si coupled to a noble-metal-free non-stoichiometric cobalt phosphate co-catalyst [419], and Si nanowires loaded with an iron phosphite co-catalyst [420].

Layered siloxene NSs (Fig. 2.25a) produced by a topotactical transformation of calcium silicide in water revealed photocatalytic properties in the water reduction without additional co-catalysts and sacrificial electron donors [421]. The siloxene is

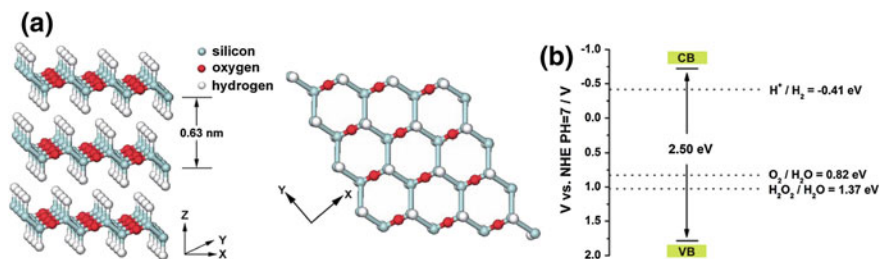


Fig. 2.25 A schematic molecular structure (a) and band structure (b) of siloxene. Reprinted and adapted with permissions from Ref. [421]. Copyright (2016) The Royal Society of Chemistry

a direct bandgap semiconductor with a strong visible light harvesting capability and a suitable bandgap of 2.5 eV. The position of both CB and VB bands of the siloxene are respectively negative and positive enough for both water reduction and oxidation to occur on the photocatalyst surface under the photoexcitation with the visible light (Fig. 2.25b) [421].

Iron silicide was reported to be able to evolve hydrogen from aqueous solutions of sodium dithionite even when illuminated with the NIR light [416]. It is a unique semiconductor material because it combines a narrow band gap of 0.8 eV with a CB position of around -0.65 V (vs. NHE) which is unprecedentedly high for such a narrow-bandgap material. Titanium disilicide is a narrow-bandgap semiconductor that can harvest light over the entire visible spectral range and serve as a stable photocatalyst for the hydrogen production without additional sacrificial donors [422].

Carbon NPs. Carbon NPs (CNPs) have recently shown a high promise for applications concerning with the light emission and absorption, including the photocatalytic solar light harvesting [169, 170]. The CNPs can be synthesized quite easily by the thermal decomposition of a single or mixed organic precursor at 200–300 °C. The structure of CNPs is still a subject of discussions, as numerous XPS studies showed them to contain simultaneously aliphatic sp^3 -hybridized and aromatic sp^2 -hybridized carbon, sometimes also the amine- and pyridine-like nitrogen. The surface of CNPs is typically decorated with hydroxyl and carboxyl groups. The CNPs are often called carbon quantum dots (QDs), however, the usage of this term seems not to be justified as no information on the possibility and character of QSEs is available for CNPs.

The CNPs can emit bright and broadband PL in the visible spectral range with a broad gamut—from blue to red, the fact determining the perspectives of the CNPs for luminescent bio-labeling. Similarly to the exact internal structure of the CNPs, the PL origins and mechanisms are also a subject of vivid discussions. A special class of CNPs is constituted by graphene quantum dots, that is, small pieces of graphene functionalized with oxygen-containing groups and N dopants that reveal a strong dependence of the spectral properties on their lateral size [169, 170].

The synthesis of CNPs typically requires very simple and available precursors making them an excellent candidate for the mass-scale photocatalytic applications.

For example, the carboxylate-terminated 2–3-nm CNPs can be produced via the pyrolysis of sodium salt of ethylenediaminetetraacetic acid (EDTA) at 350 °C. The CNPs can be then coupled to Pt NPs and the CNP/Pt heterostructure and used as an efficient visible-light-sensitive photocatalyst of the H₂ evolution from aqueous solutions of dihydronicotinamide adenine dinucleotide (NaDH) which is a convenient electron/proton sources frequently used in a biochemical research practice [423].

The CNPs produced by a hydrothermal treatment of flower pollens was successfully used to sensitize GCN NSs, the GCN/CNPs assembly evolving hydrogen under the illumination with the visible light from methanol/water mixtures with a Pt NP co-catalyst [424].

Pure CNPs produced from multi-wall carbon NTs were found to possess the capability of reducing water to hydrogen in water/methanol mixtures without additional co-catalysts [425]. In the presence of Pt NPs, the CNPs revealed a superior photoactivity as compared with the nanocrystalline TiO₂ Evonik P25.

The electrochemical etching of graphite electrodes is another convenient method of the CNPs production yielding stable suspensions of 4–5-nm CNPs. Such NPs are crystalline with a lattice regularity of 0.321 nm typical for the parental graphite indicating the CNPs to be small fragments of graphite stabilized by an outer shell of functional groups (mostly COOH as revealed by the XPS) [426]. The CNPs can be coupled with layered MoS₂ into a material with a pronounced photoelectrochemical activity in the water reduction process [427].

The scalable and benign carbonization of vegetable raw materials (such as spinach, peas, and others) was reported to produce CNPs capable of strong adsorption on the surface of nanocrystalline titania [428]. The CNPs/TiO₂ composites were tested as a photocatalyst of the hydrogen evolution from methanol/water mixtures.

Graphitic carbon nitride. The graphitic carbon nitride is probably one of the first artificially synthesized organic polymers but it emerged only relatively recently as a universal and visible-light sensitive photocatalyst with brilliant perspectives in the domains of the solar energy harvesting and the environmental photocatalysis [429–433].

Similarly to graphite, GCN is formed by planar infinite single layers that have an aromatic character and are stacked by the van-der-Waals forces ($\pi\pi$ -interactions) with an interplanar distance of around 0.34 nm. The term “carbon nitride” does not reflect exactly the structure of single layers as they are composed of heptazine (tris-s-triazine) heterocycles bounded through tertial amine N atoms into an infinite network with an intra-network periodicity of around 0.68 nm.

Two alternative structures of the single layer carbon nitride (SLCN) are proposed, one describing its as a regular net-like polyheptazine (Fig. 2.26a), the other postulating that a SLCN is composed on infinite 2D polyheptazine ribbons bound together by numerous hydrogen bonds (Fig. 2.26b) [429–435]. The exact structure of SLCN still remains a subject of discussion, however, the second structure seems to be more realistic. It can be seen that the term “carbon nitride” is only a convenient approximation to describe the stacked multilayer polyheptazine structure

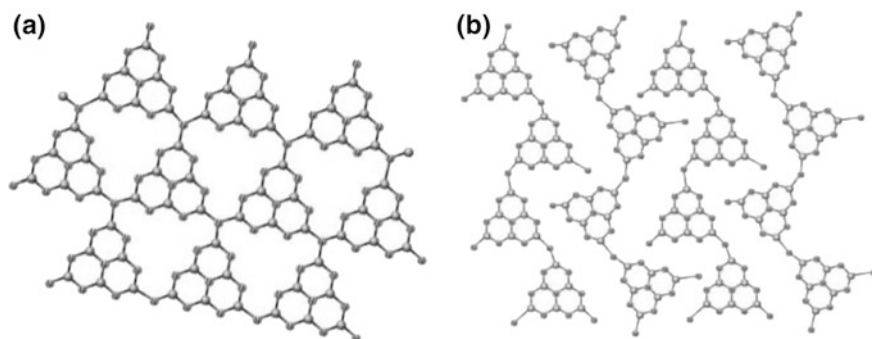


Fig. 2.26 Alternative models of the single layer carbon nitride structure. Reprinted with permissions from Ref. [435]. Copyright (2014) American Chemical Society

because the composition of the bulk undoped material is close C_3N_4 , however, this term does not reflect the exact chemical nature of this material, though used broadly by the historical reasons and convenience.

GCN is a direct bandgap semiconductor with the VB and CB formed respectively by filled and vacant $C2p$ and $N2p$ orbitals. The bandgap of bulk GCN is around 2.7 eV and can vary by 0.1–0.2 eV as a result of differences in the synthesis, possible adventitious doping, and structural defects and, therefore, GCN absorbs the UV and a portion of the visible light in a range of $\lambda < 460$ nm. Also, the GCN has a very “suitable” position of both CB and VB levels that are respectively negative and positive enough to allow the photogenerated charge carriers to participate in a variety of redox-processes, including the reduction and oxidation of water [429, 431–434]. Reported data on the exact position of CB and VB levels of GCN reveal some scatter, most probably due to the above-mentioned differences in the synthesis nuances and structural imperfection and, most often, can be found at around -1.0 and $+1.7$ V versus NHE [431–433].

The GCN has comparatively high thermal, chemical and photochemical stability as well as a low toxicity that distinguish this material from other inorganic semiconductors with similar E_g , E_{CB} and E_{VB} parameters. The bulk GCN can be produced in copious amounts from a variety of affordable precursors, such as melamine (1, 3, 5-triaminotriazine), dicyandiamide, and urea by the thermal treatment at 400–600 °C. By introducing various heteroatomic additives GCN can be doped with P, S, B etc. on the stage of the material formation [436]. Alternatively, the GCN can be annealed or treated with aggressive oxidizing/reducing agents after the synthesis to vary the C/N ratio and thus to modify its spectral and photochemical properties [429, 431–434, 436]. Various supramolecular assemblies of triazine derivatives with other carbocyclic and heterocycles compounds can be used for the synthesis of GCN with tailored electron properties, for example with an increased hydrophobicity or a more extended aromatic system [436–439]. By performing the thermal condensation of precursors in the presence of templates the GCN can be produced as porous solids. Finally, similarly to graphite, GCN can be exfoliated to form

a-few-layer and single-layer moieties or, alternatively, subjected to a partial cleavage to produce GCN NPs.

A comprehensive account on the photocatalytic systems for hydrogen evolution and other processes based on GCN can be found in reviews [430–432, 436, 440].

The compact GCN has a relatively low specific surface area of 5–15 m²/g thus limiting the efficiency of the charge carrier transfer from the photoexcited GCN to other components of the photocatalytic system. To increase the GCN surface area various “hard” (for example silica NPs [182, 441, 442]) and “soft” (organic polymers [443], sucrose [444]) templates are used resulting in the mesoporous GCN samples active in the photocatalytic H₂ evolution.

Using of uniform SiO₂ micro-beads as a hard template allows producing hollow GCN spheres with a wall thickness of around 50 nm and an inner void of several hundred nm in diameter [182, 442] (Fig. 2.27a). The wall can then be modified with a co-catalyst, like layered MoS₂ [442] or Pt NPs [182] as well as with a sensitizer, for example, CdS NPs [182], forming a complex photocatalyst for the solar hydrogen evolution. The “hollow sphere” architecture is favorable for the photocatalytic process as the co-catalyst is typically localized on the outer walls and thus the water reduction/water oxidation half-reactions can be spatially separated. Also, the hollow spheres (HSs) are well known for the ability of a more efficient light harvesting as a result of multiple light scattering in the inner voids of the spheres.

Alternatively, the GCN can be grafted to the developed surface of a photochemically inert carrier, such as mesoporous [445] and macroporous silica [446] or a zeolite [447, 448].

As in the case of inorganic semiconductor photocatalysts of the water reduction, GCN typically requires a co-catalyst to efficiently evolve hydrogen. For example, metal NP (Pt [444, 449–451], Au [91, 92], Cu [452], Ni [453]) and alloys (Au–Pt [448], Ni–Pt [454]) co-catalysts can be attached to the GCN surface or formed in situ by the chemical/photochemical deposition. Similarly to titania, GCN can be coupled with Au NPs to form plasmonic photocatalysts for the H₂ production [91, 92]. GCN can interact with MoS₂ NSs [442, 455, 456], RGO [457], and multiwall

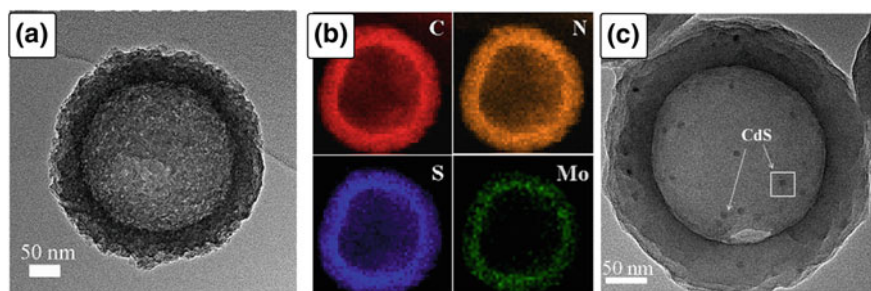


Fig. 2.27 TEM image (a) and EDX element mapping (b) of a GCN hollow sphere decorated with MoS₂ nanosheets. c TEM image of a CdS-decorated GCN hollow sphere. Reprinted with permissions from Refs. [442] (a) and [182] (b). Copyright (2015–2016) Elsevier

carbon NTs [458–460] via the $\pi\pi$ interactions forming visible-light-sensitive layered “dyads” for the hydrogen production. The assortment of sacrificial donors that can be applied in the GCN-based systems for H_2 evolution is also quite broad [436] including traditional TEA [449–451, 453], carbon acids [448], hydrazine [454], and Na_2S/Na_2SO_3 [180].

Similarly to other wide-bandgap semiconductors that can harvest only a part of the visible spectrum, GCN can be sensitized to longer wavelengths by organic dyes and narrower-bandgap semiconductor NPs. The interactions between organic dyes and GCN are especially strong due to the possibility of a multiple bonding between a dye and GCN via functional (carboxyl) groups present of the edges and outer planes of the GCN particles and via the $\pi\pi$ -stacking between the extensive aromatic systems of the dye and outer sheets of the multilayer GCN particles. In this way, visible/NIR-light-sensitive photocatalysts for the H_2 evolution were produced by coupling GCN with eosin Y [461, 462], erythrosin B [463], thiazole orange [464], and Zn phthalocyanines (an apparent QY of around 3% was observed at 730 nm) [62].

As GCN has a band structure similar to that of cadmium sulfide it can be introduced into various binary heterostructures with inorganic semiconductors, where offsets between the CB and VB edges of the components favor to an efficient spatial separation of the photogenerated charge carriers [436]. For example, the photocatalytic activity of TiO_2 NRs increases by an order of magnitude after the decoration with GCN NSs [179].

A large variety of oxide/metallate semiconductor photocatalysts can be produced by a solvothermal treatment in supercritical conditions. Introduction of GCN into the reaction mixtures offers a surface for the nucleation/deposition of oxide semiconductors and typically results in a decreased crystal size as compared to the conventional solvothermal synthesis. In this way, the heterostructures of GCN with C,N-doped TiO_2 [183], $CuFe_2O_4$ [449], CdS [180, 465], $ZnIn_2S_4$ [181] were produced with an enhanced photocatalytic activity in the H_2 evolution as compared to both individual GCN and the inorganic component.

A prolonged thermal treatment of GCN at 550–650 °C can also generate numerous lattice defects (“pinholes”) as a result of the residual ammonia elimination and splitting of the intra-layer bonds. The distortion of single layers results also in the expansion of the GCN and a partial exfoliation to NSs [466]. The formation of point defects, new surface edges and reduction in the GCN particles thickness typically result in an increase of the photocatalytic activity of this material in the water reduction [466].

The ultrasound-assisted exfoliation of bulk GCN in 2-propanol produces 2-nm thick NSs revealing an enhanced photocatalytic activity in the solar hydrogen production as compared to the compact g- C_3N_4 [467]. The exfoliation of GCN can be facilitated by the preliminary intercalation with sulfuric acid [468] in this case leading to the predominant (around 60 mass%) formation of SLCN. The SLCN showed a 3-times higher photoactivity than the non-treated GCN.

The GCN nanoribbons around 2 μm in length, ~ 200 nm in width and 3 nm thick were produced by “chemical scissors”, that is by the treatment with a mixture of concentrated HNO_3/H_2SO_4 [469]. The molar C/N ratio decreases to ~ 0.63

versus 0.76 for the stoichiometric C_3N_4 indicating the formation of carbon vacancies that can act as charge traps retarding the electron-hole recombination. As a result, the nanoribboned GCN showed a 20 times higher photocatalytic activity in the H_2 evolution as compared to the starting bulk material [469].

GCN can be effectively disintegrated by adding water to the bulk GCN mixed with the concentrated H_2SO_4 due to a strong exothermic effect (Fig. 2.28a) [450]. Following ultrasound-assisted exfoliation produces 2–3-nm thick NSs exhibiting a much higher photocatalytic activity in the H_2 evolution from aqueous TEA solutions (Fig. 2.28b) [450].

Atomically thin carbon nitride nanomeshes can be produced by the solvothermal exfoliation of mesoporous GCN intercalated with 2-propanol [451]. Along with a highly developed surface area, the holey SLCN revealed a higher bandgap of 2.75 eV (as compared to 2.59 eV for the starting material) and a CB level by ~ 0.5 eV more negative than that of mesoporous GCN. Due to these favorable factors, the SLCN nanomeshes showed an apparent QY of the H_2 production of 5.1% at $\lambda > 420$ nm, which is the highest reported for the exfoliated carbon nitrides [451].

Alternatively to the conventional polyheptazine-based GCN, formed by polyheptazine networks, a special attention is currently brought to polytriazine networks that can be produced by versatile synthetic approaches and additionally doped to obtain visible-light-harvesting photocatalysts of the hydrogen production [470–474].

Metal-organic frameworks (MOFs). The metal-organic frameworks can also be rated as an “emerging star” of the semiconductor photocatalysis with a number of reports on various redox-processes catalyzed by the photoexcited MOFs increasing drastically in recent years [475, 476]. MOFs are formed by metal-organic complex units linked by “bridge” bi- or tri-functional ligands into the 2D/3D continuous networks. Typical bridge ligands for the construction of the 2D and 3D frameworks are aromatic bi- and tri-carboxylic acids. MOFs combine a high light sensitivity with an almost unlimited versatility of possible building blocks and substituents that can alter/modify the MOF structure in a desirable manner. High-intensity ligand-to-metal (metal-to-ligand) electron transitions impart them with a strong

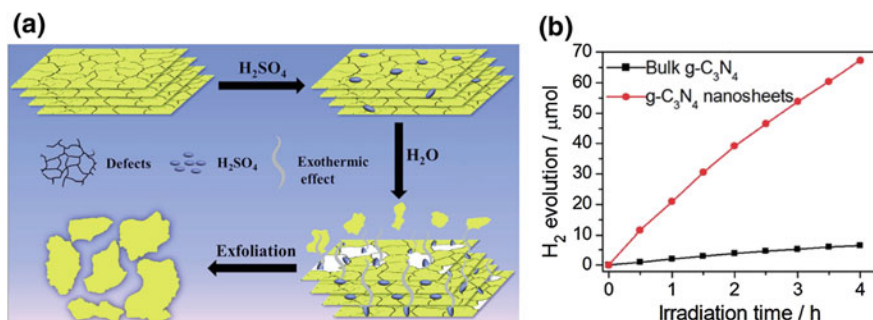


Fig. 2.28 **a** Schematic illustration of the GCN disintegration and exfoliation with H_2O/H_2SO_4 ; **b** kinetic curves of the H_2 evolution over the bulk and nanosheet GCN. Reprinted and adapted with permissions from Ref. [450]. Copyright (2015) The Royal Society of Chemistry

light harvesting capability, while the 2D/3D networks are favorable for the directed charge transport and form a system of regular pores that can be accessed by the water and sacrificial donors. The current state-of-the-art in the photocatalytic applications of MOFs is highlighted by comprehensive reviews [475, 476].

Similarly to the photocatalysis with inorganic semiconductors, no definite models were proposed allowing to predict a photocatalytic activity for a given MOF or a class of MOFs and therefore the quest for new photoactive MOFs is performed mostly empirically. As with photoactive inorganic semiconductors, there is a “club” of selected MOFs exhibiting a high photocatalytic activity and by this reason appearing most frequently in the researchers’ spotlight.

One of such MOFs is UiO-66 formed by ZrO_6 octahedra linked with p-dibenzoic acid and its derivatives (Fig. 2.29a) [477–480]. The UiO-66-type MOFs combine regular 3D porous structure, a high stability and sensitivity to the visible light. The introduction of functionalities into the bridge molecules opens a way of affecting the pore characteristics.

For example, 3 nm Pt NPs can be introduced into the inner voids of UiO-66- NH_2 MOF acting as a co-catalyst of the photocatalytic water reduction [480]. Such MOF/Pt heterostructure reveals a much higher photoactivity as compared to an analog with Pt NPs attached to the outer surface of the MOF grains. A spectral response of the UiO-66 MOF can be extended by the sensitization with dyes [483], CdS NPs [481, 482] and $\text{Cd}_x\text{Zn}_{1-x}\text{S}$ NPs [484]. After modification with RGO, a CdS/UiO-66 assembly becomes a much more active photocatalyst of the H_2 production from aqueous $\text{Na}_2\text{S}/\text{Na}_2\text{SO}_3$ solutions as compared with the “classical” TiO_2/CdS heterostructure (Fig. 2.29a).

Similar 3D structures can be assembled using oxo-zirconium units with a tetracarboxylate-derived zinc porphyrine ZnTCPP (Fig. 2.30) [482]. The MOF contains a relatively large inner channel where a hydrogenase-biomimetic metal-organic co-catalyst can be placed. The assembly shows a photocatalytic activity in the solar H_2 production from the aqueous ascorbic acid solutions [482].

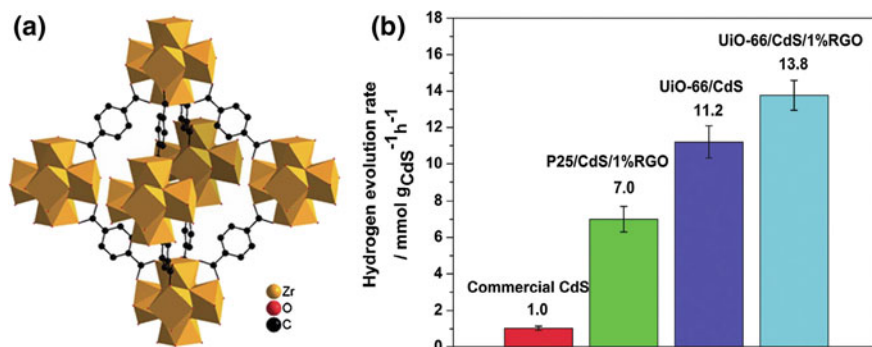


Fig. 2.29 **a** Schematic structure of UiO-66 MOF; **b** rate of the H_2 evolution using various photocatalysts. Reprinted with permissions from Refs. [483] (a) and [479] (b). Copyright (2014–2015) The Royal Society of Chemistry

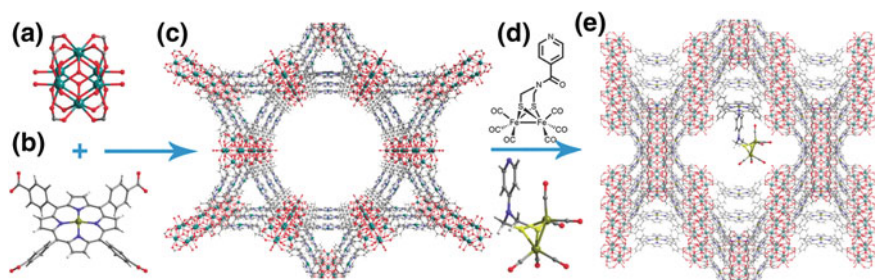


Fig. 2.30 **a** Structural building units of $\text{Zr}_6\text{O}_8(\text{CO}_2)_8(\text{H}_2\text{O})_8$, and **b** structural building unit of ZnTCPP. **c** Model MOF structure. **d** Structure of the co-catalyst. **e** Model structure of the MOF/co-catalyst assembly. Color scheme: Zr, green; Zn, dark gray; C, light gray; O, red; N, blue; Fe, light green; S, yellow. Reprinted with permissions from Ref. [484]. Copyright (2014) The Royal Society of Chemistry

A key step in the photoprocess is a charge transfer from the singlet excited state of Zn porphyrinate bridges to the incorporated co-catalyst, where the subsequent proton reduction occurs.

A popular family of photoactive MOFs includes a number of MIL-100 complexes formed by various central ions and tricarboxylic acids (like 1,3,5-benzenetricarboxylic acid) [484, 485].

A Fe^{3+} -based MIL-100 has a broad spectral response in the visible range and can be used as a photocatalyst of the H_2 evolution from water/ CH_3OH mixtures enhanced by the additional deposition of Pt NPs [484]. A La^{3+} -based 3D MOF is a wide-bandgap compound with $E_g = 3.7$ eV that can be sensitized to the visible light by CdSe NPs [485]. The MOFs with a high sensitivity to the visible light and photocatalytic activity in the H_2 evolution can be produced by using derivatives of azo-dyes [486] and rhodamines [487] as bridge ligands.

Another face of the application of MOFs in the photocatalysis is in using them as precursors for the preparation of highly dispersed visible-light-sensitive H_2 -evolving materials, for example, C,H-doped iron oxides [488].

2.7 New-Generation Co-Catalysts for the Photocatalytic Hydrogen Production

The most reported semiconductor-based photocatalytic systems for the hydrogen production contain obligatorily a co-catalyst, typically, a noble metal (Pt, Pd, Rh) that is characterized by a much lower water reduction over-voltage as compared with the semiconductor photocatalysts. The co-catalyst accepts the photogenerated CB electrons from the photocatalyst and then participates in the water/protons reduction, atomic hydrogen accumulation and recombination to the molecular hydrogen. In the photoelectrocatalytic systems where the photoexcitation of a

semiconductor anode results in the oxidation of water with simultaneous hydrogen evolution on a counter electrode the photoanode is typically coupled with appropriate oxygen evolution catalysts [489–491].

Recent studies showed that the “conventional” noble metal co-catalysts can be successfully substituted with much less expensive and more available compounds, in particular, iron group metal NPs [492], molybdenum sulfide [426, 455, 456, 493–504], oxide [505], and nitride [506], nickel oxide [507, 508] and hydroxide [408, 509], nickel sulfide [510, 511], nitride [512] and phosphide [513], tungsten carbide [514], as well as with cobalt oxide [515, 516], phosphate [176], and phosphide [517]. For example, in the CdS-based systems, the introduction of mere 0.2 wt.% MoS₂ results in a rather drastic 36-fold increase of the rate of photocatalytic hydrogen evolution from aqueous lactic acid solutions [493]. The catalytic activity of MoS₂ in the water reduction is typically associated with an efficient charge carriers separation between CdS and MoS₂, as well as with a well-known capability of molybdenum disulfide to the hydrogen activation.

The catalytic activity of MoS₂ can be boosted by the exfoliation of bulk layered material into single or a-few-layer NSs [502, 518]. As the layers of bulk MoS₂ are kept together by relatively weak van-der-Waals forces the exfoliation can be achieved by a conventional ultrasound treatment. The sonication of bulk MoS₂ in the presence of CdS NRs results in a composite photocatalyst of the H₂ evolution from aqueous lactic acid solutions that is far more active than bare CdS NRs or a mechanical NR mixture with unexfoliated molybdenum disulfide (Fig. 2.31a) [502].

Apart from the most stable semiconducting 2H-phase of MoS₂, it can form an allotropic 1T modification that is characterized by the metallic conductance. The exfoliation of 1T-MoS₂ was found to produce an even more efficient co-catalyst of the hydrogen evolution for the CdS NR photocatalyst, than conventional exfoliated 2H-MoS₂ [503] (Fig. 2.31b).

A similar catalytic activity in the H₂ evolution in the presence of nanoparticulate CdS was observed for ultrathin composite cobalt selenide/reduced graphene oxide NSs that revealed a half-metallic character [519].

The in situ photodeposition of Ni, Co, or Cu NPs on the surface of Cd_{0.4}Zn_{0.6}S resulted in a 5-fold acceleration of photocatalytic hydrogen evolution from aqueous Na₂S/Na₂SO₃ solutions [492]. The modification of nanocrystalline Cd_{0.2}Zn_{0.8}S with 3 wt.% CuS increases strongly the photocatalytic water reduction QY up to ~37% at $\lambda = 420$ nm [520]. The catalytic properties of copper sulfide were also observed in a photocatalytic hydrogen production system based on a visible-light-sensitive CuO/Al₂O₃ composite [521]. Nickel sulfide can act as a co-catalyst of the photocatalytic water reduction on the nanocrystalline CdS [522, 523], Cd_{0.5}Zn_{0.5}S [524], and a ZnS_{1-x-0.5y}O_x(OH)_y/ZnO heterostructure [525]. Cobalt sulfide revealed a catalytic activity in the photocatalytic water reduction on GCN [526].

Nickel phosphide Ni₂P NPs were proven to act as a “universal” co-catalyst of the hydrogen evolution for a broad range of semiconductor photocatalysts including TiO₂, CdS and GCN (Fig. 2.31c) and different sacrificial agents, such as lactic acid, TEA, and methanol [527].

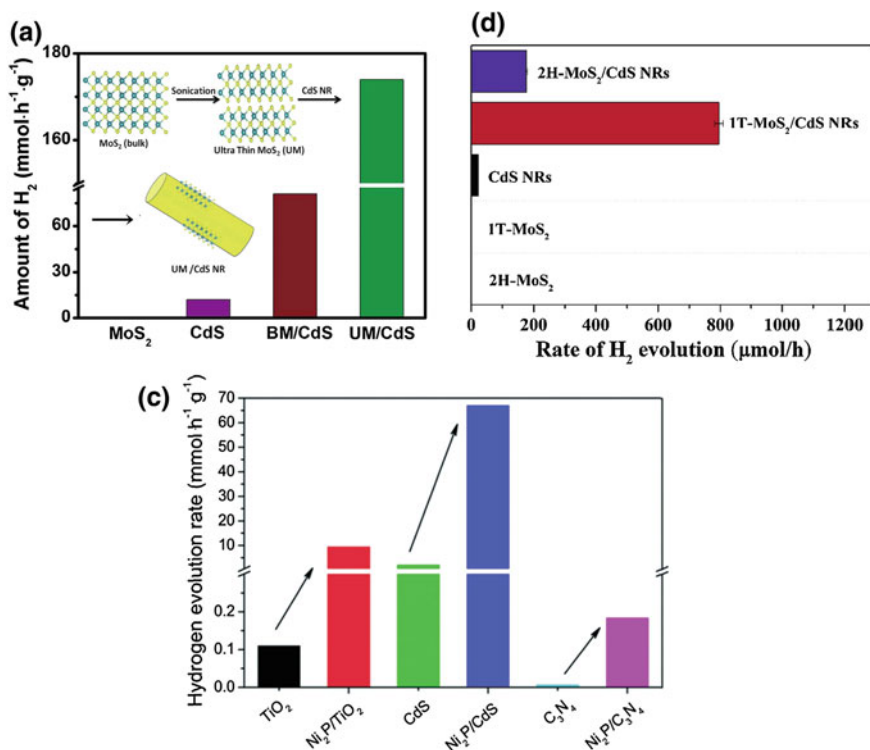


Fig. 2.31 **a, b** Rate of the photocatalytic hydrogen production in the presence of CdS NRs, a mechanical mixture of bulk 2H-MoS₂ (BM) and CdS NRs and a composite of CdS NRs with ultrathin 2H-MoS₂ NSs (UM) and 1T-MoS₂ NSs produced by the sonication. **c** Rate of the photocatalytic H₂ production from aqueous solutions of sacrificial donors with the participation of nanocrystalline TiO₂, CdS, GCN and their composites with Ni₂P NPs. Reprinted with permission from Refs. [502] (a), [503] (b), and [527] (c). Copyright (2016) The Royal Society of Chemistry

Various biological molecules, for example, hydrogenase [63, 528] as well as iron complexes mimicking an active center of the hydrogenase [482, 529], have also good perspectives as co-catalysts in the photocatalytic systems for the H₂ generation. A recent account on the hybrid artificial photosynthesis systems based on the semiconductor light harvesters and biomimetic metal-complex co-catalysts can be found in [530].

The reduced graphene oxide is often used as a hydrogen evolution co-catalyst, however, it can play other unique roles, such, for example, as a conductive 2D “mat” for assembling of various components of a photocatalytic system [531]. GO is typically produced by the ultrasound-assisted exfoliation of layered graphite oxide which, in turn, can be obtained by treating graphite with strong oxidizing agents such as KMnO₄/H₂SO₄ or KClO₃/HNO₃. The single (or a-few-layer) GO derived by the exfoliation can then be reduced by a variety of agents, like NaBH₄ and hydrazine, or via a photochemical/electrochemical/microwave treatment [531].

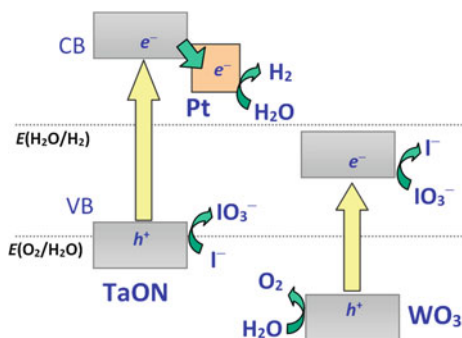
RGO bears residual functional groups such as $-\text{COH}$ and $-\text{COOH}$ that can interact with semiconductor NPs and metals bringing them together on the surface of RGO NSs. At the same time, the RGO sheets typically possess a good conductivity close to that of pristine graphite. Thus RGO enables a good electric contact among the components of a photocatalytic system that are assembled but spatially separated on the 2D RGO mat. The intermediary role of RGO NSs ensuring the electric contact between spatially separated semiconductor and metal NPs was observed for $\text{TiO}_2/\text{RGO}/\text{Ag}$ [532] and $\text{TiSi}_2/\text{RGO}/\text{RuO}_2$ [422]. Thiolated RGO NSs can strongly interact both with CdS NPs and dendritic Pt nanocrystals assembling them into a photocatalytic system for the hydrogen production from aqueous lactic acid solutions [533].

RGO can also substitute noble metal co-catalysts revealing in some cases an appealing catalytic activity for the hydrogen generation. For example, the rate of hydrogen evolution in binary TiO_2 NS/RGO NS heterostructure is more than 40 times higher than for the individual titania [534]. A catalytic effect of RGO was also observed in the photocatalytic H_2 evolution systems based on nanocrystalline CdS [500, 535, 536], Zn-doped CIS NPs [500], ZnIn_2S_4 [292], Cu_2O [537], CaIn_2O_4 [538], BiPO_4 [539], Bi_2WO_6 [540], $\text{K}_4\text{Nb}_6\text{O}_{17}$ [541], and GCN [457].

2.8 Stoichiometric Water Splitting Under the Illumination with the Visible Light

One of the conditions for the successful total water splitting consists in the spatial separation of the water reduction and water oxidation processes necessary to prevent reverse reactions between hydrogen and oxygen [2]. This challenge is typically addressed by using two separate electrode cells connected with a membrane. In the first cell the water reduction proceeds at the expense of a mediator oxidation, then the oxidized mediator diffuses through the membrane into the second cell where it participates in the water oxidation to O_2 (Fig. 2.32).

Fig. 2.32 Scheme of a photocatalytic system for total water splitting based on tantalum oxynitride, tungsten oxide and I^-/IO_3^- mediator couple



Such coupled systems are often compared to the Z-scheme of the natural photosynthesis [2, 137, 187–189, 542, 543]. The scheme is very convenient as it allows to design separately the cathode and anode cells and then combine them by an appropriate redox-pair, for example, $\text{Fe}^{3+}/\text{Fe}^{2+}$ or I^-/IO_3^- . The photocatalytic hydrogen evolution can occur on the surface of SrTiO_3/Pt doped with $\text{Cr}^{3+}/\text{Ta}^{5+}$ at the expense of the iodide ions oxidation to IO_3^- . The oxygen is evolved in a complementary cell with the regeneration of I^- on the surface of a WO_3/Pt heterostructure. Such system showed an apparent QY of around 0.1% at 420 nm [544, 545]. In the same manner, a hydrogen evolution cell based on a visible-light-sensitive GaInP_2/Pt composite was coupled with an oxygen evolution cell based on AgCl sensitized with silver bromide [546].

A number of cathode/anode cells connected by the iodide/iodate mediator was proposed, for example $\text{TiO}_2(\text{anatase})/\text{Pt}$ (H_2 evolution)— $\text{TiO}_2(\text{rutile})/\text{Pt}$ (O_2 evolution) [547], TaON/Pt (H_2 evolution)— WO_3/Pt (O_2 evolution) [548], $\text{ATaO}_2\text{N}/\text{Pt}$, $\text{A} = \text{Ca, Sr, Ba}$ (H_2)— WO_3/Pt (O_2) [549], TaON/Pt (H_2)— TaON-RuO_2 (O_2) [550], $\text{TaON}/\text{ZrO}_2/\text{Pt,Ru}$ (H_2)— WO_3/Pt (O_2) [241], sensitized layered $\text{H}_4\text{Nb}_6\text{O}_{17}/\text{Pt}$ (H_2)— WO_3/Pt (O_2) [551], BiVO_4 (H_2)—Rh-doped SrTiO_3/Ru (O_2) [198, 552], $\text{BaZrO}_3/\text{BaTaO}_2\text{N}$ (H_2)— WO_3/TiO_x (O_2) [553]. In the most part of such systems, the selective water oxidation takes place as a result of efficient IO_3^- adsorption on the semiconductor surface despite the presence of a large excess of I^- [547].

In a cell, where the photocatalytic water reduction occurs on the surface of rhodium-doped SrTiO_3/Pt and the water oxidation proceeds with the participation of BiVO_4 , $\text{Fe}^{3+}/\text{Fe}^{2+}$ redox couple is used as a mediator [554, 555]. The system performs under the Vis-illumination ($\lambda < 500$ nm) with an apparent QY of 0.3% at 440 nm. The $\text{Fe}^{3+}/\text{Fe}^{2+}$ couple was also employed as an electron carrier in a total water splitting system based on Rh-doped SrTiO_3 and WO_3 [556].

Alternatively, the Z-scheme can be realized by combining an H_2 -evolving and an O_2 -evolving cell by a conducting bridge. For example, the RhCrO_x -loaded $\text{LaMg}_{1/3}\text{Ta}_{2/3}\text{O}_2\text{N}$ crystals, acting as an H_2 evolution photocatalyst can be combined with Mo-doped BiVO_4 crystals as an oxygen-evolving photocatalyst on a shared gold substrate (Fig. 2.33a) [557]. Both components are capable of absorbing the visible light. Such composite exhibits a 5-times higher photocatalytic activity in the water splitting than a combination of corresponding suspensions. The Au substrate acts as a transport layer enabling filling of the tantalate holes with the electrons photo-generated in bismuth vanadate [557].

A similar role of an electron mediator in a Z-scheme photocatalyst can be played by the photoreduced GO (Fig. 2.33b) [558]. As opposite to the RGO, produced by a conventional reduction with hydrazine, the photoreduced RGO showed a much more expressed hydrophilic character binding strongly both to an H_2 -evolving photocatalyst (Rh-doped SrTiO_3 decorated with Ru NPs) and to an O_2 -evolving photocatalyst (BiVO_4).

By using spatially organized semiconductor materials—NRs, NTs, layered substances, etc. a spatial separation of the water reduction and water oxidation sites can be achieved within a single photocatalyst, and in such a way a short-circuited

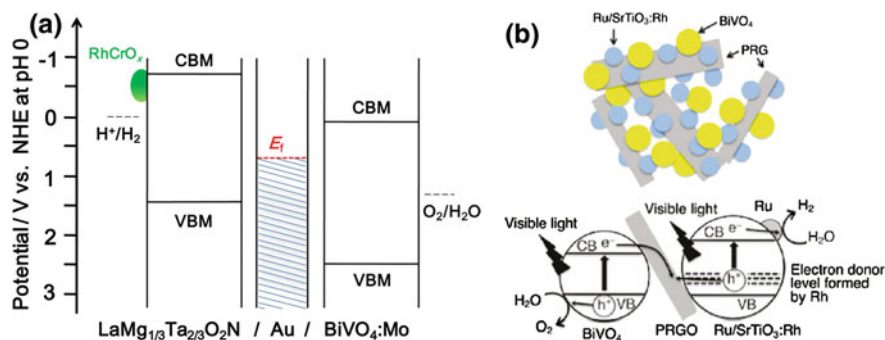


Fig. 2.33 **a** Schematic band diagram of the (RhCrO_x/LaMg_{1/3}Ta_{2/3}O₂N)/Au/BiVO₄:Mo photocatalyst; **b** scheme of the water splitting in a photocatalytic system based on Rh:SrTiO₃/Ru and BiVO₄ coupled via RGO sheets. Reprinted with permissions from Refs. [502] (a) and [558] (b). Copyright (2011, 2016) American Chemical Society

photo-electrochemical cell can be designed. For example, in a system based on a composite of titania NTs with Pt NPs [559, 560] the water reduction and oxidation half-reactions occur on different components—on Pt NPs and TiO₂ NTs, respectively, allowing to reach a water splitting QY of 0.6% [559]. In the case of a Ni/NiO_x/In_{0.9}Ni_{0.1}TaO₄ heterostructure, the co-catalyst (Ni/NiO_x) particles act as a hydrogen evolution cathode, while the surface of the Ni-doped indium tantalate—as an oxygen evolution anode [561]. A QY of the total water splitting in such system reached 0.66%. A separation of the cathodic and anodic water cleavage processes was also realized in the case of a composite photo-catalyst produced by the intercalation of Fe₂O₃ NPs into the interlayer voids of HTiNb(Ta)O₅ [562].

The hydrogen evolution and oxygen evolution processes become naturally separated in the case of two-sided nanocrystalline titania films produced by the magnetron sputtering with one side of the film decorated by Pt NPs. The photocatalytic hydrogen evolution from aqueous H₂SO₄ solution occurs on the TiO₂/Pt side of the film under the Vis-illumination, while on another side the water oxidation in the presence of NaOH takes place [221].

By oxidizing titanium foil in the presence of water vapors and NaF thin films of F-doped titania were prepared, exhibiting a photoelectrochemical activity in the total Vis-light-driven water splitting [563]. The photoelectrochemical water splitting under the Vis-illumination was also observed in the case of nanocrystalline TiO₂ films etched in HF solution [564] and was attributed to the formation of Vis-light-absorbing titanium oxyfluoride species on the film surface.

Along with the above-described complex systems where the spatial separation of cathodic and anodic processes is organized intentionally, alternative semiconductor compounds capable of simultaneous water oxidation and reduction under the Vis-excitation are explored continuously. One of the first “universal” photocatalysts of the kind was a solid solutions of gallium nitride and zinc oxide (Ga_{1-x}Zn_x)(N_{1-x}O_x) with E_g varying in a range of 2.58–2.76 eV. Gallium-zinc oxy-nitride exhibited a high

photochemical stability and, in the presence of RuO_2 , acted as a photocatalyst of the water splitting to H_2 and O_2 under the Vis-illumination [565]. A solid solution of bismuth and yttrium tungstates, BiYWO_6 ($E_g = 2.71$ eV) was also used as a total water splitting photocatalyst that showed an apparent QY of 0.17% at 420 nm in the presence of RuO_2 and $\text{Pt/Cr}_2\text{O}_3$ co-catalysts [566]. Porous films of BiVO_4 produced by the thermal decomposition of vanadium oxyacetyl acetate [567] and $\text{BiVO}_4/\text{Cu}_2\text{O}$ heterostructures [568] showed a photocatalytic activity in the water splitting under external bias [567]. The photoelectrochemical water splitting was realized on the surface of nanocrystalline hematite $\alpha\text{-Fe}_2\text{O}_3$ films synthesized by the thermal decomposition of ferrocene or iron pentacarbonyl [569, 570].

A visible-light-sensitive photoelectrochemical cell for the total water splitting was tested [571], where a Ru^{II} bipyridyl complex served simultaneously as an “antennae” and as a “bridge” connecting to the titania NPs via phosphate groups and simultaneously—to the IrO_2 NPs via COOH groups. The sensitizer photoexcitation results in the electron transfer through the following chain (Fig. 2.34): water molecules (water oxidation to O_2) \rightarrow IrO_2 NPs \rightarrow sensitizer \rightarrow TiO_2 NPs \rightarrow Pt cathode \rightarrow water molecules (water reduction to H_2).

Three new types of total water-splitting photocatalysts functioning under the UV and a portion of visible light were proposed in [572–574]: BiMnNbO_7 ($\text{M} = \text{Al}^{\text{III}}$, Ga^{III} , In^{III}), InMO_4 ($\text{M} = \text{Nb}^{\text{V}}$, Ta^{V}) and BiMO_4 ($\text{M} = \text{Nb}^{\text{V}}$, Ta^{V}) with E_g in a range of 2.4–2.7 eV. The photoactivity of the compounds increases considerably in the presence of NiO or Pt co-catalysts. The stoichiometric water splitting under the Vis-illumination was also observed in the presence of CaTaO_2N perovskite [575], complex solid solutions In-Ni-Ta-O-N [576] and Bi-Y-V-O [577], as well as gallium borate $\text{Ga}_4\text{B}_2\text{O}_9$ [385].

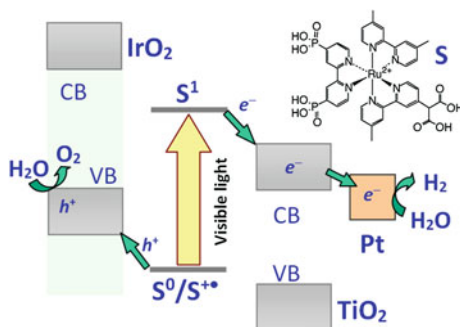
A feasibility of the photocatalytic decomposition of water confined in an inner volume of the single-wall carbon NTs was shown in [578]. Illumination of the NTs results in the evolution of a gaseous mixture with 80% hydrogen fraction.

Currently, studies are underway aimed at the search and development of new semiconductor materials capable of acting as photocatalysts of the stoichiometric water splitting, for example, GCN [579, 580], GCN/ TiO_2 nanoheterostructures [176], composites of the CNPs with BiVO_4 [581], etc.

Concluding the discussion of the large mass of experimental data on the photocatalytic systems for hydrogen production based on nanocrystalline semiconductor materials, we outline very generally the principal directions, where the highest efforts are currently applied and where a future progress could be expected.

New principles of functioning of the photocatalytic systems can open rich and unexpected directions of progress. For example, utilization of the quantum size effects allowed to create much more efficient systems for the solar water splitting based on conventional semiconductor materials, to design highly efficient nanoheterostructures based on the same materials but in different phase compositions and grain size, and to “invoke life” into some semiconductor materials that are passive in the bulk form but reveal pronounced photocatalytic properties in the

Fig. 2.34 Scheme of a photoelectrochemical system for the stoichiometric water splitting based on a heterostructure of Ti^{IV} and Ir^{IV} oxides and a visible-light-sensitive Ru^{II} complex (S). Details of the system—in [571]



water reduction/splitting when introduced in a nanocrystalline form. Also, the phenomenon of plasmonic photocatalysis is a vivid example of the new principle of light energy harvesting making a great impact on the development of semiconductor-based photocatalytic light-harvesting systems.

New photocatalysts should be continuously searched for, in particular, among the available and Earth-abundant materials. The example of graphitic carbon nitride, that was known since the middle of 19th century but discovered as an excellent photocatalyst only at the end of 20th century, shows that new solutions for the challenges of the solar light harvesting can be just before our eyes and wait to be discovered and realized. Very high expectations are currently associated with inexpensive and abundant materials based on carbon NPs, that can be produced from a variety of available natural sources, as well as with ternary and more complex metal chalcogenides based on broadly available copper, tin, zinc and other elements, that can act as excellent harvesters of the visible and near IR solar irradiation.

New co-catalysts are continuously discovered and such materials can enhance dramatically the performance of conventional semiconductor-based photocatalytic systems as well as to reduce a need for expensive noble and platinum-group metals.

Finally, *new sacrificial donors* derived from sustainable sources, such as biomass, when coupled to the above-discussed benefits of new photocatalysts and co-catalyst can make the photocatalytic water splitting a really competitive and lucrative process and assist to its broad implementation in our everyday life. This road should be paved by simultaneous development of the theoretical backgrounds of the solar-light-induced water splitting and predictive modelling of the most optimized designs and constructions of the photochemical reactors and water splitting solar cells as well as their operational regimes [582].

References

1. Calvert JG, Pitts, JN Jr (1966) Photochemistry. Wiley, New-York, London, Sydney
2. Maeda K, Domen K (2007) New non-oxide photocatalysts designed for overall water splitting under visible light. *J Phys Chem C* 111:7851–7861. doi:[10.1021/jp070911w](https://doi.org/10.1021/jp070911w)
3. van de Krol R, Liang Y, Schoonman J (2008) Solar hydrogen production with nanostructured metal oxides. *J Mater Chem* 18:2311–2320. doi:[10.1039/B718969A](https://doi.org/10.1039/B718969A)
4. Babu VJ, Vempati S, Uyar T, Ramakrishna S (2015) Review of one-dimensional and two-dimensional nanostructured materials for hydrogen generation. *Phys Chem Chem Phys* 17:2960–2986. doi:[10.1039/c4cp04245j](https://doi.org/10.1039/c4cp04245j)
5. Walter MG, Warren EL, McKone JR et al (2010) Solar water splitting cells. *Chem Rev* 110:6446–6473. doi:[10.1021/cr1002326](https://doi.org/10.1021/cr1002326)
6. Kitano M, Hara M (2010) Heterogeneous photocatalytic cleavage of water. *J Mater Chem* 20:627–641. doi:[10.1039/B910180B](https://doi.org/10.1039/B910180B)
7. Maeda K, Domen K (2010) Photocatalytic water splitting: recent progress and future challenges. *J Phys Chem Lett* 1:2655–2661. doi:[10.1021/jz1007966](https://doi.org/10.1021/jz1007966)
8. Jing D, Guo L, Zhao L et al (2010) Efficient solar hydrogen production by photocatalytic water splitting: from fundamental study to pilot demonstration. *Inter J Hydrogen En* 35:7087–7097. doi:[10.1016/j.ijhydene.2010.01.030](https://doi.org/10.1016/j.ijhydene.2010.01.030)
9. Maeda K (2011) Photocatalytic water splitting using semiconductor particles: history and recent developments. *J Photochem Photobiol, C* 12:237–268. doi:[10.1016/j.jphotochemrev.2011.07.001](https://doi.org/10.1016/j.jphotochemrev.2011.07.001)
10. Abe R (2010) Recent progress on photocatalytic and photoelectrochemical water splitting under visible light irradiation. *J Photochem Photobiol C* 11:179–209. doi:[10.1016/j.jphotochemrev.2011.02.003](https://doi.org/10.1016/j.jphotochemrev.2011.02.003)
11. Moriya Y, Takata T, Domen K (2013) Recent progress in the development of (oxy)nitride photocatalysts for water splitting under visible-light irradiation. *Coord Chem Rev* 257:1957–1969. doi:[10.1016/j.ccr.2013.01.021](https://doi.org/10.1016/j.ccr.2013.01.021)
12. Du P, Eisenberg R (2012) Catalysts made of earth-abundant elements (Co, Ni, Fe) for water splitting: recent progress and future challenges. *Environ Sci* 5:6012–6021. doi:[10.1039/C2EE03250C](https://doi.org/10.1039/C2EE03250C)
13. Warren SC, Thimsen E (2012) Plasmonic solar water splitting. *Environ Sci* 5:5133–5146. doi:[10.1039/C1EE02875H](https://doi.org/10.1039/C1EE02875H)
14. Valdes A, Brillet J, Grätzel M et al (2012) Solar hydrogen production with semiconductor metal oxides: new directions in experiment and theory. *Phys Chem Chem Phys* 14:49–70. doi:[10.1039/C1CP23212F](https://doi.org/10.1039/C1CP23212F)
15. Zhou H, Qu Y, Zeid T, Duan X (2012) Towards highly efficient photocatalysts using semiconductor nanoarchitectures. *Environ Sci* 5:6732–6743. doi:[10.1039/C2EE03447F](https://doi.org/10.1039/C2EE03447F)
16. Wang P, Huang B, Dai Y, Whangbo MH (2012) Plasmonic photocatalysts: harvesting visible light with noble metal nanoparticles. *Phys Chem Chem Phys* 14:9813–9825. doi:[10.1039/C2CP40823F](https://doi.org/10.1039/C2CP40823F)
17. Horiuchi Y, Toyao T, Takeuchi M et al (2013) Recent advances in visible-light-responsive photocatalysts for hydrogen production and solar energy conversion—from semiconducting TiO₂ to MOF/PCP photocatalysts. *Phys Chem Chem Phys* 15:13243–13253. doi:[10.1039/C3CP51427G](https://doi.org/10.1039/C3CP51427G)
18. Prevot MS, Sivula K (2013) Photoelectrochemical tandem cells for solar water splitting. *J Phys Chem C* 117:17879–17893. doi:[10.1021/jp405291g](https://doi.org/10.1021/jp405291g)
19. Zhang K, Guo L (2013) Metal sulphide semiconductors for photocatalytic hydrogen production. *Catal Sci Technol* 3:1672–1690. doi:[10.1039/C3CY00018D](https://doi.org/10.1039/C3CY00018D)
20. Osterloh FE (2013) Inorganic nanostructures for photoelectrochemical and photocatalytic water splitting. *Chem Soc Rev* 42:2294–2320. doi:[10.1039/C2CS35266D](https://doi.org/10.1039/C2CS35266D)

21. Fresno F, Portela R, Suarez S, Coronado JM (2014) Photocatalytic materials: recent achievements and near future trends. *J Mater Chem A* 2:2863–2884. doi:[10.1039/C3TA13793G](https://doi.org/10.1039/C3TA13793G)
22. Zhang P, Zhang J, Gong J (2014) Tantalum-based semiconductors for solar water splitting. *Chem Soc Rev* 43:4395–4422. doi:[10.1039/C3CS60438A](https://doi.org/10.1039/C3CS60438A)
23. Ran J, Zhang J, Yu J et al (2014) Earth-abundant cocatalysts for semiconductor-based photocatalytic water splitting. *Chem Soc Rev* 43:7787–7812. doi:[10.1039/C3CS60425J](https://doi.org/10.1039/C3CS60425J)
24. Huang ZF, Pan L, Zou JJ et al (2014) Nanostructured bismuth vanadate-based materials for solar-energy-driven water oxidation: a review on recent progress. *Nanoscale* 6:14044–14063. doi:[10.1039/C4NR05245E](https://doi.org/10.1039/C4NR05245E)
25. Ida S, Ishihara T (2014) Recent progress in two-dimensional oxide photocatalysts for water splitting. *J Phys Chem Lett* 5:2533–2542. doi:[10.1021/jz5010957](https://doi.org/10.1021/jz5010957)
26. Hisatomi T, Kubota J, Domen K (2014) Recent advances in semiconductors for photocatalytic and photoelectrochemical water splitting. *Chem Soc Rev* 43:7520–7535. doi:[10.1039/C3CS60378D](https://doi.org/10.1039/C3CS60378D)
27. Vaneski A, Schneider J, Susha AS, Rogach AL (2014) Colloidal hybrid heterostructures based on II–VI semiconductor nanocrystals for photocatalytic hydrogen generation. *J Photochem Photobiol C* 19:52–61. doi:[10.1016/j.jphotochemrev.2013.12.001](https://doi.org/10.1016/j.jphotochemrev.2013.12.001)
28. Zong X, Wang L (2014) Ion-exchangeable semiconductor materials for visible light-induced photocatalysis. *J Photochem Photobiol C* 18:32–49. doi:[10.1016/j.jphotochemrev.2013.10.001](https://doi.org/10.1016/j.jphotochemrev.2013.10.001)
29. Chen X, Liu L, Huang F (2015) Black titanium dioxide (TiO₂) nanomaterials. *Chem Soc Rev* 44:1861–1885. doi:[10.1039/C4CS00330F](https://doi.org/10.1039/C4CS00330F)
30. Moniz SJA, Shevlin SA, Martin DJ et al (2015) Visible-light driven heterojunction photocatalysts for water splitting—a critical review. *Environ Sci* 8:731–759. doi:[10.1039/C4EE03271C](https://doi.org/10.1039/C4EE03271C)
31. Wang M, Han K, Zhang S, Sun L (2015) Integration of organometallic complexes with semiconductors and other nanomaterials for photocatalytic H₂ production. *Coord Chem Rev* 287:1–14. doi:[10.1016/j.ccr.2014.12.005](https://doi.org/10.1016/j.ccr.2014.12.005)
32. Gholipour MR, Dinh CT, Beland F, Do TO (2015) Nanocomposite heterojunctions as sunlight-driven photocatalysts for hydrogen production from water splitting. *Nanoscale* 7:8187–8208. doi:[10.1039/C4NR07224C](https://doi.org/10.1039/C4NR07224C)
33. Tachibana Y, Vayssieres L, Durrant JR (2012) Artificial photosynthesis for solar water-splitting. *Nat Photonics* 6:511–518. doi:[10.1038/nphoton.2012.175](https://doi.org/10.1038/nphoton.2012.175)
34. Zhou N, Lopez-Puente V, Wang Q et al (2015) Plasmon-enhanced light harvesting: applications in enhanced photocatalysis, photodynamic therapy and photovoltaics. *RSC Adv* 5:29076–29097. doi:[10.1039/C5RA01819F](https://doi.org/10.1039/C5RA01819F)
35. Ghirardi ML, Dubini A, Yu J, Maness PC (2009) Photobiological hydrogen-producing systems. *Chem Soc Rev* 38:52–61. doi:[10.1039/B718939G](https://doi.org/10.1039/B718939G)
36. Szacilowski K, Macyk W, Drzewiecka-Matuszek A et al (2005) Bioinorganic photochemistry: frontiers and mechanisms. *Chem Rev* 105:2647–2694. doi:[10.1021/cr030707e](https://doi.org/10.1021/cr030707e)
37. Allakhverdiev SI, Kreslavski VD, Thavasi V et al (2009) Hydrogen photoproduction by use of photosynthetic organisms and biomimetic systems. *Photochem Photobiol Sci* 8:148–156. doi:[10.1039/B814932A](https://doi.org/10.1039/B814932A)
38. Zhang X, Peng T, Song S (2016) Recent advances in dye-sensitized semiconductor systems for photocatalytic hydrogen production. *J Mater Chem A* 4:2365–2402. doi:[10.1039/c5ta08939e](https://doi.org/10.1039/c5ta08939e)
39. Nada AA, Hamed HA, Barakat MH et al (2008) Enhancement of photocatalytic hydrogen production rate using photosensitized TiO₂/RuO₂-MV²⁺. *Inter J Hydrogen En* 33:3264–3269. doi:[10.1016/j.ijhydene.2008.04.027](https://doi.org/10.1016/j.ijhydene.2008.04.027)
40. Jin Z, Zhang X, Lu G, Li S (2006) Improved quantum yield for photocatalytic hydrogen generation under visible light irradiation over eosin sensitized TiO₂—Investigation of different noble metal loading. *J Mol Catal A* 259:275–280. doi:[10.1016/j.molcata.2006.06.035](https://doi.org/10.1016/j.molcata.2006.06.035)

41. Tiwari A, Mondal I, Pal U (2015) Visible light induced hydrogen production over thiophenothiazine-based dye sensitized TiO_2 photocatalyst in neutral water. *RSC Adv* 5:31415–31421. doi:[10.1039/C5RA03039K](https://doi.org/10.1039/C5RA03039K)
42. Lee J, Kwak J, Ko KC et al (2012) Phenothiazine-based organic dyes with two anchoring groups on TiO_2 for highly efficient visible light-induced water splitting. *Chem Commun* 48:11431–11433. doi:[10.1039/C2CC36501D](https://doi.org/10.1039/C2CC36501D)
43. Tiwari A, Pal U (2015) Effect of donor-donor- π -acceptor architecture of triphenylamine-based organic sensitizers over TiO_2 photocatalysts for visible-light-driven hydrogen production. *Inter J Hydrogen En* 40:9069–9079. doi:[10.1016/j.ijhydene.2015.05.101](https://doi.org/10.1016/j.ijhydene.2015.05.101)
44. Chen S, Li Y, Wang C (2015) Enhancement of visible-light-driven photocatalytic H_2 evolution from water over $\text{g-C}_3\text{N}_4$ through combination with perylene diimide aggregates. *RSC Adv* 5:15880–15885. doi:[10.1016/j.apcata.2015.03.026](https://doi.org/10.1016/j.apcata.2015.03.026)
45. Zhang J, Du P, Schneider J et al (2007) Photogeneration of hydrogen from water using an integrated system based on TiO_2 and platinum(II) diimine dithiolate sensitizers. *J Am Chem Soc* 129:7726–7727. doi:[10.1021/ja071789h](https://doi.org/10.1021/ja071789h)
46. Astuti Y, Palomares E, Haque SA, Durrant JR (2005) Triplet state photosensitization of nanocrystalline metal oxide electrodes by zinc-substituted cytochrome c: application to hydrogen evolution. *J Am Chem Soc* 127:15120–15126. doi:[10.1021/ja0533444](https://doi.org/10.1021/ja0533444)
47. Bala S, Mondal I, Goswami A et al (2014) Synthesis, crystal structure and optical properties of a naphthylbisimide-Ni complex: a framework on TiO_2 for visible light H_2 production. *Dalton Trans* 43:15704–15707. doi:[10.1039/C4DT02006E](https://doi.org/10.1039/C4DT02006E)
48. Li Q, Jin Z, Peng Z et al (2007) High-efficient photocatalytic hydrogen evolution on Eosin Y-sensitized Ti – MCM41 zeolite under visible-light irradiation. *J Phys Chem C* 111:8237–8241. doi:[10.1021/jp068703b](https://doi.org/10.1021/jp068703b)
49. Li Q, Lu G (2007) Visible-light driven photocatalytic hydrogen generation on Eosin Y-sensitized Pt-loaded nanotube $\text{Na}_2\text{Ti}_2\text{O}_4(\text{OH})_2$. *J Mol Catal A* 266:75–79. doi:[10.1016/j.molcata.2006.10.047](https://doi.org/10.1016/j.molcata.2006.10.047)
50. Li Y, Xie C, Peng S et al (2008) Eosin Y-sensitized nitrogen-doped TiO_2 for efficient visible light photocatalytic hydrogen evolution. *J Mol Catal A* 282:117–123. doi:[10.1016/j.molcata.2007.12.005](https://doi.org/10.1016/j.molcata.2007.12.005)
51. Abe R, Sayama K, Arakawa H (2004) Dye-sensitized photocatalysts for efficient hydrogen production from aqueous I^- solution under visible light irradiation. *J Photochem Photobiol A* 166:115–122. doi:[10.1016/j.jphotochem.2004.04.031](https://doi.org/10.1016/j.jphotochem.2004.04.031)
52. Puangpetch T, Sommakettarin P, Chavadej S, Sreethawong T (2010) Hydrogen production from water splitting over Eosin Y-sensitized mesoporous-assembled perovskite titanate nanocrystal photocatalysts under visible light irradiation. *Inter J Hydrogen En* 35:12428–12442. doi:[10.1016/j.ijhydene.2010.08.138](https://doi.org/10.1016/j.ijhydene.2010.08.138)
53. Zhang N, Shi J, Niu F et al (2015) A cocatalyst-free Eosin Y-sensitized p-type of Co_3O_4 quantum dot for highly efficient and stable visible-light-driven water reduction and hydrogen production. *Phys Chem Chem Phys* 17:21397–21400. doi:[10.1039/c5cp02983j](https://doi.org/10.1039/c5cp02983j)
54. Ikeda S, Abe C, Torimoto T, Ohtani B (2003) Photochemical hydrogen evolution from aqueous triethanolamine solutions sensitized by binaphthol-modified titanium(IV) oxide under visible-light irradiation. *J Photochem Photobiol A* 160:61–67. doi:[10.1016/S1010-6030\(03\)00222-3](https://doi.org/10.1016/S1010-6030(03)00222-3)
55. Fu N, Lu G (2009) Hydrogen evolution over heteropoly blue-sensitized Pt/TiO_2 under visible light irradiation. *Catal Lett* 127:319–322. doi:[10.1007/s10562-008-9681-4](https://doi.org/10.1007/s10562-008-9681-4)
56. Fu N, Lu G (2009) Photo-catalytic H_2 evolution over a series of Keggin-structure heteropoly blue sensitized Pt/TiO_2 under visible light irradiation. *Appl Surf Sci* 255:4378–4383. doi:[10.1016/j.apsusc.2008.11.056](https://doi.org/10.1016/j.apsusc.2008.11.056)
57. Kuchmiy SY, Korzhak AV, Guba NF et al (1995) Sensitization of cadmium sulfide by cyanine dyes in the photocatalytic production of hydrogen. *Theoret Experim Chem* 31:370–374. doi:[10.1007/BF00531245](https://doi.org/10.1007/BF00531245)

58. Xu J, Li Y, Peng S et al (2013) Eosin Y-sensitized graphitic carbon nitride fabricated by heating urea for visible light photocatalytic hydrogen evolution: the effect of the pyrolysis temperature of urea. *Phys Chem Chem Phys* 15:7657–7665. doi:[10.1039/C3CP44687E](https://doi.org/10.1039/C3CP44687E)
59. Wang Y, Hong J, Zhang W, Xu R (2013) Carbon nitride nanosheets for photocatalytic hydrogen evolution: remarkably enhanced activity by dye sensitization. *Catal Sci Technol* 3:1703–1711. doi:[10.1039/C3CY20836B](https://doi.org/10.1039/C3CY20836B)
60. Xu J, Li Y, Peng S (2015) Photocatalytic hydrogen evolution over erythrosin B-sensitized graphitic carbon nitride with in situ grown molybdenum sulfide cocatalyst. *Inter J Hydrogen En* 40:353–362. doi:[10.1016/j.ijhydene.2014.10.150](https://doi.org/10.1016/j.ijhydene.2014.10.150)
61. Takanabe K, Kamata K, Wang X et al (2010) Photocatalytic hydrogen evolution on dye-sensitized mesoporous carbon nitride photocatalyst with magnesium phthalocyanine. *Phys Chem Chem Phys* 12:13020–13025. doi:[10.1039/C0CP00611D](https://doi.org/10.1039/C0CP00611D)
62. Song S, Guo Y, Peng T et al (2016) Effects of the symmetry and carboxyl anchoring group of zinc phthalocyanine derivatives on g-C₃N₄ for photosensitized H₂ production. *RSC Adv* 6:77366–77374. doi:[10.1039/c6ra15890k](https://doi.org/10.1039/c6ra15890k)
63. Reisner E, Fontecilla-Camps JC, Armstrong FA (2009) Catalytic electrochemistry of a [NiFeSe]-hydrogenase on TiO₂ and demonstration of its suitability for visible-light driven H₂ production. *Chem Commun* 550–552. doi:[10.1039/B817371K](https://doi.org/10.1039/B817371K)
64. Peng T, Ke D, Cai P et al (2008) Influence of different ruthenium(II) bipyridyl complex on the photocatalytic H₂ evolution over TiO₂ nanoparticles with mesostructures. *J Power Sources* 180:498–505. doi:[10.1016/j.jpowsour.2008.02.002](https://doi.org/10.1016/j.jpowsour.2008.02.002)
65. Lakshminarasimhan N, Bae E, Choi W (2007) Enhanced photocatalytic production of H₂ on mesoporous TiO₂ prepared by template-free method: role of interparticle charge transfer. *J Phys Chem C* 111:15244–15250. doi:[10.1021/jp0752724](https://doi.org/10.1021/jp0752724)
66. Li J, E Y, Lian L, Ma W (2013) Visible light induced dye-sensitized photocatalytic hydrogen production over platinumized TiO₂ derived from decomposition of platinum complex precursor. *Inter J Hydrogen En* 38:10746–10753. doi:[10.1016/j.ijhydene.2013.02.121](https://doi.org/10.1016/j.ijhydene.2013.02.121)
67. Maeda K, Eguchi M, Youngblood WJ, Mallouk TE (2008) Niobium oxide nanoscrolls as building blocks for dye-sensitized hydrogen production from water under visible light irradiation. *Chem Mater* 20:6770–6778. doi:[10.1021/cm801807b](https://doi.org/10.1021/cm801807b)
68. Maeda K, Eguchi M, Lee SH et al (2009) Photocatalytic hydrogen evolution from hexaniobate nanoscrolls and calcium niobate nanosheets sensitized by ruthenium(II) bipyridyl complexes. *J Phys Chem C* 113:7962–7969. doi:[10.1021/jp900842e](https://doi.org/10.1021/jp900842e)
69. Peng T, Dai K, Yi H et al (2008) Photosensitization of different ruthenium(II) complex dyes on TiO₂ for photocatalytic H₂ evolution under visible-light. *Chem Phys Lett* 460:216–219. doi:[10.1016/j.cplett.2008.06.001](https://doi.org/10.1016/j.cplett.2008.06.001)
70. Ueno K, Misawa H (2013) Surface plasmon-enhanced photochemical reactions. *J Photochem Photobiol C* 15:31–52. doi:[10.1016/j.jphotochemrev.2013.04.001](https://doi.org/10.1016/j.jphotochemrev.2013.04.001)
71. Valenti M, Jonsson MP, Biskos G et al (2016) Plasmonic nanoparticle-semiconductor composites for efficient solar water splitting. *J Mater Chem A* 4:17891–17912. doi:[10.1039/c6ta06405a](https://doi.org/10.1039/c6ta06405a)
72. Clavero C (2014) Plasmon-induced hot-electron generation at nanoparticle/metal-oxide interfaces for photovoltaic and photocatalytic devices. *Nat Photonics* 8:95–103. doi:[10.1038/NPHOTON.2013.238](https://doi.org/10.1038/NPHOTON.2013.238)
73. Nguyen BH, Nguyen VH (2015) Recent advances in research on plasmonic enhancement of photocatalysis. *Adv Nat Sci Nanosci Nanotechnol* 6:043001. doi:[10.1088/2043-6262/6/4/043001](https://doi.org/10.1088/2043-6262/6/4/043001)
74. Mendez-Medrano MG, Kowalska E, Lehoux A et al (2016) Surface modification of TiO₂ with Au nanoclusters for efficient water treatment and hydrogen generation under visible light. *J Phys Chem C* 120:25010–25022. doi:[10.1021/acs.jpcc.6b06854](https://doi.org/10.1021/acs.jpcc.6b06854)
75. Fang J, Cao SW, Wang Z et al (2012) Mesoporous plasmonic Au–TiO₂ nanocomposites for efficient visible-light-driven photocatalytic water reduction. *Inter J Hydrogen En* 37:17853–17861. doi:[10.1016/j.ijhydene.2012.09.023](https://doi.org/10.1016/j.ijhydene.2012.09.023)

76. Zhang X, Liu Y, Kang Z (2014) 3D branched ZnO nanowire arrays decorated with plasmonic Au nanoparticles for high-performance photoelectrochemical water splitting. *ACS Appl Mater Interfaces* 6:4480–4489. doi:[10.1021/am500234v](https://doi.org/10.1021/am500234v)
77. DeSario PA, Pietron JJ, DeVantier DE et al (2013) Plasmonic enhancement of visible-light water splitting with Au–TiO₂ composite aerogels. *Nanoscale* 5:8073–8083. doi:[10.1039/c3nr01429k](https://doi.org/10.1039/c3nr01429k)
78. Ingram DB, Linic S (2011) Water splitting on composite plasmonic-metal/semiconductor photoelectrodes: evidence for selective plasmon-induced formation of charge carriers near the semiconductor surface. *J Am Chem Soc* 133:5202–5205. doi:[10.1021/ja200086g](https://doi.org/10.1021/ja200086g)
79. Meng F, Cushing SK, Li J et al (2015) Enhancement of solar hydrogen generation by synergistic interaction of La₂Ti₂O₇ photocatalyst with plasmonic gold nanoparticles and reduced graphene oxide nanosheets. *ACS Catal* 5:1949–1955. doi:[10.1021/cs5016194](https://doi.org/10.1021/cs5016194)
80. Hou W, Cronin SB (2012) A review of surface plasmon resonance-enhanced photocatalysis. *Adv Funct Mater* 23:1612–1619. doi:[10.1002/adfm.201202148](https://doi.org/10.1002/adfm.201202148)
81. Wu B, Liu D, Mubeen S et al (2016) Anisotropic growth of TiO₂ onto gold nanorods for plasmon-enhanced hydrogen production from water reduction. *J Am Chem Soc* 138:1114–1117. doi:[10.1021/jacs.5b11341](https://doi.org/10.1021/jacs.5b11341)
82. Chen JJ, Wu JCS, Wu PC, Tsai DP (2011) Plasmonic photocatalyst for H₂ evolution in photocatalytic water splitting. *J Phys Chem C* 115:210–216. doi:[10.1021/jp1074048](https://doi.org/10.1021/jp1074048)
83. Mubeen S, Hernandez-Sosa G, Moses D et al (2011) Plasmonic photosensitization of a wide band gap semiconductor: converting plasmons to charge carriers. *Nano Lett* 11:5548–5552. doi:[10.1021/nl203457v](https://doi.org/10.1021/nl203457v)
84. Priebe JB, Radnik J, Lennox AJJ et al (2015) Solar hydrogen production by plasmonic Au – TiO₂ catalysts: impact of synthesis protocol and TiO₂ phase on charge transfer efficiency and H₂ evolution rates. *ACS Catal* 5:2137–2148. doi:[10.1021/cs5018375](https://doi.org/10.1021/cs5018375)
85. Zhan Z, An J, Zhang H et al (2014) Three-dimensional plasmonic photoanodes based on Au-Embedded TiO₂ structures for enhanced visible-light water splitting. *ACS App Mater Interfaces* 6:1139–1144. doi:[10.1021/am404738a](https://doi.org/10.1021/am404738a)
86. Zhang Z, Zhang L, Hedhili MN et al (2013) Plasmonic gold nanocrystals coupled with photonic crystal seamlessly on TiO₂ nanotube photoelectrodes for efficient visible light photoelectrochemical water splitting. *Nano Lett* 13:14–20. doi:[10.1021/nl3029202](https://doi.org/10.1021/nl3029202)
87. Chen C, Kuai L, Chen Y et al (2015) Au/Pt co-loaded ultrathin TiO₂ nanosheets for photocatalyzed H₂ evolution by the synergistic effect of plasmonic enhancement and co-catalysis. *RSC Adv* 5:98254–98259. doi:[10.1039/c5ra17732d](https://doi.org/10.1039/c5ra17732d)
88. Yu G, Wang X, Cao J et al (2016) Plasmonic Au nanoparticles embedding enhances the activity and stability of CdS for photocatalytic hydrogen evolution. *Chem Commun* 52:2394–2397. doi:[10.1039/c5cc10066f](https://doi.org/10.1039/c5cc10066f)
89. Luo Y, Liu X, Tang X et al (2014) Gold nanoparticles embedded in Ta₂O₅/Ta₃N₅ as active visible-light plasmonic photocatalysts for solar hydrogen evolution. *J Mater Chem A* 2:14927–14939. doi:[10.1039/c4ta02991g](https://doi.org/10.1039/c4ta02991g)
90. Wu M, Chen WJ, Shen YH et al (2014) In situ growth of matchlike ZnO/Au plasmonic heterostructure for enhanced photoelectrochemical water splitting. *ACS Appl Mater Interfaces* 6:15052–15060. doi:[10.1021/am503044f](https://doi.org/10.1021/am503044f)
91. Zeng J, Song T, Lv M et al (2016) Plasmonic photocatalyst Au/g-C₃N₄/NiFe₂O₄ nanocomposites for enhanced visible-light-driven photocatalytic hydrogen evolution. *RSC Adv* 6:54964–54975. doi:[10.1039/c6ra08356k](https://doi.org/10.1039/c6ra08356k)
92. Patnaik S, Martha S, Madras G, Parida K (2016) The effect of sulfate pre-treatment to improve the deposition of Au-nanoparticles in a gold-modified sulfated g-C₃N₄ plasmonic photocatalyst towards visible light induced water reduction reaction. *Phys Chem Chem Phys* 18:28502–28514. doi:[10.1039/c6cp04262g](https://doi.org/10.1039/c6cp04262g)
93. Zhang X, Zhao J, Wang S et al (2014) Shape-dependent localized surface plasmon enhanced photocatalytic effect of ZnO nanorods decorated with Ag. *Inter J Hydrogen En* 39:8238–8245. doi:[10.1016/j.ijhydene.2014.03.153](https://doi.org/10.1016/j.ijhydene.2014.03.153)

94. Yi J, She X, Song Y et al (2016) A silver on 2D white- C_3N_4 support photocatalyst for mechanistic insights: synergetic utilization of plasmonic effect for solar hydrogen evolution. *RSC Adv* 6:112420–112428. doi:[10.1039/c6ra23964a](https://doi.org/10.1039/c6ra23964a)
95. Kryukov AI, Kuchmiy SY, Korzhak AV et al (1993) Synergism in an organized photocatalytic system based on cadmium sulfide and titanium complexes. *Theoret Exp Chem* 29:312–316. doi:[10.1007/BF00532100](https://doi.org/10.1007/BF00532100)
96. Kryukov AI, Kuchmiy SY, Kulik SV et al (1994) New photocatalysts: dispersed semiconductor materials with microheterojunctions. *Theoret Exp Chem* 30:182–186. doi:[10.1007/BF00531180](https://doi.org/10.1007/BF00531180)
97. Kryukov AI, Kuchmiy SY, Pokhodenko VD (1994) Molecular design in photo-catalysis: physicochemical principles for designing high-efficiency photocatalytic oxidation-reduction systems. *Theoret Exp Chem* 30:141–157. doi:[10.1007/BF00534653](https://doi.org/10.1007/BF00534653)
98. Kryukov A, Kuchmiy SY, Pokhodenko VD (1997) Nanostructural composite photocatalysts based on polycrystalline cadmium sulfide. *Theoret Exp Chem* 33:306–321. doi:[10.1007/BF02522707](https://doi.org/10.1007/BF02522707)
99. Kryukov AI, Kuchmiy SY, Pokhodenko VD (2000) Energetics of electron processes in semiconductor photocatalytic systems. *Theoret Exp Chem* 36:69–89. doi:[10.1007/BF02529022](https://doi.org/10.1007/BF02529022)
100. Fedoseev BI, Savinov EI, Parmon VN (1987) Photocatalytic hydrogen evolution from Na₂S solution in the presence of highly disperse cadmium and copper sulfides. *Kinetics Catal* 28:1111–1115
101. Ogisu K, Takanabe K, Lu D et al (2009) CdS nanoparticles exhibiting quantum size effect by dispersion on TiO₂: photocatalytic H₂ evolution and photoelectrochemical measurements. *Bull Chem Soc Jpn* 82:528–535. doi:[10.1246/bcsj.82.528](https://doi.org/10.1246/bcsj.82.528)
102. Hirai T, Suzuki K, Komasaawa I (2001) Preparation and photocatalytic properties of composite cds nanoparticles-titanium dioxide particles. *J Colloid Interface Sci* 244:262–265. doi:[10.1006/jcis.2001.7982](https://doi.org/10.1006/jcis.2001.7982)
103. Stroyuk OL, Kryukov AI, Kuchmiy SY, Pokhodenko VD (2005) Quantum size effects in the photonics of semiconductor nanoparticles. *Theoret Exp Chem* 41:67–91. doi:[10.1007/s11237-005-0025-9](https://doi.org/10.1007/s11237-005-0025-9)
104. Stroyuk OL, Kryukov AI, Kuchmiy SY, Pokhodenko VD (2005) Quantum size effects in semiconductor photocatalysis. *Theoret Exp Chem* 41:207–228. doi:[10.1007/s11237-005-0042-8](https://doi.org/10.1007/s11237-005-0042-8)
105. Lian Z, Xu P, Wang W et al (2015) C₆₀-decorated CdS/TiO₂ mesoporous architectures with enhanced photostability and photocatalytic activity for H₂ evolution. *ACS Appl Mater Interfaces* 7:4533–4540. doi:[10.1021/am5088665](https://doi.org/10.1021/am5088665)
106. Ji SM, Jun H, Jang JS et al (2007) Photocatalytic hydrogen production from natural seawater. *J Photochem Photobiol A* 189:141–144. doi:[10.1016/j.jphotochem.2007.01.011](https://doi.org/10.1016/j.jphotochem.2007.01.011)
107. Park H, Choi W, Hoffmann MR (2008) Effects of the preparation method of the ternary CdS/TiO₂/Pt hybrid photocatalysts on visible light-induced hydrogen production. *J Mater Chem* 18:2379–2385. doi:[10.1039/B718759A](https://doi.org/10.1039/B718759A)
108. Jang JS, Choi SH, Kim HG, Lee JS (2008) Location and state of Pt in platinized CdS/TiO₂ photocatalysts for hydrogen production from water under visible light. *J Phys Chem C* 112:17200–17205. doi:[10.1021/jp804699c](https://doi.org/10.1021/jp804699c)
109. Cui X, Jiang G, Zhu M et al (2013) TiO₂/CdS composite hollow spheres with controlled synthesis of platinum on the internal wall for the efficient hydrogen evolution. *Inter J Hydrogen En* 38:9065–9073. doi:[10.1016/j.ijhydene.2013.05.062](https://doi.org/10.1016/j.ijhydene.2013.05.062)
110. Zhou H, Pan J, Ding L et al (2014) Biomass-derived hierarchical porous CdS/M/TiO₂ (M = Au, Ag, pt, pd) ternary heterojunctions for photocatalytic hydrogen evolution *Inter J Hydrogen En* 39:16293–16301. doi:[10.1016/j.ijhydene.2014.08.032](https://doi.org/10.1016/j.ijhydene.2014.08.032)
111. Cui X, Wang Y, Jiang G et al (2014) A photonic crystal-based CdS–Au–WO₃ heterostructure for efficient visible-light photocatalytic hydrogen and oxygen evolution. *RSC Adv* 4:15689–15694. doi:[10.1039/C4RA01415D](https://doi.org/10.1039/C4RA01415D)
112. Vaishnav JK, Arbuj SS, Rane SB, Amalnerkar DP (2014) One dimensional CdS/ZnO nanocomposites: an efficient photocatalyst for hydrogen generation. *RSC Adv* 4:47637–47642. doi:[10.1039/C4RA08561B](https://doi.org/10.1039/C4RA08561B)

113. Yang G, Yan W, Zhang Q et al (2013) One-dimensional CdS/ZnO core/shell nanofibers via single-spinneret electrospinning: tunable morphology and efficient photocatalytic hydrogen production. *Nanoscale* 5:12432–12439. doi:[10.1039/C3NR03462C](https://doi.org/10.1039/C3NR03462C)
114. Shen S, Guo L (2008) Growth of quantum-confined CdS nanoparticles inside Ti-MCM-41 as a visible light photocatalyst. *Mater Res Bull* 43:437–446. doi:[10.1016/j.materresbull.2007.02.034](https://doi.org/10.1016/j.materresbull.2007.02.034)
115. Liu Z, Shen S, Guo L (2012) Study on photocatalytic performance for hydrogen evolution over CdS/M-MCM-41 (M = Zr, Ti) composite photocatalysts under visible light illumination. *Inter J Hydrogen En* 37:816–821. doi:[10.1016/j.ijhydene.2011.04.052](https://doi.org/10.1016/j.ijhydene.2011.04.052)
116. Zhang YJ, Yan W, Wu YP, Wang ZH (2008) Synthesis of TiO₂ nanotubes coupled with CdS nanoparticles and production of hydrogen by photocatalytic water decomposition. *Mater Lett* 62(2008):3846–3848. doi:[10.1016/j.matlet.2008.04.084](https://doi.org/10.1016/j.matlet.2008.04.084)
117. Xing C, Jing D, Liu M, Guo L (2009) Photocatalytic hydrogen production over Na₂Ti₂O₄(OH)₂ nanotube sensitized by CdS nanoparticles. *Mater Res Bull* 44:442–445. doi:[10.1016/j.materresbull.2008.04.016](https://doi.org/10.1016/j.materresbull.2008.04.016)
118. Kim JC, Choi J, Lee YB et al (2006) Enhanced photocatalytic activity in composites of TiO₂ nanotubes and CdS nanoparticles. *Chem Commun* 48(2006):5024–5026. doi:[10.1039/B612572G](https://doi.org/10.1039/B612572G)
119. Chen Y, Guo L (2012) Highly efficient visible-light-driven photocatalytic hydrogen production from water using Cd_{0.5}Zn_{0.5}S/TNTs (titanate nanotubes) nanocomposites without noble metals. *J Mater Chem* 22:7507–7514. doi:[10.1039/C2JM16797B](https://doi.org/10.1039/C2JM16797B)
120. Qi L, Yu J, Jaroniec M (2011) Preparation and enhanced visible-light photocatalytic H₂-production activity of CdS-sensitized Pt/TiO₂ nanosheets with exposed (001) facets. *Phys Chem Chem Phys* 13:8915–8923. doi:[10.1039/C1CP20079H](https://doi.org/10.1039/C1CP20079H)
121. Gao B, Yuan X, Lu P et al (2015) Enhanced visible-light-driven photocatalytic H₂-production activity of CdS-loaded TiO₂ microspheres with exposed (001) facets. *J Phys Chem Sol* 87:171–176. doi:[10.1016/j.jpcs.2015.08.018](https://doi.org/10.1016/j.jpcs.2015.08.018)
122. Guan G, Kida T, Kusakabe K et al (2005) Photocatalytic activity of CdS nanoparticles incorporated in titanium silicate molecular sieves of ETS-4 and ETS-10. *Appl Catal A* 295:71–78. doi:[10.1016/j.apcata.2005.08.010](https://doi.org/10.1016/j.apcata.2005.08.010)
123. Shangguan W, Yoshida A (2001) Synthesis and photocatalytic properties of CdS-intercalated metal oxides. *Sol En Mater Sol Cells* 69:189–194. doi:[10.1016/S0927-0248\(01\)00020-4](https://doi.org/10.1016/S0927-0248(01)00020-4)
124. Shangguan W, Yoshida A (2002) Photocatalytic hydrogen evolution from water on nanocomposites incorporating cadmium sulfide into the interlayer. *J Phys Chem B* 106:12227–12230. doi:[10.1021/jp0212500](https://doi.org/10.1021/jp0212500)
125. Dinh CT, Pham NH, Kleitz F, Do TO (2013) Design of water-soluble CdS–titanate–nickel nanocomposites for photocatalytic hydrogen production under sunlight. *J Mater Chem A* 1:13308–13313. doi:[10.1039/C3TA12914D](https://doi.org/10.1039/C3TA12914D)
126. Xiao J, Peng T, Ke D et al (2007) Synthesis, characterization of CdS/rectorite nanocomposites and its photocatalytic activity. *Phys Chem Miner* 34:275–285. doi:[10.1007/s00269-007-0146-x](https://doi.org/10.1007/s00269-007-0146-x)
127. Parayil SK, Baltrusaitis J, Wu CM, Koodali RT (2013) Synthesis and characterization of ligand stabilized CdS-Trititanate composite materials for visible light-induced photocatalytic water splitting. *Inter J Hydrogen En* 38:2656–2669. doi:[10.1016/j.ijhydene.2012.12.042](https://doi.org/10.1016/j.ijhydene.2012.12.042)
128. Ryu SY, Choi J, Balcerski W et al (2007) Photocatalytic production of H₂ on nanocomposite catalysts. *Ind Eng Chem Res* 46:7476–7488. doi:[10.1021/ie0703033](https://doi.org/10.1021/ie0703033)
129. Shangguan W (2007) Hydrogen evolution from water splitting on nanocomposite photocatalysts. *Sci Technol Adv Mater* 8:76–81. doi:[10.1016/j.stam.2006.09.007](https://doi.org/10.1016/j.stam.2006.09.007)
130. Choi J, Ryu Y, Balcerski W et al (2008) Photocatalytic production of hydrogen on Ni/NiO/KNbO₃/CdS nanocomposites using visible light. *J Mater Chem* 18:2371–2378. doi:[10.1039/B718535A](https://doi.org/10.1039/B718535A)

131. Chen W, Gao H, Yuan J et al (2013) Structure characteristics of $\text{CdS}/\text{H}_{1.9}\text{K}_{0.3}\text{La}_{0.5}\text{Bi}_{0.1}\text{Ta}_2\text{O}_7$ and photocatalytic activity for hydrogen evolution under visible light. *Inter J Hydrogen En* 38:10754–10760. doi:[10.1016/j.ijhydene.2013.02.067](https://doi.org/10.1016/j.ijhydene.2013.02.067)
132. Yu J, Lei SL, Chen TC et al (2014) A new $\text{CdS}/\text{Bi}_{1-x}\text{In}_x\text{TaO}_4$ heterostructured photocatalyst containing solid solutions for H_2 evolution from water splitting. *Inter J Hydrogen En* 39:13105–13113. doi:[10.1016/j.ijhydene.2014.06.148](https://doi.org/10.1016/j.ijhydene.2014.06.148)
133. Zhang G, Lin B, Yang W et al (2015) Highly efficient photocatalytic hydrogen generation by incorporating CdS into ZnCr-layered double hydroxide interlayer. *RSC Adv* 5:5823–5829. doi:[10.1039/C4RA11757C](https://doi.org/10.1039/C4RA11757C)
134. Wu J, Lin J, Yin S, Sato T (2001) Synthesis and photocatalytic properties of layered $\text{HfNbWO}_6/(\text{Pt}, \text{Cd}_{0.8}\text{Zn}_{0.2}\text{S})$ nanocomposites. *J Mater Chem* 11:3343–3347. doi:[10.1039/B103838A](https://doi.org/10.1039/B103838A)
135. So WW, Kim KJ, Moon SJ (2004) Photo-production of hydrogen over the $\text{CdS}-\text{TiO}_2$ nanocomposite particulate films treated with TiCl_4 . *Inter J Hydrogen En* 29:229–234. doi:[10.1016/S0360-3199\(03\)00211-8](https://doi.org/10.1016/S0360-3199(03)00211-8)
136. Wang H, Zhu W, Chong B, Qin K (2014) Improvement of photocatalytic hydrogen generation from $\text{CdSe}/\text{CdS}/\text{TiO}_2$ nanotube-array coaxial heterogeneous structure. *Inter J Hydrogen En* 39:90–99. doi:[10.1016/j.ijhydene.2013.10.048](https://doi.org/10.1016/j.ijhydene.2013.10.048)
137. Kudo A, Miseki Y (2009) Heterogeneous photocatalyst materials for water splitting. *Chem Soc Rev* 38:253–278. doi:[10.1039/B800489G](https://doi.org/10.1039/B800489G)
138. Moon GD, Joo JB, Lee I, Yin Y (2014) Decoration of size-tunable CuO nanodots on TiO_2 nanocrystals for noble metal-free photocatalytic H_2 production. *Nanoscale* 6:12002–12008. doi:[10.1039/C4NR03521F](https://doi.org/10.1039/C4NR03521F)
139. Jang JS, Ji SM, Bae SW et al (2007) Optimization of CdS/TiO_2 nano-bulk composite photocatalysts for hydrogen production from $\text{Na}_2\text{S}/\text{Na}_2\text{SO}_3$ aqueous electrolyte solution under visible light ($\lambda \geq 420$ nm). *J Photochem Photobiol, A* 188:112–119. doi:[10.1016/j.jphotochem.2006.11.027](https://doi.org/10.1016/j.jphotochem.2006.11.027)
140. Jang JS, Kim HG, Borse PH, Lee JS (2007) Simultaneous hydrogen production and decomposition of H_2S dissolved in alkaline water over $\text{CdS}-\text{TiO}_2$ composite photocatalysts under visible light irradiation. *Inter J Hydrogen En* 32:4786–4791. doi:[10.1016/j.ijhydene.2007.06.026](https://doi.org/10.1016/j.ijhydene.2007.06.026)
141. Jang JS, Kim HG, Joshi UA et al (2008) Fabrication of CdS nanowires decorated with TiO_2 nanoparticles for photocatalytic hydrogen production under visible light irradiation. *Inter J Hydrogen En* 33:5975–5980. doi:[10.1016/j.ijhydene.2008.07.105](https://doi.org/10.1016/j.ijhydene.2008.07.105)
142. Li C, Xi Z, Fang W et al (2015) Enhanced photocatalytic hydrogen evolution activity of CuInS_2 loaded TiO_2 under solar light irradiation. *J Sol State Chem* 226:94–100. doi:[10.1016/j.jssc.2015.02.011](https://doi.org/10.1016/j.jssc.2015.02.011)
143. Guo K, Liu Z, Han J et al (2014) Hierarchical $\text{TiO}_2-\text{CuInS}_2$ core-shell nanoarrays for photoelectrochemical water splitting. *Phys Chem Chem Phys* 16:16204–16213. doi:[10.1039/C4CP01971G](https://doi.org/10.1039/C4CP01971G)
144. Li K, Xu J, Zhang X et al (2013) Low-temperature preparation of $\text{AgIn}_5\text{S}_8/\text{TiO}_2$ heterojunction nanocomposite with efficient visible-light-driven hydrogen production. *Inter J Hydrogen En* 38:15965–15975. doi:[10.1016/j.ijhydene.2013.09.147](https://doi.org/10.1016/j.ijhydene.2013.09.147)
145. Cheng Z, Zhan X, Wang F et al (2015) Construction of CuInS_2/Ag sensitized ZnO nanowire arrays for efficient hydrogen generation. *RSC Adv* 5:81723–81727. doi:[10.1039/c5ra14188e](https://doi.org/10.1039/c5ra14188e)
146. Choi Y, Baek M, Zhang Z et al (2015) A two-storey structured photoanode of a 3D $\text{Cu}_2\text{ZnSnS}_4/\text{CdS}/\text{ZnO}$ @steel composite nanostructure for efficient photoelectrochemical hydrogen generation. *Nanoscale* 7:15291–15299. doi:[10.1039/c5nr04107d](https://doi.org/10.1039/c5nr04107d)
147. Kandiel TA, Takanabe K (2016) Solvent-induced deposition of Cu–Ga–In–S nanocrystals onto titanium dioxide surface for visible-light-driven photocatalytic hydrogen production. *Appl Catal B* 184:264–269. doi:[10.1016/j.apcatb.2015.11.036](https://doi.org/10.1016/j.apcatb.2015.11.036)
148. Brahimi R, Bessekhoud Y, Bouguelia A, Trari M (2007) Visible light induced hydrogen evolution over the heterosystem $\text{Bi}_2\text{S}_3/\text{TiO}_2$. *Catal Today* 122:62–65. doi:[10.1016/j.cattod.2007.01.030](https://doi.org/10.1016/j.cattod.2007.01.030)

149. Kim J, Kang M (2012) High photocatalytic hydrogen production over the band gap-tuned urchin-like Bi₂S₃-loaded TiO₂ composites system. *Inter J Hydrogen En* 37:8249–8256. doi:[10.1016/j.ijhydene.2012.02.057](https://doi.org/10.1016/j.ijhydene.2012.02.057)
150. Senevirathna N, Pitigaka P, Tennakone K (2005) Water photoreduction with Cu₂O quantum dots on TiO₂ nanoparticles. *J Photochem Photobiol A* 171:257–259. doi:[10.1016/j.jphotochem.2004.10.018](https://doi.org/10.1016/j.jphotochem.2004.10.018)
151. Zhang S, Zhang S, Peng F et al (2011) Electrodeposition of polyhedral Cu₂O on TiO₂ nanotube arrays for enhancing visible light photocatalytic performance. *Electrochem Commun* 13:861–864. doi:[10.1016/j.elecom.2011.05.022](https://doi.org/10.1016/j.elecom.2011.05.022)
152. Kumar DP, Reddy NL, Kumari MM et al (2015) Cu₂O-sensitized TiO₂ nanorods with nanocavities for highly efficient photocatalytic hydrogen production under solar irradiation. *Sol En Mater Sol Cells* 136:157–166. doi:[10.1016/j.solmat.2015.01.009](https://doi.org/10.1016/j.solmat.2015.01.009)
153. Zhang S, Peng B, Yang S et al (2013) The influence of the electrodeposition potential on the morphology of Cu₂O/TiO₂ nanotube arrays and their visible-light-driven photocatalytic activity for hydrogen evolution. *Inter J Hydrogen En* 38:13866–13871. doi:[10.1016/j.ijhydene.2013.08.081](https://doi.org/10.1016/j.ijhydene.2013.08.081)
154. Li L, Xu L, Shi W, Guan J (2013) Facile preparation and size-dependent photocatalytic activity of Cu₂O nanocrystals modified titania for hydrogen evolution. *Inter J Hydrogen En* 38:816–822. doi:[10.1016/j.ijhydene.2012.10.064](https://doi.org/10.1016/j.ijhydene.2012.10.064)
155. Sharma D, Upadhyay S, Satsangi VR et al (2014) Improved photoelectrochemical water splitting performance of Cu₂O/SrTiO₃ heterojunction photoelectrode. *J Phys Chem C* 118:25320–25329. doi:[10.1021/jp507039n](https://doi.org/10.1021/jp507039n)
156. Jung M, Scott J, Ng YH et al (2014) CuO_x dispersion and reducibility on TiO₂ and its impact on photocatalytic hydrogen evolution. *Inter J Hydrogen En* 39:12499–12506. doi:[10.1016/j.ijhydene.2014.06.020](https://doi.org/10.1016/j.ijhydene.2014.06.020)
157. Bandara J, Udawatta C, Rajapakse C (2005) Highly stable CuO incorporated TiO₂ catalyst for photocatalytic hydrogen production from H₂O. *Photochem Photobiol Sci* 4:857–861. doi:[10.1039/B507816D](https://doi.org/10.1039/B507816D)
158. Yu Z, Meng J, Li Y et al (2013) Efficient photocatalytic hydrogen production from water over a CuO and carbon fiber comodified TiO₂ nanocomposite photocatalyst. *Inter J Hydrogen En* 38:6649–16655. doi:[10.1016/j.ijhydene.2013.07.056](https://doi.org/10.1016/j.ijhydene.2013.07.056)
159. Xu S, Du AJ, Liu J et al (2011) Highly efficient CuO incorporated TiO₂ nanotube photocatalyst for hydrogen production from water. *Inter J Hydrogen En* 36:6560–6568. doi:[10.1016/j.ijhydene.2011.02.103](https://doi.org/10.1016/j.ijhydene.2011.02.103)
160. Kumar SP, Shankar MV, Kumari MM et al (2013) Nano-size effects on CuO/TiO₂ catalysts for highly efficient H₂ production under solar light irradiation. *Chem Commun* 49:9443–9445. doi:[10.1039/C3CC44742A](https://doi.org/10.1039/C3CC44742A)
161. Yue X, Yi S, Wang R et al (2016) A novel and highly efficient earth-abundant Cu₃P with TiO₂ “P–N” heterojunction nanophotocatalyst for hydrogen evolution from water. *Nanoscale* 8:17516–17523. doi:[10.1039/c6nr06620h](https://doi.org/10.1039/c6nr06620h)
162. Yang X, Xu J, Wong T et al (2013) Synthesis of In₂O₃–In₂S₃ core–shell nanorods with inverted type-I structure for photocatalytic H₂ generation. *Phys Chem Chem Phys* 15:12688–12693. doi:[10.1039/C3CP51722E](https://doi.org/10.1039/C3CP51722E)
163. Liu Z, Bai H, Xu S, Sun DD (2011) Hierarchical CuO/ZnO “corn-like” architecture for photocatalytic hydrogen generation. *Inter J Hydrogen En* 36:13473–13480. doi:[10.1016/j.ijhydene.2011.07.137](https://doi.org/10.1016/j.ijhydene.2011.07.137)
164. Rajaambal S, Mapa M, Gopinath CS (2014) In_{1–x}Ga_xN@ZnO: a rationally designed and quantum dot integrated material for water splitting and solar harvesting applications. *Dalton Trans* 43:12546–12554. doi:[10.1039/C4DT01268B](https://doi.org/10.1039/C4DT01268B)
165. Derbal A, Omeiri S, Bouguelia A, Trari M (2008) Characterization of new heterosystem CuFeO₂/SnO₂ application to visible-light induced hydrogen evolution. *Inter J Hydrogen En* 33:4274–4282. doi:[10.1016/j.ijhydene.2008.05.067](https://doi.org/10.1016/j.ijhydene.2008.05.067)

166. Nguyen-Phan TD, Luo S, Vovchok D et al (2016) Visible light-driven H_2 production over highly dispersed ruthenium on rutile TiO_2 nanorods. *ACS Catal* 6:407–417. doi:[10.1021/acscatal.5b02318](https://doi.org/10.1021/acscatal.5b02318)
167. Brahimi R, Bessekhoud Y, Bouguelia A, Trari M (2007) $CuAlO_2/TiO_2$ heterojunction applied to visible light H_2 production. *J Photochem Photobiol A* 186:242–247. doi:[10.1016/j.jphotochem.2006.08.013](https://doi.org/10.1016/j.jphotochem.2006.08.013)
168. Ou Y, Lin J, Fang S, Liao D (2006) MWNT– TiO_2 : Ni composite catalyst: a new class of catalyst for photocatalytic H_2 evolution from water under visible light illumination. *Chem Phys Lett* 429:199–203. doi:[10.1016/j.cplett.2006.08.024](https://doi.org/10.1016/j.cplett.2006.08.024)
169. Yu H, Shi R, Zhao Y et al (2016) Smart utilization of carbon dots in semiconductor photocatalysis. *Adv Mater* 28:9454–9477. doi:[10.1002/adma.201602581](https://doi.org/10.1002/adma.201602581)
170. Cao S, Yu J (2016) Carbon-based H_2 -production photocatalytic materials. *J Photochem Photobiol C* 27:72–99. doi:[10.1016/j.jphotochemrev.2016.04.002](https://doi.org/10.1016/j.jphotochemrev.2016.04.002)
171. Wang J, Gao M, Ho GW (2014) Bidentate-complex-derived TiO_2 /carbon dot photocatalysts: in situ synthesis, versatile heterostructures, and enhanced H_2 evolution. *J Mater Chem A* 2 (2014):5703–5709. doi:[10.1039/C3TA15114J](https://doi.org/10.1039/C3TA15114J)
172. Yu H, Zhao Y, Zhou C et al (2014) Carbon quantum dots/ TiO_2 composites for efficient photocatalytic hydrogen evolution. *J Mater Chem A* 2:3344–3351. doi:[10.1039/C3TA14108J](https://doi.org/10.1039/C3TA14108J)
173. Tang Y, Hao R, Fu Y et al (2016) Carbon quantum dot/mixed crystal TiO_2 composites via a hydrogenation process: an efficient photocatalyst for the hydrogen evolution reaction. *RSC Adv* 6:96803–96808. doi:[10.1039/c6ra17597j](https://doi.org/10.1039/c6ra17597j)
174. Wang J, Huang J, Xie H, Qu A (2014) Synthesis of $g-C_3N_4/TiO_2$ with enhanced photocatalytic activity for H_2 evolution by a simple method. *Inter J Hydrogen En* 39:6354–6363. doi:[10.1016/j.ijhydene.2014.02.020](https://doi.org/10.1016/j.ijhydene.2014.02.020)
175. Zang Y, Li L, Xu Y et al (2014) Hybridization of brookite TiO_2 with $g-C_3N_4$: a visible-light-driven photocatalyst for As^{3+} oxidation, MO degradation and water splitting for hydrogen evolution. *J Mater Chem A* 2:15774–15780. doi:[10.1039/C4TA02082K](https://doi.org/10.1039/C4TA02082K)
176. Li Y, Wang R, Li H et al (2015) Efficient and stable photoelectrochemical seawater splitting with $TiO_2@g-C_3N_4$ nanorod arrays decorated by Co-Pi. *J Phys Chem C* 119:20283–20292. doi:[10.1021/acs.jpcc.5b05427](https://doi.org/10.1021/acs.jpcc.5b05427)
177. Pany S, Parida KM (2015) A facile in situ approach to fabricate N, S- $TiO_2/g-C_3N_4$ nanocomposite with excellent activity for visible light induced water splitting for hydrogen evolution. *Phys Chem Chem Phys* 17:8070–8077. doi:[10.1039/C4CP05582A](https://doi.org/10.1039/C4CP05582A)
178. Zhong X, Jin M, Dong H et al (2014) TiO_2 nanobelts with a uniform coating of $g-C_3N_4$ as a highly effective heterostructure for enhanced photocatalytic activities. *J Sol State Chem* 220:54–59. doi:[10.1016/j.jssc.2014.08.016](https://doi.org/10.1016/j.jssc.2014.08.016)
179. Jiang Y, Guo S, Hao R et al (2016) A hybridized heterojunction structure between TiO_2 nanorods and exfoliated graphitic carbon nitride sheets for hydrogen evolution under visible light. *CrystEngComm* 18:6875–6880. doi:[10.1039/c6ce01442a](https://doi.org/10.1039/c6ce01442a)
180. Cheng F, Yin H, Xiang Q (2017) Low-temperature solid-state preparation of ternary $CdS/g-C_3N_4/CuS$ nanocomposites for enhanced visible-light photocatalytic H_2 -production activity. *Appl Surf Sci* 391:432–439. doi:[10.1016/j.apsusc.2016.06.169](https://doi.org/10.1016/j.apsusc.2016.06.169)
181. Liu H, Jin Z, Xu Z et al (2015) Fabrication of $ZnIn_2S_4-g-C_3N_4$ sheet-on-sheet nanocomposites for efficient visible-light photocatalytic H_2 -evolution and degradation of organic pollutants. *RSC Adv* 5:97951–97961. doi:[10.1039/c5ra17028a](https://doi.org/10.1039/c5ra17028a)
182. Zheng D, Zhang G, Wang X (2015) Integrating CdS quantum dots on hollow graphitic carbon nitride nanospheres for hydrogen evolution photocatalysis. *Appl Catal B* 179:479–488. doi:[10.1016/j.apcatb.2015.05.060](https://doi.org/10.1016/j.apcatb.2015.05.060)
183. Chen W, Liu TY, Huang T et al (2015) A novel yet simple strategy to fabricate visible light responsive C, N- $TiO_2/g-C_3N_4$ heterostructures with significantly enhanced photocatalytic hydrogen generation. *RSC Adv* 5:101214–101220. doi:[10.1039/c5ra18302b](https://doi.org/10.1039/c5ra18302b)

184. Hu B, Cai F, Chen T et al (2015) Hydrothermal synthesis g-C₃N₄/Nano-InVO₄ nanocomposites and enhanced photocatalytic activity for hydrogen production under visible light irradiation. *ACS Appl Mater Interfaces* 7:18247–18256. doi:[10.1021/acsami.5b05715](https://doi.org/10.1021/acsami.5b05715)
185. Kudo A (2007) Recent progress in the development of visible light-driven powdered photocatalysts for water splitting. *Inter J Hydrogen En* 32:2673–2678. doi:[10.1016/j.ijhydene.2006.09.010](https://doi.org/10.1016/j.ijhydene.2006.09.010)
186. Ni M, Leung M, Leung D, Sumathy K (2007) A review and recent developments in photocatalytic water-splitting using TiO₂ for hydrogen production. *Renew Sustain En Rev* 11:401–425. doi:[10.1016/j.rser.2005.01.009](https://doi.org/10.1016/j.rser.2005.01.009)
187. Matsuoka M, Kitano M, Takeuchi M et al (2007) Photocatalysis for new energy production: recent advances in photocatalytic water splitting reactions for hydrogen production. *Catal Today* 122:51–61. doi:[10.1016/j.cattod.2007.01.042](https://doi.org/10.1016/j.cattod.2007.01.042)
188. Lee JS (2005) Photocatalytic water splitting under visible light with particulate semiconductor catalysts. *Catal Surv Asia* 9:217–227. doi:[10.1007/s10563-005-9157-0](https://doi.org/10.1007/s10563-005-9157-0)
189. Kudo A (2003) Photocatalyst materials for water splitting. *Catal Surv Asia* 7:31–38. doi:[10.1023/A:1023480507710](https://doi.org/10.1023/A:1023480507710)
190. Tsuji I, Kudo A (2003) H₂ evolution from aqueous sulfite solutions under visible-light irradiation over Pb and halogen-codoped ZnS photocatalysts. *J Photochem Photobiol A* 156:249–252. doi:[10.1016/S1010-6030\(02\)00433-1](https://doi.org/10.1016/S1010-6030(02)00433-1)
191. Kudo A, Sekizawa M (2000) Photocatalytic H₂ evolution under visible light irradiation on Ni-doped ZnS photocatalyst. *Chem Commun* 1371–1372. doi:[10.1039/B003297M](https://doi.org/10.1039/B003297M)
192. Kudo A, Sekizawa M (1999) Photocatalytic H₂ evolution under visible light irradiation on Zn_{1-x}Cu_xS solid solution. *Catal Lett* 58:241–243. doi:[10.1023/A:1019067025917](https://doi.org/10.1023/A:1019067025917)
193. Mei Z, Ouyang S, Zhang Y, Kako T (2013) Ultrafine Zn_{1-x}Cu_xS (0 ≤ x ≤ 0.066) nanocrystallites for photocatalytic H₂ evolution under visible light irradiation. *RSC Adv* 3:10654–10657. doi:[10.1039/C3RA41076E](https://doi.org/10.1039/C3RA41076E)
194. Wu Y, Lu G, Li S (2009) The doping effect of Bi on TiO₂ for photocatalytic hydrogen generation and photodecolorization of rhodamine B. *J Phys Chem C* 113:9950–9955. doi:[10.1021/jp9009433](https://doi.org/10.1021/jp9009433)
195. Ishii T, Kato H, Kudo A (2004) H₂ evolution from an aqueous methanol solution on SrTiO₃ photocatalysts codoped with chromium and tantalum ions under visible light irradiation. *J Photochem Photobiol A* 163:181–186. doi:[10.1016/S1010-6030\(03\)00442-8](https://doi.org/10.1016/S1010-6030(03)00442-8)
196. Wang D, Ye J, Kako T, Kimura T (2006) Photophysical and photocatalytic properties of SrTiO₃ doped with Cr cations on different sites. *J Phys Chem B* 110:15824–15830. doi:[10.1021/jp062487p](https://doi.org/10.1021/jp062487p)
197. Iwashina K, Kudo A (2011) Rh-doped SrTiO₃ photocatalyst electrode showing cathodic photocurrent for water splitting under visible-light irradiation. *J Am Chem Soc* 133:13272–13275
198. Kato H, Sasaki Y, Shirakura N, Kudo A (2013) Synthesis of highly active rhodium-doped SrTiO₃ powders in Z-scheme systems for visible-light-driven photocatalytic overall water splitting. *J Mater Chem A* 1:12327–12333. doi:[10.1039/C3TA12803B](https://doi.org/10.1039/C3TA12803B)
199. Niishiro R, Kato H, Kudo A (2005) Nickel and either tantalum or niobium-codoped TiO₂ and SrTiO₃ photocatalysts with visible-light response for H₂ or O₂ evolution from aqueous solutions. *Phys Chem Chem Phys* 7:2241–2245. doi:[10.1039/B502147B](https://doi.org/10.1039/B502147B)
200. Kato H, Kudo A (2002) Visible-light-response and photocatalytic activities of TiO₂ and SrTiO₃ photocatalysts codoped with antimony and chromium. *J Phys Chem B* 106:5029–5034. doi:[10.1021/jp0255482](https://doi.org/10.1021/jp0255482)
201. Hwang DW, Kim HG, Lee JS et al (2005) Photocatalytic hydrogen production from water over M-doped La₂Ti₂O₇ (M = Cr, Fe) under visible light irradiation (λ > 420 nm). *J Phys Chem B* 109:2093–2102. doi:[10.1021/jp0493226](https://doi.org/10.1021/jp0493226)
202. Hwang DW, Kim HG, Jang JS et al (2004) Photocatalytic decomposition of water–methanol solution over metal-doped layered perovskites under visible light irradiation. *Catal Today* 93–95:845–850. doi:[10.1016/j.cattod.2004.06.084](https://doi.org/10.1016/j.cattod.2004.06.084)

203. Kanhere P, Zheng J, Chen Z (2012) Visible light driven photocatalytic hydrogen evolution and photophysical properties of Bi³⁺ doped NaTaO₃. *Inter J Hydrogen En* 37:4889–4896. doi:[10.1016/j.ijhydene.2011.12.056](https://doi.org/10.1016/j.ijhydene.2011.12.056)
204. Zou JP, Zhang LZ, Luo SL et al (2012) Preparation and photocatalytic activities of two new Zn-doped SrTiO₃ and BaTiO₃ photocatalysts for hydrogen production from water without cocatalysts loading. *Inter J Hydrogen En* 37:17068–17077. doi:[10.1016/j.ijhydene.2012.08.133](https://doi.org/10.1016/j.ijhydene.2012.08.133)
205. Xue Y, Wang X (2015) The effects of Ag doping on crystalline structure and photocatalytic properties of BiVO₄. *Inter J Hydrogen En* 40:5878–5888. doi:[10.1016/j.ijhydene.2015.03.028](https://doi.org/10.1016/j.ijhydene.2015.03.028)
206. Jana P, Montero CM, Pizzarro P et al (2014) Photocatalytic hydrogen production in the water/methanol system using Pt/RE:NaTaO₃ (RE = Y, La, Ce, Yb) catalysts. *Inter J Hydrogen En* 39:5283–5290. doi:[10.1016/j.ijhydene.2013.12.182](https://doi.org/10.1016/j.ijhydene.2013.12.182)
207. Shimura K, Yoshida H (2012) Effect of doped zinc species on the photocatalytic activity of gallium oxide for hydrogen production. *Phys Chem Chem Phys* 14:2678–2684. doi:[10.1039/C2CP23220K](https://doi.org/10.1039/C2CP23220K)
208. Kudo A, Niishiro R, Iwase A, Kato H (2007) Effects of doping of metal cations on morphology, activity, and visible light response of photocatalysts. *Chem Phys* 339:104–110. doi:[10.1016/j.chemphys.2007.07.024](https://doi.org/10.1016/j.chemphys.2007.07.024)
209. Zou Z, Arakawa H (2003) Direct water splitting into H₂ and O₂ under visible light irradiation with a new series of mixed oxide semiconductor photocatalysts. *J Photochem Photobiol A* 158:145–162. doi:[10.1016/S1010-6030\(03\)00029-7](https://doi.org/10.1016/S1010-6030(03)00029-7)
210. Zou Z, Ye J, Sayama K, Arakawa H (2002) Photocatalytic hydrogen and oxygen formation under visible light irradiation with M-doped InTaO₄ (M = Mn, Fe, Co, Ni and Cu) photocatalysts. *J Photochem Photobiol A* 148:65–69. doi:[10.1016/S1010-6030\(02\)00068-0](https://doi.org/10.1016/S1010-6030(02)00068-0)
211. Wang D, Zou Z, Ye J (2005) Photocatalytic water splitting with the Cr-doped Ba₂In₂O₅/In₂O₃ composite oxide semiconductors. *Chem Mater* 17:3255–3261. doi:[10.1021/cm0477117](https://doi.org/10.1021/cm0477117)
212. Gurunathan K (2004) Photocatalytic hydrogen production using transition metal ions-doped γ-Bi₂O₃ semiconductor particles. *Inter J Hydrogen En* 29:933–940. doi:[10.1016/j.ijhydene.2003.04.001](https://doi.org/10.1016/j.ijhydene.2003.04.001)
213. Jing D, Zhang Y, Guo L (2005) Study on the synthesis of Ni doped mesoporous TiO₂ and its photocatalytic activity for hydrogen evolution in aqueous methanol solution. *Chem Phys Lett* 415:74–78. doi:[10.1016/j.cplett.2005.08.080](https://doi.org/10.1016/j.cplett.2005.08.080)
214. Liu Q, Ding D, Ning C, Wang X (2015) Black Ni-doped TiO₂ photoanodes for high-efficiency photoelectrochemical water-splitting. *Inter J Hydrogen En* 40:2107–2114. doi:[10.1016/j.ijhydene.2014.12.064](https://doi.org/10.1016/j.ijhydene.2014.12.064)
215. Wang D, Ye J, Kitazawa H, Kimura T (2007) Photophysical and photocatalytic properties of three isostructural oxide semiconductors In₆NiTi₆O₂₂, In₃CrTi₂O₁₀, and In₁₂NiCr₂Ti₁₀O₄₂ with different 3d transition metals. *J Phys Chem C* 111:12848–12854. doi:[10.1021/jp0678599](https://doi.org/10.1021/jp0678599)
216. Wang D, Zou Z, Ye J (2005) Photocatalytic H₂ evolution over a new visible-light-driven photocatalyst In₁₂NiCr₂Ti₁₀O₄₂. *Chem Phys Lett* 411:285–290. doi:[10.1016/j.cplett.2005.05.124](https://doi.org/10.1016/j.cplett.2005.05.124)
217. Konta R, Ishii T, Kato H, Kudo A (2004) Photocatalytic activities of noble metal ion doped SrTiO₃ under visible light irradiation. *J Phys Chem B* 108:8992–8995. doi:[10.1021/jp049556p](https://doi.org/10.1021/jp049556p)
218. Kitano M, Takeuchi M, Matsuoka M et al (2007) Photocatalytic water splitting using Pt-loaded visible light-responsive TiO₂ thin film photocatalysts. *Catal Today* 120:133–138. doi:[10.1016/j.cattod.2006.07.043](https://doi.org/10.1016/j.cattod.2006.07.043)
219. Fukumoto S, Kitano M, Takeuchi M et al (2009) Photocatalytic hydrogen production from aqueous solutions of alcohol as model compounds of biomass using visible light-responsive TiO₂ thin films. *Catal Lett* 127:39–43. doi:[10.1007/s10562-008-9769-x](https://doi.org/10.1007/s10562-008-9769-x)

220. Kitano M, Tsujimaru K, Anpo M (2008) Hydrogen production using highly active titanium oxide-based photocatalysts. *Topics Catal* 49:4–17. doi:[10.1007/s11244-008-9059-2](https://doi.org/10.1007/s11244-008-9059-2)
221. Selli E, Chiarello GL, Quartarone E et al (2007) A photocatalytic water splitting device for separate hydrogen and oxygen evolution. *Chem Commun* 5022–5024. doi:[10.1039/B711747G](https://doi.org/10.1039/B711747G)
222. Matsuoka M, Kitano M, Fukumoto S et al (2008) The effect of the hydrothermal treatment with aqueous NaOH solution on the photocatalytic and photoelectrochemical properties of visible light-responsive TiO₂ thin films. *Catal Today* 132:159–164. doi:[10.1016/j.cattod.2007.12.032](https://doi.org/10.1016/j.cattod.2007.12.032)
223. Kitano M, Takeuchi M, Matsuoka M et al (2005) Preparation of visible light-responsive TiO₂ thin film photocatalysts by an RF magnetron sputtering deposition method and their photocatalytic reactivity. *Chem Lett* 34:616–617. doi:[10.1246/cl.2005.616](https://doi.org/10.1246/cl.2005.616)
224. Dholam R, Patel N, Adami M, Miotello A (2008) Physically and chemically synthesized TiO₂ composite thin films for hydrogen production by photocatalytic water splitting. *Inter J Hydrogen En* 33:6896–6903. doi:[10.1016/j.ijhydene.2008.08.061](https://doi.org/10.1016/j.ijhydene.2008.08.061)
225. Matsuoka M, Kitano M, Takeuchi M et al (2005) Photocatalytic water splitting on visible light-responsive TiO₂ thin films prepared by a RF magnetron sputtering deposition method. *Topics Catal* 35:305–310. doi:[10.1007/s11244-005-3838-9](https://doi.org/10.1007/s11244-005-3838-9)
226. Wang Z, Yang C, Lin T et al (2013) Visible-light photocatalytic, solar thermal and photoelectrochemical properties of aluminium-reduced black titania. *Environ Sci* 6:3007–3014. doi:[10.1039/c3ee41817k](https://doi.org/10.1039/c3ee41817k)
227. Cui H, Zhao W, Yang C et al (2014) Black TiO₂ nanotube arrays for high-efficiency photoelectrochemical water-splitting. *J Mater Chem A* 2:8612–8616. doi:[10.1039/c4ta00176a](https://doi.org/10.1039/c4ta00176a)
228. Zhang K, Zhou W, Zhang X et al (2016) Large-scale synthesis of stable mesoporous black TiO₂ nanosheets for efficient solar-driven photocatalytic hydrogen evolution via an earth-abundant low-cost biotemplate. *RSC Adv* 6:50506–50512. doi:[10.1039/c6ra06751d](https://doi.org/10.1039/c6ra06751d)
229. Yuan J, Chen M, Shi J, Shanguang W (2006) Preparations and photocatalytic hydrogen evolution of N-doped TiO₂ from urea and titanium tetrachloride. *Inter J Hydrogen En* 31:1326–1331. doi:[10.1016/j.ijhydene.2005.11.016](https://doi.org/10.1016/j.ijhydene.2005.11.016)
230. Sreethawong T, Laehsatee S, Chavadej S (2009) Use of Pt/N-doped mesoporous-assembled nanocrystalline TiO₂ for photocatalytic H₂ production under visible light irradiation. *Catal Commun* 10:538–543. doi:[10.1016/j.catcom.2008.10.029](https://doi.org/10.1016/j.catcom.2008.10.029)
231. Sreethawong T, Laehsatee S, Chavadej S (2008) Comparative investigation of mesoporous- and non-mesoporous-assembled TiO₂ nanocrystals for photocatalytic H₂ production over N-doped TiO₂ under visible light irradiation. *Inter J Hydrogen En* 33:5947–5957. doi:[10.1016/j.ijhydene.2008.08.007](https://doi.org/10.1016/j.ijhydene.2008.08.007)
232. Liu SH, Syu HR (2013) High visible-light photocatalytic hydrogen evolution of C, N-codoped mesoporous TiO₂ nanoparticles prepared via an ionic-liquid-template approach. *Inter J Hydrogen En* 38:13856–13865. doi:[10.1016/j.ijhydene.2013.08.094](https://doi.org/10.1016/j.ijhydene.2013.08.094)
233. Kim H, Monllor-Satoca D, Kim W, Choi W (2015) N-doped TiO₂ nanotubes coated with a thin TaO_xN_y layer for photoelectrochemical water splitting: dual bulk and surface modification of photoanodes. *Environ Sci* 8:247–257. doi:[10.1039/C4EE02169J](https://doi.org/10.1039/C4EE02169J)
234. Lin WC, Yang WD, Huang IL et al (2009) Hydrogen production from methanol/water photocatalytic decomposition using Pt/TiO_{2-x}N_x catalyst. *Environ Sci* 23:2192–2196
235. Pei F, Liu Y, Xu S et al (2013) Nanocomposite of graphene oxide with nitrogen-doped TiO₂ exhibiting enhanced photocatalytic efficiency for hydrogen evolution. *Inter J Hydrogen En* 38:2670–2677. doi:[10.1016/j.ijhydene.2012.12.045](https://doi.org/10.1016/j.ijhydene.2012.12.045)
236. Pei F, Xu S, Zuo W et al (2014) Effective improvement of photocatalytic hydrogen evolution via a facile in-situ solvothermal N-doping strategy in N-TiO₂/N-graphene nanocomposite. *Inter J Hydrogen En* 39:6845–6852. doi:[10.1016/j.ijhydene.2014.02.173](https://doi.org/10.1016/j.ijhydene.2014.02.173)
237. Hara M, Nunoshige J, Takata T et al (2003) Unusual enhancement of H₂ evolution by Ru on TaON photocatalyst under visible light irradiation. *Chem Commun* 3000–3001. doi:[10.1039/B309935K](https://doi.org/10.1039/B309935K)

238. Hara M, Hitoki G, Takata T et al (2003) TaON and Ta₃N₅ as new visible light driven photocatalysts. *Catal Today* 78:555–560. doi:[10.1016/S0920-5861\(02\)00354-1](https://doi.org/10.1016/S0920-5861(02)00354-1)
239. Suzuki TM, Nakamura T, Saeki S et al (2012) Visible light-sensitive mesoporous N-doped Ta₂O₅ spheres: synthesis and photocatalytic activity for hydrogen evolution and CO₂ reduction. *J Mater Chem* 22:24584–24590. doi:[10.1039/C2JM33980C](https://doi.org/10.1039/C2JM33980C)
240. Mishima T, Matsuda M, Miyake M (2007) Visible-light photocatalytic properties and electronic structure of Zr-based oxynitride, Zr₂ON₂, derived from nitridation of ZrO₂. *Appl Catal A* 324:77–82. doi:[10.1016/j.apcata.2007.03.017](https://doi.org/10.1016/j.apcata.2007.03.017)
241. Maeda K, Terashima H, Kase K et al (2008) Surface modification of TaON with monoclinic ZrO₂ to produce a composite photocatalyst with enhanced hydrogen evolution activity under visible light. *Bull Chem Soc Jpn* 81:927–937. doi:[10.1246/bcsj.81.927](https://doi.org/10.1246/bcsj.81.927)
242. Liu M, You W, Lei Z et al (2004) Water reduction and oxidation on Pt–Ru/Y₂Ta₂O₅N₂ catalyst under visible light irradiation. *Chem Commun* 2192–2193. doi:[10.1039/B407892F](https://doi.org/10.1039/B407892F)
243. Ji SM, Borse PH, Kim HG et al (2005) Photocatalytic hydrogen production from water–methanol mixtures using N-doped Sr₂Nb₂O₇ under visible light irradiation: effects of catalyst structure. *Phys Chem Chem Phys* 7:1315–1321. doi:[10.1039/B417052K](https://doi.org/10.1039/B417052K)
244. Maeda K, Teramura K, Domen K (2008) Effect of post-calcination on photocatalytic activity of (Ga_{1–x}Zn_x)(N_{1–x}O_x) solid solution for overall water splitting under visible light. *J Catal* 254:198–204. doi:[10.1016/j.jcat.2007.12.009](https://doi.org/10.1016/j.jcat.2007.12.009)
245. Maeda K, Teramura K, Lu D et al (2007) Roles of Rh/Cr₂O₃ (core/shell) nanoparticles photodeposited on visible-light-responsive (Ga_{1–x}Zn_x)(N_{1–x}O_x) solid solutions in photocatalytic overall water splitting. *J Phys Chem C* 111:7554–7560. doi:[10.1021/jp071056j](https://doi.org/10.1021/jp071056j)
246. Maeda K, Teramura K, Lu D et al (2006) Characterization of Rh–Cr mixed-oxide nanoparticles dispersed on (Ga_{1–x}Zn_x)(N_{1–x}O_x) as a cocatalyst for visible-light-driven overall water splitting. *J Phys Chem B* 110:13753–13758. doi:[10.1021/jp061829o](https://doi.org/10.1021/jp061829o)
247. Teramura K, Maeda K, Saito T et al (2005) Characterization of ruthenium oxide nanocluster as a cocatalyst with (Ga_{1–x}Zn_x)(N_{1–x}O_x) for photocatalytic overall water splitting. *J Phys Chem B* 109:21915–21921. doi:[10.1021/jp054313y](https://doi.org/10.1021/jp054313y)
248. Maeda K, Teramura K, Takata T et al (2005) Overall water splitting on (Ga_{1–x}Zn_x)(N_{1–x}O_x) solid solution photocatalyst: relationship between physical properties and photocatalytic activity. *J Phys Chem B* 109:20504–20510. doi:[10.1021/jp053499y](https://doi.org/10.1021/jp053499y)
249. Lee Y, Terashima H, Shimodaira Y et al (2007) Zinc germanium oxynitride as a photocatalyst for overall water splitting under visible light. *J Phys Chem C* 111:1042–1048. doi:[10.1021/jp065653z](https://doi.org/10.1021/jp065653z)
250. Reyes-Gil KR, Reyes-Garcia EA, Raftery D (2007) Nitrogen-doped In₂O₃ thin film electrodes for photocatalytic water splitting. *J Phys Chem C* 111:14579–14588. doi:[10.1021/jp072831y](https://doi.org/10.1021/jp072831y)
251. Mohapatra SK, Misra M, Mahajan VK, Raja KS (2007) Design of a highly efficient photoelectrolytic cell for hydrogen generation by water splitting: application of TiO_{2–x}C_x nanotubes as a photoanode and Pt/TiO₂ nanotubes as a cathode. *J Phys Chem C* 111:8677–8685. doi:[10.1021/jp071906v](https://doi.org/10.1021/jp071906v)
252. Park JH, Kim S, Bard AJ (2006) Novel carbon-doped TiO₂ nanotube arrays with high aspect ratios for efficient solar water splitting. *Nano Lett* 6:24–28. doi:[10.1021/nl051807y](https://doi.org/10.1021/nl051807y)
253. Liu Z, Pesic B, Raja KS et al (2009) Hydrogen generation under sunlight by self ordered TiO₂ nanotube arrays. *Inter J Hydrogen En* 34:3250–3257. doi:[10.1016/j.ijhydene.2009.02.044](https://doi.org/10.1016/j.ijhydene.2009.02.044)
254. Shaban YA, Khan SU (2008) Visible light active carbon modified n-TiO₂ for efficient hydrogen production by photoelectrochemical splitting of water. *Inter J Hydrogen En* 33:1118–1126. doi:[10.1016/j.ijhydene.2007.11.026](https://doi.org/10.1016/j.ijhydene.2007.11.026)
255. Shaban YA, Khan SU (2009) Carbon modified (CM)-n-TiO₂ thin films for efficient water splitting to H₂ and O₂ under xenon lamp light and natural sunlight illuminations. *J Sol State Electrochem* 13:1025–1036. doi:[10.1007/s10008-009-0823-4](https://doi.org/10.1007/s10008-009-0823-4)

256. Randeniya LK, Murphy AB, Plumb IC (2008) A study of S-doped TiO₂ for photoelectrochemical hydrogen generation from water. *J Mater Sci* 43:1389–1399. doi:[10.1007/s10853-007-2309-z](https://doi.org/10.1007/s10853-007-2309-z)
257. Ogisu K, Ishikawa A, Teramura K et al (2007) Lanthanum-indium oxysulfide as a visible light driven photocatalyst for water splitting. *Chem Lett* 36:854–855. doi:[10.1246/cl.2007.854](https://doi.org/10.1246/cl.2007.854)
258. Ryu SY, Balcerski W, Lee TK, Hoffmann MR (2007) Photocatalytic production of hydrogen from water with visible light using hybrid catalysts of CdS attached to microporous and mesoporous silicas. *J Phys Chem C* 111:18195–18203. doi:[10.1021/jp074860e](https://doi.org/10.1021/jp074860e)
259. Hirai T, Nanba M, Komasaawa I (2003) Dithiol-mediated incorporation of CdS nanoparticles from reverse micellar system into Zn-doped SBA-15 mesoporous silica and their photocatalytic properties. *J Colloid Interface Sci* 268:394–399. doi:[10.1016/j.jcis.2003.09.011](https://doi.org/10.1016/j.jcis.2003.09.011)
260. Khatamian M, Oskoui MS, Haghighi M (2014) Photocatalytic hydrogen generation over CdS–metallosilicate composites under visible light irradiation. *New J Chem* 38:1684–1693. doi:[10.1039/C3NJ01348K](https://doi.org/10.1039/C3NJ01348K)
261. Peng R, Zhao D, Baltrusaitis J et al (2012) Visible light driven photocatalytic evolution of hydrogen from water over CdS encapsulated MCM-48 materials. *RSC Adv* 2:5754–5767. doi:[10.1039/C2RA20714A](https://doi.org/10.1039/C2RA20714A)
262. Peng R, Wu CM, Baltrusaitis J et al (2013) Ultra-stable CdS incorporated Ti-MCM-48 mesoporous materials for efficient photocatalytic decomposition of water under visible light illumination. *Chem Commun* 49:3221–3223. doi:[10.1039/C3CC41362D](https://doi.org/10.1039/C3CC41362D)
263. Peng R, Lin C, Baltrusaitis J et al (2014) Insight into band positions and inter-particle electron transfer dynamics between CdS nanoclusters and spatially isolated TiO₂ dispersed in cubic MCM-48 mesoporous materials: a highly efficient system for photocatalytic hydrogen evolution under visible light illumination. *Phys Chem Chem Phys* 16:2048–2061. doi:[10.1039/C3CP52801D](https://doi.org/10.1039/C3CP52801D)
264. Henglein A, Gutierrez M (1983) Photochemistry of colloidal metal sulfides. 5. Fluorescence and chemical reactions of ZnS and ZnS/CdS co-colloids. *Ber Bunsenges Phys Chem* 87:852–858. doi:[10.1002/bbpc.19830871005](https://doi.org/10.1002/bbpc.19830871005)
265. Deshpande A, Shah P, Gholap RS, Gupta NM (2009) Interfacial and physico-chemical properties of polymer-supported CdS–ZnS nanocomposites and their role in the visible-light mediated photocatalytic splitting of water. *J Colloid Interface Sci* 333:263–268. doi:[10.1016/j.jcis.2009.01.037](https://doi.org/10.1016/j.jcis.2009.01.037)
266. Lunawat PS, Senapati S, Kumar R, Gupta NM (2007) Visible light-induced splitting of water using CdS nanocrystallites immobilized over water-repellant polymeric surface. *Inter J Hydrogen En* 32:2784–2790. doi:[10.1016/j.ijhydene.2007.04.001](https://doi.org/10.1016/j.ijhydene.2007.04.001)
267. Kim YK, Kim M, Hwang SH et al (2015) CdS-loaded flexible carbon nanofiber mats as a platform for solar hydrogen production. *Inter J Hydrogen En* 40:136–145. doi:[10.1016/j.ijhydene.2014.11.011](https://doi.org/10.1016/j.ijhydene.2014.11.011)
268. Hirai T, Bando Y, Komasaawa I (2002) Immobilization of CdS nanoparticles formed in reverse micelles onto alumina particles and their photocatalytic properties. *J Phys Chem B* 106:8967–8970. doi:[10.1021/jp020386v](https://doi.org/10.1021/jp020386v)
269. Hirai T, Nanba M, Komasaawa I (2002) Dithiol-mediated immobilization of CdS nanoparticles from reverse micellar system onto Zn-doped silica particles and their high photocatalytic activity. *J Colloid Interface Sci* 252:89–92. doi:[10.1006/jcis.2002.8430](https://doi.org/10.1006/jcis.2002.8430)
270. Yu G, Geng L, Wu S et al (2015) Highly-efficient cocatalyst-free H₂-evolution over silica-supported CdS nanoparticle photocatalysts under visible light. *Chem Commun* 51:10676–10679. doi:[10.1039/C5CC02249E](https://doi.org/10.1039/C5CC02249E)
271. Yu G, Zhang W, Sun Y et al (2016) A highly active cocatalyst-free semiconductor photocatalyst for visible-light-driven hydrogen evolution: synergistic effect of surface defects and spatial bandgap engineering. *J Mater Chem A* 4:13803–13808. doi:[10.1039/c6ta03803d](https://doi.org/10.1039/c6ta03803d)

272. Bb Kale, Baeg JO, Apte SK et al (2007) Confinement of nano CdS in designated glass: a novel functionality of quantum dot–glass nanosystems in solar hydrogen production. *J Mater Chem* 17:4297–4303. doi:[10.1039/B708269J](https://doi.org/10.1039/B708269J)
273. Apte SK, Garaje SN, Valant M, Kale BB (2012) Eco-friendly solar light driven hydrogen production from copious waste H₂S and organic dye degradation by stable and efficient orthorhombic CdS quantum dots–GeO₂ glass photocatalyst. *Green Chem* 14:1455–1462. doi:[10.1039/C2GC16416G](https://doi.org/10.1039/C2GC16416G)
274. Kanade KG, Baeg JO, Mulik UP et al (2006) Nano-CdS by polymer-inorganic solid-state reaction: visible light pristine photocatalyst for hydrogen generation. *Mater Res Bull* 41:2219–2225. doi:[10.1016/j.materresbull.2006.04.031](https://doi.org/10.1016/j.materresbull.2006.04.031)
275. Li W, O'Dowd G, Whittles TJ et al (2015) Colloidal dual-band gap cell for photocatalytic hydrogen generation. *Nanoscale* 7:16606–16610. doi:[10.1039/c5nr04950d](https://doi.org/10.1039/c5nr04950d)
276. Baldovi HG, Latorre-Sanchez M, Esteve-Adell I et al (2016) Generation of MoS₂ quantum dots by laser ablation of MoS₂ particles in suspension and their photocatalytic activity for H₂ generation. *J Nanopart Res* 18:240–248. doi:[10.1007/s11051-016-3540-9](https://doi.org/10.1007/s11051-016-3540-9)
277. Hirai T, Nomura Y, Komasaawa I (2003) Immobilization of RuS₂ nanoparticles prepared in reverse micellar system onto thiol-modified polystyrene particles and their photocatalytic properties. *J Nanoparticle Res* 5:61–67. doi:[10.1023/A:102442226598](https://doi.org/10.1023/A:102442226598)
278. Barawi M, Ferrer IJ, Flores E et al (2016) Hydrogen photoassisted generation by visible light and an earth abundant photocatalyst: pyrite (FeS₂). *J Phys Chem C* 120:9547–9552. doi:[10.1021/acs.jpcc.5b11482](https://doi.org/10.1021/acs.jpcc.5b11482)
279. Li G, Su R, Rao J et al (2016) Band gap narrowing of SnS₂ superstructures with improved hydrogen production. *J Mater Chem A* 4:209–216. doi:[10.1039/c5ta07283b](https://doi.org/10.1039/c5ta07283b)
280. Shen S, Zhao L, Guo L (2008) Cetyltrimethylammoniumbromide (CTAB)-assisted hydrothermal synthesis of ZnIn₂S₄ as an efficient visible-light-driven photocatalyst for hydrogen production. *Inter J Hydrogen En* 33:4501–4510. doi:[10.1016/j.ijhydene.2008.05.043](https://doi.org/10.1016/j.ijhydene.2008.05.043)
281. Lei Z, You W, Liu M et al (2003) Photocatalytic water reduction under visible light on a novel ZnIn₂S₄ catalyst synthesized by hydrothermal method. *Chem Commun* 2142–2143. doi:[10.1039/B306813G](https://doi.org/10.1039/B306813G)
282. Guijun M, Hongjian Y, Xu Z et al (2008) Photocatalytic splitting of H₂S to produce hydrogen by gas-solid phase reaction. *Chin J Catal* 29:313–315. doi:[10.1016/S1872-2067\(08\)60029-7](https://doi.org/10.1016/S1872-2067(08)60029-7)
283. Shen S, Zhao L, Guo L (2009) Crystallite, optical and photocatalytic properties of visible-light-driven ZnIn₂S₄ photocatalysts synthesized via a surfactant-assisted hydrothermal method. *Mater Res Bull* 44:100–105. doi:[10.1016/j.materresbull.2008.03.027](https://doi.org/10.1016/j.materresbull.2008.03.027)
284. Shen J, Zai J, Yuan Y, Qian X (2012) 3D hierarchical ZnIn₂S₄: the preparation and photocatalytic properties on water splitting. *Inter J Hydrogen En* 37:16986–16993. doi:[10.1016/j.ijhydene.2012.08.038](https://doi.org/10.1016/j.ijhydene.2012.08.038)
285. Fan WJ, Zhou ZF, Xu WB et al (2010) Preparation of ZnIn₂S₄/fluoropolymer fiber composites and its photocatalytic H₂ evolution from splitting of water using Xe lamp irradiation. *Inter J Hydrogen En* 35:6525–6530. doi:[10.1016/j.ijhydene.2010.04.036](https://doi.org/10.1016/j.ijhydene.2010.04.036)
286. Li Y, Zhang K, Peng S et al (2012) Photocatalytic hydrogen generation in the presence of ethanolamines over Pt/ZnIn₂S₄ under visible light irradiation. *J Mol Catal A* 363–364:354–361. doi:[10.1016/j.molcata.2012.07.011](https://doi.org/10.1016/j.molcata.2012.07.011)
287. Chaudhari NS, Bhirud AP, Sonawane RS et al (2011) Ecofriendly hydrogen production from abundant hydrogen sulfide using solar light-driven hierarchical nanostructured ZnIn₂S₄ photocatalyst. *Green Chem* 13:2500–2506. doi:[10.1039/C1GC15515F](https://doi.org/10.1039/C1GC15515F)
288. Li F, Luo J, Chen G et al (2014) Hydrothermal synthesis of zinc indium sulfide microspheres with Ag⁺ doping for enhanced H₂ production by photocatalytic water splitting under visible light. *Catal Sci Technol* 4:1144–1150. doi:[10.1039/C3CY00952A](https://doi.org/10.1039/C3CY00952A)

289. Shang L, Zhou C, Bian T et al (2013) Facile synthesis of hierarchical ZnIn_2S_4 submicrospheres composed of ultrathin mesoporous nanosheets as a highly efficient visible-light-driven photocatalyst for H_2 production. *J Mater Chem A* 1:4552–4558. doi:[10.1039/C3TA01685D](https://doi.org/10.1039/C3TA01685D)
290. Xu Z, Li Y, Peng S et al (2012) NaCl-assisted low temperature synthesis of layered Zn-In-S photocatalyst with high visible-light activity for hydrogen evolution. *RSC Adv* 2:3458–3466. doi:[10.1039/C2RA01159J](https://doi.org/10.1039/C2RA01159J)
291. Chen Y, He J, Li J et al (2016) Hydrilla derived ZnIn_2S_4 photocatalyst with hexagonal-cubic phase junctions: A bio-inspired approach for H_2 evolution. *Catal Commun* 87:1–5. doi:[10.1016/j.catcom.2016.08.031](https://doi.org/10.1016/j.catcom.2016.08.031)
292. Tian F, Zhu R, Zhong J et al (2016) An efficient preparation method of RGO/ ZnIn_2S_4 for photocatalytic hydrogen generation under visible light. *Inter J Hydrogen En* 41:20156–20171. doi:[10.1016/j.ijhydene.2016.08.063](https://doi.org/10.1016/j.ijhydene.2016.08.063)
293. Shen S, Zhao L, Zhou Z, Guo L (2008) Enhanced photocatalytic hydrogen evolution over Cu-doped ZnIn_2S_4 under visible light irradiation. *J Phys Chem C* 112:16148–16155. doi:[10.1021/jp804525q](https://doi.org/10.1021/jp804525q)
294. Ding J, Sun S, Yan W et al (2013) Photocatalytic H_2 evolution on a novel CaIn_2S_4 photocatalyst under visible light irradiation. *Inter J Hydrogen En* 38:13153–13158. doi:[10.1016/j.ijhydene.2013.07.109](https://doi.org/10.1016/j.ijhydene.2013.07.109)
295. Ding J, Li X, Chen L et al (2016) Au–Pt alloy nanoparticles site-selectively deposited on CaIn_2S_4 nanosteps as efficient photocatalysts for hydrogen production. *J Mater Chem A* 4:12630–12637. doi:[10.1039/c6ta04468a](https://doi.org/10.1039/c6ta04468a)
296. Zhou Q, Kang SZ, Li X et al (2015) AgGaS_2 nanoplates loaded with CuS: an efficient visible photocatalyst for rapid H_2 evolution. *Inter J Hydrogen En* 40:4119–4128. doi:[10.1016/j.ijhydene.2015.01.143](https://doi.org/10.1016/j.ijhydene.2015.01.143)
297. Iwase A, Ng YH, Amal R, Kudo A (2015) Solar hydrogen evolution using a CuGaS_2 photocathode improved by incorporating reduced graphene oxide. *J Mater Chem A* 3:8566–8570. doi:[10.1039/C5TA01237F](https://doi.org/10.1039/C5TA01237F)
298. Yu X, An X, Shavel A et al (2014) The effect of the Ga content on the photocatalytic hydrogen evolution of $\text{CuIn}_{1-x}\text{Ga}_x\text{S}_2$ nanocrystals. *J Mater Chem A* 2:12317–12322. doi:[10.1039/C4TA01315H](https://doi.org/10.1039/C4TA01315H)
299. Kato T, Hakari Y, Ikeda S et al (2015) Utilization of metal sulfide material of $(\text{CuGa})_{1-x}\text{Zn}_x\text{S}_2$ solid solution with visible light response in photocatalytic and photoelectrochemical solar water splitting systems. *J Phys Chem Lett* 6:1042–1047. doi:[10.1021/acs.jpclett.5b00137](https://doi.org/10.1021/acs.jpclett.5b00137)
300. Kandiel TA, Hutton GA, Reisner E (2016) Visible light driven hydrogen evolution with a noble metal free $\text{CuGa}_2\text{In}_3\text{S}_8$ nanoparticle system in water. *Catal Sci Technol* 6:6536–6541. doi:[10.1039/c6cy01103a](https://doi.org/10.1039/c6cy01103a)
301. Quintans CS, Kato H, Kobayashi M et al (2015) Improvement of hydrogen evolution under visible light over $\text{Zn}_{1-2x}(\text{CuGa})_x\text{Ga}_2\text{S}_4$ photocatalysts by synthesis utilizing a polymerizable complex method. *J Mater Chem A* 3:14239–14244. doi:[10.1039/C5TA02114F](https://doi.org/10.1039/C5TA02114F)
302. Chen F, Zai J, Xu M, Qian X (2013) 3D-hierarchical Cu_3SnS_4 flowerlike micro-spheres: controlled synthesis, formation mechanism and photocatalytic activity for H_2 evolution from water. *J Mater Chem A* 1:4316–4323. doi:[10.1039/C3TA01491F](https://doi.org/10.1039/C3TA01491F)
303. Kush P, Deori K, Kumar A, Deka S (2015) Efficient hydrogen/oxygen evolution and photocatalytic dye degradation and reduction of aqueous Cr(VI) by surfactant free hydrophilic $\text{Cu}_2\text{ZnSnS}_4$ nanoparticles. *J Mater Chem A* 3:8098–8106. doi:[10.1039/C4TA06551D](https://doi.org/10.1039/C4TA06551D)
304. Yu X, Shavel A, An X et al (2014) $\text{Cu}_2\text{ZnSnS}_4$ -Pt and $\text{Cu}_2\text{ZnSnS}_4$ -Au heterostructured nanoparticles for photocatalytic water splitting and pollutant degradation. *J Am Chem Soc* 136:9236–9239. doi:[10.1021/ja502076b](https://doi.org/10.1021/ja502076b)
305. Gonce MK, Dogru M, Aslan E et al (2015) Photocatalytic hydrogen evolution based on $\text{Cu}_2\text{ZnSnS}_4$, $\text{Cu}_2\text{ZnSnSe}_4$ and $\text{Cu}_2\text{ZnSnSe}_{4-x}\text{S}_x$ nanofibers. *RSC Adv* 5:94025–94028. doi:[10.1039/c5ra18877f](https://doi.org/10.1039/c5ra18877f)

306. Yu X, An X, Genç A et al (2015) $\text{Cu}_2\text{ZnSnS}_4$ -PtM (M = Co, Ni) nanoheterostructures for photocatalytic hydrogen evolution. *J Phys Chem C* 119:21882–21888. doi:[10.1021/acs.jpcc.5b06199](https://doi.org/10.1021/acs.jpcc.5b06199)
307. Zhang ZX, Chong RF, Meng YN et al (2015) High temperature recrystallization of kersterite $\text{Cu}_2\text{ZnSnS}_4$ towards enhanced photocatalytic H_2 evolution. *Inter J Hydrogen En* 40:13456–13462. doi:[10.1016/j.ijhydene.2015.08.032](https://doi.org/10.1016/j.ijhydene.2015.08.032)
308. Zheng L, Xu Y, Song Y et al (2009) Nearly monodisperse CuInS_2 hierarchical micro-architectures for photocatalytic H_2 evolution under visible light. *Inorg Chem* 48:4003–4009. doi:[10.1021/ic802399f](https://doi.org/10.1021/ic802399f)
309. Gannouni M, Assaker IB, Chtourou R (2015) Photoelectrochemical cell based on n- CuInS_8 film as photoanodes for photocatalytic water splitting. *Inter J Hydrogen En* 40:7252–7259. doi:[10.1016/j.ijhydene.2015.04.057](https://doi.org/10.1016/j.ijhydene.2015.04.057)
310. Guan Z, Luo W, Feng J et al (2015) Selective etching of metastable phase induced an efficient $\text{CuIn}_{0.7}\text{Ga}_{0.3}\text{S}_2$ nano-photocathode for solar water splitting. *J Mater Chem A* 3:7840–7848. doi:[10.1039/C5TA01259G](https://doi.org/10.1039/C5TA01259G)
311. Hu P, Ngaw CK, Tay YY et al (2015) A “uniform” heterogeneous photocatalyst: integrated p–n type $\text{CuInS}_2/\text{NaInS}_2$ nanosheets by partial ion exchange reaction for efficient H_2 evolution. *Chem Commun* 51:9381–9384. doi:[10.1039/C5CC02237A](https://doi.org/10.1039/C5CC02237A)
312. Zhang X, Du Y, Zhou Z, Guo L (2010) A simplified method for synthesis of band-structure-controlled $(\text{CuIn})_x\text{Zn}_{2(1-x)}\text{S}_2$ solid solution photocatalysts with high activity of photocatalytic H_2 evolution under visible-light irradiation. *Inter J Hydrogen En* 35:3313–3321. doi:[10.1016/j.ijhydene.2010.01.111](https://doi.org/10.1016/j.ijhydene.2010.01.111)
313. Zhang X, Yang M, Zhao J, Guo L (2013) Photocatalytic hydrogen evolution with simultaneous degradation of organics over $(\text{CuIn})_{0.2}\text{Zn}_{1.6}\text{S}_2$ solid solution. *Inter J Hydrogen En* 38:15985–15991. doi:[10.1016/j.ijhydene.2013.10.014](https://doi.org/10.1016/j.ijhydene.2013.10.014)
314. Huang Y, Chen J, Zou W et al (2015) Enhanced photocatalytic hydrogen evolution efficiency using hollow microspheres of $(\text{CuIn})_x\text{Zn}_{2(1-x)}\text{S}_2$ solid solutions. *Dalton Trans* 44:10991–10996. doi:[10.1039/C5DT01269D](https://doi.org/10.1039/C5DT01269D)
315. Lin y, Zhang F, Pan D (2012) A facile route to $(\text{ZnS})_x(\text{CuInS}_2)_{1-x}$ hierarchical microspheres with excellent water-splitting ability. *J Mater Chem* 22:22619–22623. doi:[10.1039/C2JM35166H](https://doi.org/10.1039/C2JM35166H)
316. Tang X, Tay Q, Chen Z et al (2013) Cu–In–Zn–S nanoporous spheres for highly efficient visible-light-driven photocatalytic hydrogen evolution. *New J Chem* 37:1878–1882. doi:[10.1039/C3NJ00266G](https://doi.org/10.1039/C3NJ00266G)
317. Xu M, Zai J, Yuan Y, Qian X (2012) Band gap-tunable $(\text{CuIn})_x\text{Zn}_{2(1-x)}\text{S}_2$ solid solutions: preparation and efficient photocatalytic hydrogen production from water under visible light without noble metals. *J Mater Chem* 22:23929–23934. doi:[10.1039/C2JM35375J](https://doi.org/10.1039/C2JM35375J)
318. Tang X, Tay Q, Chen Z et al (2013) CuInZnS -decorated graphene nanosheets for highly efficient visible-light-driven photocatalytic hydrogen production. *J Mater Chem A* 1:6359–6365. doi:[10.1039/C3TA01602A](https://doi.org/10.1039/C3TA01602A)
319. Zhang G, Zhang W, Wang P et al (2013) Stability of an H_2 -producing photo-catalyst $(\text{Ru}/(\text{CuAg})_{0.15}\text{In}_{0.3}\text{Zn}_{1.4}\text{S}_2)$ in aqueous solution under visible light irradiation. *Inter J Hydrogen En* 38:1286–1296. doi:[10.1016/j.ijhydene.2012.11.033](https://doi.org/10.1016/j.ijhydene.2012.11.033)
320. Zhang G, Zhang W, Minakata D et al (2013) The pH effects on H_2 evolution kinetics for visible light water splitting over the $\text{Ru}/(\text{CuAg})_{0.15}\text{In}_{0.3}\text{Zn}_{1.4}\text{S}_2$ photocatalyst. *Inter J Hydrogen En* 38:11727–11736. doi:[10.1016/j.ijhydene.2013.06.140](https://doi.org/10.1016/j.ijhydene.2013.06.140)
321. Tsuji I, Kato H, Kudo A (2006) Photocatalytic hydrogen evolution on $\text{ZnS} - \text{CuInS}_2 - \text{AgInS}_2$ solid solution photocatalysts with wide visible light absorption bands. *Chem Mater* 18:1969–1975. doi:[10.1021/cm0527017](https://doi.org/10.1021/cm0527017)
322. Tsuji I, Kato H, Kobayashi H, Kudo A (2005) Photocatalytic H_2 evolution under visible-light irradiation over band-structure-controlled $(\text{CuIn})_x\text{Zn}_{2(1-x)}\text{S}_2$ solid solutions. *J Phys Chem B* 109:7323–7329. doi:[10.1021/jp044722e](https://doi.org/10.1021/jp044722e)

323. Li Y, Chen G, Zhou C, Sun J (2009) A simple template-free synthesis of nanoporous ZnS–In₂S₃–Ag₂S solid solutions for highly efficient photocatalytic H₂ evolution under visible light. *Chem Commun* 2020–2022. doi:[10.1039/B819300B](https://doi.org/10.1039/B819300B)
324. Kudo A, Tsuji I, Kato H (2002) AgInZn₇S₉ solid solution photocatalyst for H₂ evolution from aqueous solutions under visible light irradiation. *Chem Commun* 1958–1959. doi:[10.1039/B204259B](https://doi.org/10.1039/B204259B)
325. Kale BB, Baeg JO, Lee SM et al (2006) CdIn₂S₄ nanotubes and “marigold” nanostructures: a visible-light photocatalyst. *Adv Func Mater* 16:1349–1354. doi:[10.1002/adfm.200500525](https://doi.org/10.1002/adfm.200500525)
326. Yu Y, Chen G, Wang G, Lv Z (2013) Visible-light-driven ZnIn₂S₄/CdIn₂S₄ composite photocatalyst with enhanced performance for photocatalytic H₂ evolution. *Inter J Hydrogen En* 38:1278–1285. doi:[10.1016/j.ijhydene.2012.11.020](https://doi.org/10.1016/j.ijhydene.2012.11.020)
327. Chen X, Li L, Zhang W et al (2016) Fabricate globular flower-like CuS/CdIn₂S₄/ZnIn₂S₄ with high visible light response via microwave-assisted one – step method and its multipathway photoelectron migration properties for hydrogen evolution and pollutant degradation. *ACS Sustainable Chem Eng* 4:6680–6688. doi:[10.1021/acssuschemeng.6b01543](https://doi.org/10.1021/acssuschemeng.6b01543)
328. Mei Z, Ouyang S, Tang DM et al (2013) An ion-exchange route for the synthesis of hierarchical In₂S₃/ZnIn₂S₄ bulk composite and its photocatalytic activity under visible-light irradiation. *Dalton Trans* 42:2687–2690. doi:[10.1039/C2DT32271D](https://doi.org/10.1039/C2DT32271D)
329. Hou J, Yang C, Cheng H et al (2013) Ternary 3D architectures of CdS QDs/graphene/ZnIn₂S₄ heterostructures for efficient photocatalytic H₂ production. *Phys Chem Chem Phys* 15:15660–15668. doi:[10.1039/C3CP51857D](https://doi.org/10.1039/C3CP51857D)
330. Chen D, Ye J (2007) Photocatalytic H₂ evolution under visible light irradiation on AgIn₅S₈ photocatalyst. *J Phys Chem Sol* 68:2317–2320. doi:[10.1016/j.jpcs.2007.07.059](https://doi.org/10.1016/j.jpcs.2007.07.059)
331. Kudo A, Nagane A, Tsuji I, Kato H (2002) H₂ evolution from aqueous potassium sulfite solutions under visible light irradiation over a novel sulfide photocatalyst NaInS₂ with a layered structure. *Chem Lett* 31:882–883. doi:[10.1246/cl.2002.882](https://doi.org/10.1246/cl.2002.882)
332. Shen S, Guo L (2006) Structural, textural and photocatalytic properties of quantum-sized In₂S₃-sensitized Ti-MCM-41 prepared by ion-exchange and sulfidation methods. *J Sol State Chem* 179:2629–2635. doi:[10.1016/j.jssc.2006.05.010](https://doi.org/10.1016/j.jssc.2006.05.010)
333. Li S, Wang C, Qiu H (2015) Single- and few-layer ZrS₂ as efficient photocatalysts for hydrogen production under visible light. *Inter J Hydrogen En* 40:15503–15509. doi:[10.1016/j.ijhydene.2015.08.110](https://doi.org/10.1016/j.ijhydene.2015.08.110)
334. Wang F, Shifa TA, Zhan X et al (2015) Recent advances in transition-metal dichalcogenide based nanomaterials for water splitting. *Nanoscale* 7:19764–19788. doi:[10.1039/c5nr06718a](https://doi.org/10.1039/c5nr06718a)
335. Lin Z, Ning S, Yang Z et al (2016) Large-scale preparation of heterometallic chalcogenide MnSb₂S₄ monolayer nanosheets with a high visible-light photocatalytic activity for H₂ evolution. *Chem Commun* 52:13381–13384. doi:[10.1039/c6cc07127a](https://doi.org/10.1039/c6cc07127a)
336. Bessekhouad Y, Mohammedi M, Trari M (2002) Hydrogen photoproduction from hydrogen sulfide on Bi₂S₃ catalyst. *Sol En Mater Sol Cells* 73:339–350. doi:[10.1016/S0927-0248\(01\)00218-5](https://doi.org/10.1016/S0927-0248(01)00218-5)
337. Abdi A, Denoyelle A, Commenges-Bernole M, Trari M (2013) Photocatalytic hydrogen evolution on new mesoporous material Bi₂S₃/Y-zeolite. *Inter J Hydrogen En* 38:2070–2078. doi:[10.1016/j.ijhydene.2012.11.085](https://doi.org/10.1016/j.ijhydene.2012.11.085)
338. Zhang K, Jing D, Xing C, Guo L (2007) Significantly improved photocatalytic hydrogen production activity over Cd_{1-x}Zn_xS photocatalysts prepared by a novel thermal sulfuration method. *Inter J Hydrogen En* 32:4685–4691. doi:[10.1016/j.ijhydene.2007.08.022](https://doi.org/10.1016/j.ijhydene.2007.08.022)
339. del Valle F, Ishikawa A, Domen K et al (2009) Influence of Zn concentration in the activity of Cd_{1-x}Zn_xS solid solutions for water splitting under visible light. *Catal Today* 143:51–56. doi:[10.1016/j.cattod.2008.09.024](https://doi.org/10.1016/j.cattod.2008.09.024)
340. Chan CC, Chang CC, Hsu CH et al (2014) Efficient and stable photocatalytic hydrogen production from water splitting over Zn_xCd_{1-x}S solid solutions under visible light irradiation. *Inter J Hydrogen En* 39:1630–1639. doi:[10.1016/j.ijhydene.2013.11.059](https://doi.org/10.1016/j.ijhydene.2013.11.059)

341. Du H, Liang K, Yuan CZ et al (2016) Bare $\text{Cd}_{1-x}\text{Zn}_x\text{S}$ ZB/WZ heterophase nano-junctions for visible light photocatalytic hydrogen production with high efficiency. *ACS Appl Mater Interfaces* 8:24550–24558. doi:[10.1021/acsami.6b06182](https://doi.org/10.1021/acsami.6b06182)
342. Roy AM, De GC (2003) Immobilisation of CdS, ZnS and mixed ZnS–CdS on filter paper: effect of hydrogen production from alkaline $\text{Na}_2\text{S}/\text{Na}_2\text{S}_2\text{O}_3$ solution. *J Photochem Photobiol A* 157:87–92. doi:[10.1016/S1010-6030\(02\)00430-6](https://doi.org/10.1016/S1010-6030(02)00430-6)
343. Zhang X, Jing D, Liu M, Guo L (2008) Efficient photocatalytic H_2 production under visible light irradiation over Ni doped $\text{Cd}_{1-x}\text{Zn}_x\text{S}$ microsphere photocatalysts. *Catal Commun* 9:1720–1724. doi:[10.1016/j.catcom.2008.01.032](https://doi.org/10.1016/j.catcom.2008.01.032)
344. Stroyuk AL, Raevskaya AE, Korzhak AV et al (2009) Photocatalytic production of hydrogen in systems based on $\text{Cd}_x\text{Zn}_{1-x}\text{S}/\text{Ni}^0$ nanostructures. *Theoret Exp Chem* 45:12–22
345. Kimi M, Yuliati L, Shamsuddin M (2011) Photocatalytic hydrogen production under visible light over $\text{Cd}_{0.1}\text{Sn}_x\text{Zn}_{0.9-2x}\text{S}$ solid solution photocatalysts. *Inter J Hydrogen En* 36:9453–9461. doi:[10.1016/j.ijhydene.2011.05.044](https://doi.org/10.1016/j.ijhydene.2011.05.044)
346. Peng S, An R, Li Y et al (2012) Remarkable enhancement of photocatalytic hydrogen evolution over $\text{Cd}_{0.5}\text{Zn}_{0.5}\text{S}$ by bismuth-doping. *Inter J Hydrogen En* 37:1366–1374. doi:[10.1016/j.ijhydene.2011.09.140](https://doi.org/10.1016/j.ijhydene.2011.09.140)
347. Sathish M, Viswanath RP (2007) Photocatalytic generation of hydrogen over mesoporous CdS nanoparticle: effect of particle size, noble metal and support. *Catal Today* 129:421–427. doi:[10.1016/j.cattod.2006.12.008](https://doi.org/10.1016/j.cattod.2006.12.008)
348. Li Y, Du Y, Peng S et al (2008) Enhancement of photocatalytic activity of cadmium sulfide for hydrogen evolution by photoetching. *Inter J Hydrogen En* 33:2007–2013. doi:[10.1016/j.ijhydene.2008.02.023](https://doi.org/10.1016/j.ijhydene.2008.02.023)
349. Chang CM, Orchard KL, Martindale CM, Reisner E (2016) Ligand removal from CdS quantum dots for enhanced photocatalytic H_2 generation in pH neutral water. *J Mater Chem A* 4:2856–2862. doi:[10.1039/c5ta04136h](https://doi.org/10.1039/c5ta04136h)
350. Jana MK, Gupta U, Rao CNR (2016) Hydrazine as a hydrogen carrier in the photocatalytic generation of H_2 using CdS quantum dots. *Dalton Trans* 45:15137–15141. doi:[10.1039/c6dt02505f](https://doi.org/10.1039/c6dt02505f)
351. Silva LA, Ryu SY, Choi J et al (2008) Photocatalytic hydrogen production with visible light over Pt-interlinked hybrid composites of cubic-phase and hexagonal-phase CdS. *J Phys Chem C* 112:12069–12073. doi:[10.1021/jp8037279](https://doi.org/10.1021/jp8037279)
352. Li K, Han M, Chen R et al (2016) Hexagonal@Cubic CdS Core@Shell nanorod photocatalyst for highly active production of H_2 with unprecedented stability. *Adv Mater* 28:8906–8911. doi:[10.1002/adma.201601047](https://doi.org/10.1002/adma.201601047)
353. Baran MP, Korsunskaya NE, Stara TR et al (2016) Graded $\text{ZnS}/\text{Zn}_x\text{O}_{1-x}$ heterostructures produced by oxidative photolysis of zinc sulfide: structure, optical properties and photocatalytic evolution of molecular hydrogen. *J Photochem Photobiol A* 329:213–220. doi:[10.1016/j.jphotochem.2016.07.003](https://doi.org/10.1016/j.jphotochem.2016.07.003)
354. Jang JS, Joshi UA, Lee JS (2007) Solvothermal synthesis of CdS nanowires for photocatalytic hydrogen and electricity production. *J Phys Chem C* 111:13280–13287. doi:[10.1021/jp072683b](https://doi.org/10.1021/jp072683b)
355. Kida T, Guan G, Minami Y et al (2003) Photocatalytic hydrogen production from water over a $\text{LaMnO}_3/\text{CdS}$ nanocomposite prepared by the reverse micelle method. *J Mater Chem* 13:1186–1191. doi:[10.1039/B211812B](https://doi.org/10.1039/B211812B)
356. Kida T, Guan G, Yamada N et al (2004) Hydrogen production from sewage sludge solubilized in hot-compressed water using photocatalyst under light irradiation. *Inter J Hydrogen En* 29:269–274. doi:[10.1016/j.ijhydene.2003.08.007](https://doi.org/10.1016/j.ijhydene.2003.08.007)
357. Ma G, Yan H, Shi J et al (2008) Direct splitting of H_2S into H_2 and S on CdS-based photocatalyst under visible light irradiation. *J Catal* 260:134–140. doi:[10.1016/j.jcat.2008.09.017](https://doi.org/10.1016/j.jcat.2008.09.017)
358. Frame FA, Carroll EC, Larsen DS et al (2008) First demonstration of CdSe as a photocatalyst for hydrogen evolution from water under UV and visible light. *Chem Commun* 2206–2208. doi:[10.1039/B718796C](https://doi.org/10.1039/B718796C)

359. Holmes MA, Townsend TK, Osterloh FE (2012) Quantum confinement controlled photocatalytic water splitting by suspended CdSe nanocrystals. *Chem Commun* 48:371–373. doi:[10.1039/C1CC16082F](https://doi.org/10.1039/C1CC16082F)
360. Grigioni I, Bernareggi M, Sinibaldi G et al (2016) Size-dependent performance of CdSe quantum dots in the photocatalytic evolution of hydrogen under visible light irradiation. *Appl Catal A* 518:176–180. doi:[10.1016/j.apcata.2015.09.021](https://doi.org/10.1016/j.apcata.2015.09.021)
361. Zhao J, Holmes MA, Osterloh FE (2013) Quantum confinement controls photocatalysis: a free energy analysis for photocatalytic proton reduction at CdSe nanocrystals. *ACS Nano* 7:4316–4325. doi:[10.1021/nn400826h](https://doi.org/10.1021/nn400826h)
362. Rasamani KD, Li Z, Sun Y (2016) Significant enhancement of photocatalytic water splitting enabled by elimination of surface traps in Pt-tipped CdSe nanorods *Nanoscale* 8:18621–18625. doi:[10.1039/c6nr06902a](https://doi.org/10.1039/c6nr06902a)
363. Costi R, Young ER, Bulović V, Nocera DG (2013) Stabilized CdSe–CoPi composite photoanode for light-assisted water oxidation by transformation of a CdSe/Cobalt metal thin film. *ACS Appl Mater Interfaces* 5:2364–2367. doi:[10.1021/am400364u](https://doi.org/10.1021/am400364u)
364. Yang S, Xu CY, Yang L et al (2016) Solution-phase synthesis of g-In₂Se₃ nanoparticles for highly efficient photocatalytic hydrogen generation under simulated sunlight irradiation. *RSC Adv* 6:106671–106675. doi:[10.1039/c6ra21784b](https://doi.org/10.1039/c6ra21784b)
365. Gurunathan K, Baeg JO, Lee SM et al (2008) Visible light active pristine and Fe³⁺ doped CuGa₂O₄ spinel photocatalysts for solar hydrogen production. *Inter J Hydrogen En* 33:2646–2652. doi:[10.1016/j.ijhydene.2008.03.018](https://doi.org/10.1016/j.ijhydene.2008.03.018)
366. Saadi S, Bouguelia A, Derbal A, Trari M (2007) Hydrogen photoproduction over new catalyst CuLaO₂. *J Photochem Photobiol A* 187:97–104. doi:[10.1016/j.jphotochem.2006.09.017](https://doi.org/10.1016/j.jphotochem.2006.09.017)
367. Koriche N, Bouguelia A, Trari M (2006) Photocatalytic hydrogen production over new oxide CuLaO_{2.62}. *Inter J Hydrogen En* 31:1196–1203. doi:[10.1016/j.ijhydene.2005.08.015](https://doi.org/10.1016/j.ijhydene.2005.08.015)
368. Koriche N, Bouguelia A, Aider A, Trari M (2005) Photocatalytic hydrogen evolution over delafossite CuAlO₂. *Inter J Hydrogen En* 30:693–699. doi:[10.1016/j.ijhydene.2004.06.011](https://doi.org/10.1016/j.ijhydene.2004.06.011)
369. Zhou C, Zhao Y, Shang L et al (2016) Facile synthesis of ultrathin SnNb₂O₆ nanosheets towards improved visible-light photocatalytic H₂-production activity. *Chem Commun* 52:8239–8242. doi:[10.1039/c6cc03739a](https://doi.org/10.1039/c6cc03739a)
370. Ye J, Zou Z, Arakawa H et al (2002) Correlation of crystal and electronic structures with photophysical properties of water splitting photocatalysts InMO₄ (M = V⁵⁺, Nb⁵⁺, Ta⁵⁺). *J Photochem Photobiol A* 148:79–83. doi:[10.1016/S1010-6030\(02\)00074-6](https://doi.org/10.1016/S1010-6030(02)00074-6)
371. Zhu H, Fang M, Hyang Z et al (2016) Novel carbon-incorporated porous ZnFe₂O₄ nanospheres for enhanced photocatalytic hydrogen generation under visible light irradiation. *RSC Adv* 6:56069–56076. doi:[10.1039/c6ra05098k](https://doi.org/10.1039/c6ra05098k)
372. Pai YH, Tsai CT, Fang SY (2013) Enhanced photocatalytic hydrogen generation with Pt Nanoparticles on multi-phase polycrystalline microporous MnO₂ photocatalyst. *J Power Sources* 223:107–113. doi:[10.1016/j.jpowsour.2012.09.024](https://doi.org/10.1016/j.jpowsour.2012.09.024)
373. Jin S, Wang X, Ju M et al (2015) Effect of phase junction structure on the photocatalytic performance in overall water splitting: Ga₂O₃ photocatalyst as an example. *J Phys Chem C* 119:18221–18228. doi:[10.1021/acs.jpcc.5b04092](https://doi.org/10.1021/acs.jpcc.5b04092)
374. Hu C, Chu K, Zhao Y, Teoh WY (2014) Efficient photoelectrochemical water splitting over anodized p-Type NiO porous films. *ACS Appl Mater Interfaces* 6:18558–18568. doi:[10.1021/am507138b](https://doi.org/10.1021/am507138b)
375. Manikandan M, Tanabe T, Li P et al (2014) Photocatalytic water splitting under visible light by mixed-valence Sn₃O₄. *ACS Appl Mater Interfaces* 6:3790–3793. doi:[10.1021/am500157u](https://doi.org/10.1021/am500157u)
376. Tijare SN, Joshi MV, Padole PS et al (2012) Photocatalytic hydrogen generation through water splitting on nano-crystalline LaFeO₃ perovskite. *Inter J Hydrogen En* 37:10451–10456. doi:[10.1016/j.ijhydene.2012.01.120](https://doi.org/10.1016/j.ijhydene.2012.01.120)

377. May KJ, Fenning DP, Ming T et al (2015) Thickness-dependent photoelectrochemical water splitting on ultrathin LaFeO_3 films grown on Nb:SrTiO_3 . *J Phys Chem Lett* 6:977–985. doi:[10.1021/acs.jpcllett.5b00169](https://doi.org/10.1021/acs.jpcllett.5b00169)
378. Pan C, Takata T, Nakabayashi M et al (2015) A complex perovskite-type oxynitride: the first photocatalyst for water splitting operable at up to 600 nm. *Angew Chem Int Ed* 54:1–6. doi:[10.1002/anie.201410961](https://doi.org/10.1002/anie.201410961)
379. Lee CW, Kim DW, Cho IS et al (2012) Simple synthesis and characterization of SrSnO_3 nanoparticles with enhanced photocatalytic activity. *Inter J Hydrogen En* 37:10557–10563. doi:[10.1016/j.ijhydene.2012.04.063](https://doi.org/10.1016/j.ijhydene.2012.04.063)
380. Shibli SMA, Arun PS, Raj AV (2015) Exploration of octahedrally shaped MnCo_2O_4 catalyst particles for visible light driven photocatalytic water splitting reaction. *RSC Adv* 5:19393–19399. doi:[10.1039/C4RA12646G](https://doi.org/10.1039/C4RA12646G)
381. Liu J, Wen S, Zou X et al (2013) Visible-light-responsive copper(II) borate photocatalysts with intrinsic midgap states for water splitting. *J Mater Chem A* 1:1553–1556. doi:[10.1039/C2TA00522K](https://doi.org/10.1039/C2TA00522K)
382. Luan J, Guo N, Chen B (2014) Hydrogen production with $\text{Ga}_2\text{BiSbO}_7$, $\text{Fe}_2\text{BiSbO}_7$ and $\text{Gd}_2\text{BiSbO}_7$ as photocatalysts under visible light irradiation. *Inter J Hydrogen En* 39:1228–1236. doi:[10.1016/j.ijhydene.2013.11.020](https://doi.org/10.1016/j.ijhydene.2013.11.020)
383. Mahapure SA, Palei PK, Nikam LK et al (2013) Novel nanocrystalline zinc silver antimonate ($\text{ZnAg}_3\text{SbO}_4$): an efficient & ecofriendly visible light photocatalyst with enhanced hydrogen generation. *J Mater Chem A* 1:12835–12840. doi:[10.1039/C3TA12883K](https://doi.org/10.1039/C3TA12883K)
384. Guo S, Han S (2014) Constructing a novel hierarchical 3D flower-like nano/micro titanium phosphate with efficient hydrogen evolution from water splitting. *J Power Sources* 267:9–13. doi:[10.1016/j.jpowsour.2014.05.011](https://doi.org/10.1016/j.jpowsour.2014.05.011)
385. Wang G, Jing Y, Ju J et al (2015) $\text{Ga}_4\text{B}_2\text{O}_9$: an efficient borate photocatalyst for overall water splitting without cocatalyst. *Inorg Chem* 54:2945–2949. doi:[10.1021/ic5031087](https://doi.org/10.1021/ic5031087)
386. Liang J, Xu J, Gu Q et al (2013) A novel Zn_2GeO_4 superstructure for effective photocatalytic hydrogen generation. *J Mater Chem A* 1:7798–7805. doi:[10.1039/C3TA11374D](https://doi.org/10.1039/C3TA11374D)
387. Yan S, Wan L, Li Z, Zou Z (2011) Facile temperature-controlled synthesis of hexagonal Zn_2GeO_4 nanorods with different aspect ratios toward improved photocatalytic activity for overall water splitting and photoreduction of CO_2 . *Chem Commun* 47:5632–5634. doi:[10.1039/C1CC10513B](https://doi.org/10.1039/C1CC10513B)
388. Pan B, Xie Q, Wang H et al (2013) Synthesis and photocatalytic hydrogen production of a novel photocatalyst LaCO_3OH . *J Mater Chem A* 1:6629–6634. doi:[10.1039/C3TA01553J](https://doi.org/10.1039/C3TA01553J)
389. Ruiz-Gomez MA, Torres-Martinez LM, Figueroa-Torres MZ et al (2013) Hydrogen evolution from pure water over a new advanced photocatalyst $\text{Sm}_2\text{GaTaO}_7$. *Inter J Hydrogen En* 38:12554–12561. doi:[10.1016/j.ijhydene.2012.11.131](https://doi.org/10.1016/j.ijhydene.2012.11.131)
390. Ye J, Zou Z, Oshikiri M et al (2002) A novel hydrogen-evolving photocatalyst InVO_4 active under visible light irradiation. *Chem Phys Lett* 356:221–226. doi:[10.1016/S0009-2614\(02\)00254-3](https://doi.org/10.1016/S0009-2614(02)00254-3)
391. Lv M, Liu G, Xu X (2016) Homologous compounds $\text{Zn}_n\text{In}_2\text{O}_{3+n}$ ($n = 4, 5$, and 7) containing laminated functional groups as efficient photocatalysts for hydrogen production. *ACS Appl Mater Interfaces* 8:28700–28708. doi:[10.1021/acsami.6b10951](https://doi.org/10.1021/acsami.6b10951)
392. Huang Q, Ye Z, Xiao X (2015) Recent progress in photocathodes for hydrogen evolution. *J Mater Chem A* 3:15824–15837. doi:[10.1039/c5ta03594e](https://doi.org/10.1039/c5ta03594e)
393. Luo J, Steier L, Son MK et al (2016) Cu_2O nanowire photocathodes for efficient and durable solar water splitting. *Nano Lett* 16:1848–1857. doi:[10.1021/acs.nanolett.5b04929](https://doi.org/10.1021/acs.nanolett.5b04929)
394. Dubale AA, Su WN, Tamirat AG et al (2014) The synergetic effect of graphene on Cu_2O nanowire arrays as a highly efficient hydrogen evolution photocathode in water splitting. *J Mater Chem A* 2:18383–18397. doi:[10.1039/c4ta03464c](https://doi.org/10.1039/c4ta03464c)
395. Dubale AA, Tamirat AG, Chen H-M (2016) A highly stable CuS and CuS–Pt modified $\text{Cu}_2\text{O}/\text{CuO}$ heterostructure as an efficient photocathode for the hydrogen evolution reaction. *J Mater Chem A* 4:2205–2216. doi:[10.1039/c5ta09464j](https://doi.org/10.1039/c5ta09464j)

396. Dong Y, Chen Y, Jiang P et al (2016) A novel g-C₃N₄ based photocathode for photoelectrochemical hydrogen evolution. *RSC Adv* 6:7465–7473. doi:[10.1039/c5ra23265a](https://doi.org/10.1039/c5ra23265a)
397. Basu M, Zhang ZW, Chen CJ et al (2016) CoSe₂ embedded in C₃N₄: an efficient photocathode for photoelectrochemical water splitting. *ACS Appl Mater Interfaces* 8:26690–26696. doi:[10.1021/acsami.6b06520](https://doi.org/10.1021/acsami.6b06520)
398. Li S, Zhang P, Song X, Gao L (2015) Photoelectrochemical hydrogen production of TiO₂ passivated Pt/Si-nanowire composite photocathode. *ACS Appl Mater Interfaces* 7:18560–18565. doi:[10.1021/acsami.5b04936](https://doi.org/10.1021/acsami.5b04936)
399. Bao XQ, Cerqueira MF, Alpuimab P, Liu L (2015) Silicon nanowire arrays coupled with cobalt phosphide spheres as low-cost photocathodes for efficient solar hydrogen evolution. *Chem Commun* 51:10742–10745. doi:[10.1039/c5cc02331a](https://doi.org/10.1039/c5cc02331a)
400. Lewis NS (2016) Developing a scalable artificial photosynthesis technology through nanomaterials by design. *Nat Nanotechnol* 11:1010–1019. doi:[10.1038/nnano.2016.194](https://doi.org/10.1038/nnano.2016.194)
401. Chandrasekaran S, McInnes SJP, Macdonald TJ (2015) Porous silicon nanoparticles as a nanophotocathode for photoelectrochemical water splitting. *RSC Adv* 5:85978–85982. doi:[10.1039/c5ra12559f](https://doi.org/10.1039/c5ra12559f)
402. Reece SY, Hamel JA, Sung K, Jarvi TD, Esswein AJ, Pijpers JJH, Nocera DG (2011) Wireless solar water splitting using silicon-based semiconductors and earth-abundant catalysts. *Science* 34:645–648. doi:[10.1126/science.1209816](https://doi.org/10.1126/science.1209816)
403. Patra BK, Khilari S, Pradhan D, Pradhan N (2016) Hybrid dot-disk Au-CuInS₂ nanostructures as active photocathode for efficient evolution of hydrogen from water. *Chem Mater* 28:4358–4366. doi:[10.1021/acs.chemmater.6b01357](https://doi.org/10.1021/acs.chemmater.6b01357)
404. Chae SY, Park SJ, Han SG et al (2016) Enhanced photocurrents with ZnS passivated Cu(In, Ga)(Se, S)₂ photocathodes synthesized using a nonvacuum process for solar water splitting. *J Am Chem Soc* 138:15673–15681. doi:[10.1021/jacs.6b09595](https://doi.org/10.1021/jacs.6b09595)
405. Kaneko H, Minegishi T, Nakabayashi M et al (2016) Enhanced hydrogen evolution under simulated sunlight from neutral electrolytes on (ZnSe)_{0.85}(CuIn_{0.7}Ga_{0.3}Se₂)_{0.15} photocathodes prepared by a bilayer method. *Angew Chem Int Ed* 55:15329–15333. doi:[10.1002/anie.201609202](https://doi.org/10.1002/anie.201609202)
406. Abe T, Fukui K, Kawai Y et al (2016) A water splitting system using an organophotocathode and titanium dioxide photoanode capable of bias-free H₂ and O₂ evolution. *Chem Commun* 52:7735–7737. doi:[10.1039/c6cc01225f](https://doi.org/10.1039/c6cc01225f)
407. Hu Z, Yuan L, Liu Z et al (2016) An elemental phosphorus photocatalyst with a record high hydrogen evolution efficiency. *Angew Chem Int Ed* 55:9580–9585. doi:[10.1002/anie.201603331](https://doi.org/10.1002/anie.201603331)
408. Dang H, Dong X, Dong Y et al (2014) Enhancing the photocatalytic H₂ evolution activity of red phosphorous by using noble-metal-free Ni(OH)₂ under photoexcitation up to 700 nm. *RSC Adv* 4:44823–44826. doi:[10.1039/c4ra06867j](https://doi.org/10.1039/c4ra06867j)
409. Gao Y, Wang Y, Wang Y (2007) Photocatalytic hydrogen evolution from water on SiC under visible light irradiation. *React Kin Catal Lett* 91:13–19. doi:[10.1007/s11144-007-5064-x](https://doi.org/10.1007/s11144-007-5064-x)
410. Wang M, Chen J, Liao X et al (2014) Highly efficient photocatalytic hydrogen production of platinum nanoparticle-decorated SiC nanowires under simulated sunlight irradiation. *Inter J Hydrogen En* 39:14581–14587. doi:[10.1016/j.ijhydene.2014.07.068](https://doi.org/10.1016/j.ijhydene.2014.07.068)
411. Wang D, Guo Z, Peng Y, Yuan W (2015) Visible light induced photocatalytic overall water splitting over micro-SiC driven by the Z-scheme system. *Catal Commun* 61:53–56. doi:[10.1016/j.catcom.2014.12.008](https://doi.org/10.1016/j.catcom.2014.12.008)
412. Wang Y, Guo X, Dong L et al (2013) Enhanced photocatalytic performance of chemically bonded SiC-graphene composites for visible-light-driven overall water splitting. *Inter J Hydrogen En* 38:12733–12738. doi:[10.1016/j.ijhydene.2013.07.062](https://doi.org/10.1016/j.ijhydene.2013.07.062)
413. Liu H, She G, Mu L, Shi W (2012) Porous SiC nanowire arrays as stable photocatalyst for water splitting under UV irradiation. *Mater Res Bull* 47:917–920. doi:[10.1016/j.materresbull.2011.12.046](https://doi.org/10.1016/j.materresbull.2011.12.046)

414. Wang B, Wang Y, Lei Y et al (2016) Mesoporous silicon carbide nanofibers with in situ embedded carbon for co-catalyst free photocatalytic hydrogen production. *Nano Res* 9:886–898. doi:[10.1007/s12274-015-0971-z](https://doi.org/10.1007/s12274-015-0971-z)
415. Kida T, Minami Y, Guan G et al (2006) Photocatalytic activity of gallium nitride for producing hydrogen from water under light irradiation. *J Mater Sci* 41:3527–3534. doi:[10.1007/s10853-005-5655-8](https://doi.org/10.1007/s10853-005-5655-8)
416. Yoshimizu M, Kobayashi R, Saegusa M et al (2015) Photocatalytic hydrogen evolution over β -iron silicide under infrared-light irradiation. *Chem Commun* 51:2818–2820. doi:[10.1039/C4CC08093A](https://doi.org/10.1039/C4CC08093A)
417. Yoneyama H, Matsumoto N, Tamura H (1986) Photocatalytic decomposition of formic acid on platinized n-type silicon powder in aqueous solution. *Bull Chem Soc Jpn* 59:3302–3304. doi:[10.1246/bcsj.59.3302](https://doi.org/10.1246/bcsj.59.3302)
418. Jang YJ, Ryu J, Hong D et al (2016) A multi-stacked hyperporous silicon flake for highly active solar hydrogen production. *Chem Commun* 52:10221–10224. doi:[10.1039/c6cc04775k](https://doi.org/10.1039/c6cc04775k)
419. Zhang H, Li A, Wang Z et al (2016) Decorating mesoporous silicon with amorphous metal–phosphorous-derived nanocatalysts towards enhanced photoelectrochemical water reduction. *J Mater Chem A* 4:14960–14967. doi:[10.1039/c6ta05725j](https://doi.org/10.1039/c6ta05725j)
420. Lv C, Chen Z, Chen Z et al (2015) Silicon nanowires loaded with iron phosphide for effective solar-driven hydrogen production. *J Mater Chem A* 3:17669–17675. doi:[10.1039/c5ta03438h](https://doi.org/10.1039/c5ta03438h)
421. Li S, Wang H, Li D et al (2016) Siloxene nanosheets: a metal-free semiconductor for water splitting. *J Mater Chem A* 4:15841–15844. doi:[10.1039/c6ta07545b](https://doi.org/10.1039/c6ta07545b)
422. Mou Z, Yin S, Zhu M et al (2013) $\text{RuO}_2/\text{TiSi}_2$ /graphene composite for enhanced photocatalytic hydrogen generation under visible light irradiation. *Phys Chem Chem Phys* 15:2793–2799. doi:[10.1039/c2cp44270a](https://doi.org/10.1039/c2cp44270a)
423. Wu W, Zhan L, Ohkubo K et al (2015) Photocatalytic H_2 evolution from NADH with carbon quantum dots/Pt and 2-phenyl-4-(1-naphthyl)quinolinium ion. *J Photochem Photobiol, B* 152:63–70. doi:[10.1016/j.jphotobiol.2014.10.018](https://doi.org/10.1016/j.jphotobiol.2014.10.018)
424. Liu Q, Chen T, Guo Y et al (2016) Ultrathin g- C_3N_4 nanosheets coupled with carbon nanodots as 2D/0D composites for efficient photocatalytic H_2 evolution. *Appl Catal B* 193:248–258. doi:[10.1016/j.apcatb.2016.04.034](https://doi.org/10.1016/j.apcatb.2016.04.034)
425. Yang P, Zhao J, Wang J et al (2015) Pure carbon nanodots for excellent photocatalytic hydrogen generation. *RSC Adv* 5:21332–21335. doi:[10.1039/c5ra01924a](https://doi.org/10.1039/c5ra01924a)
426. Ming H, Ma Z, Liu Y et al (2012) Large scale electrochemical synthesis of high quality carbon nanodots and their photocatalytic property. *Dalton Trans* 41:9526–9531. doi:[10.1039/C2DT30985H](https://doi.org/10.1039/C2DT30985H)
427. Zhao S, Li C, Wang L et al (2016) Carbon quantum dots modified MoS_2 with visible-light-induced high hydrogen evolution catalytic ability. *Carbon* 99:599–606. doi:[10.1016/j.carbon.2015.12.088](https://doi.org/10.1016/j.carbon.2015.12.088)
428. Wang J, Ng YH, Lim YF, Ho GW (2014) Vegetable-extracted carbon dots and their nanocomposites for enhanced photocatalytic H_2 production. *RSC Adv* 4:44117–44123. doi:[10.1039/c4ra07290a](https://doi.org/10.1039/c4ra07290a)
429. Thomas A, Fischer A, Goettmann F et al (2008) Graphitic carbon nitride materials: variation of structure and morphology and their use as metal-free catalysts. *J Mater Chem* 18:4893–4908. doi:[10.1039/b800274f](https://doi.org/10.1039/b800274f)
430. Zhou L, Zhang H, Sun H et al (2016) Recent advances in non-metal modification of graphitic carbon nitride for photocatalysis: a historic review. *Catal Sci Technol* 6:002–7023. doi:[10.1039/c6cy01195k](https://doi.org/10.1039/c6cy01195k)
431. Wen J, Xie J, Chen X, Li X (2017) A review on g- C_3N_4 -based photocatalysts. *Appl Surf Sci* 391:72–123. doi:[10.1016/j.apsusc.2016.07.030](https://doi.org/10.1016/j.apsusc.2016.07.030)
432. Zheng Y, Lin L, Wang B, Wang X (2015) Graphitic carbon nitride polymers toward sustainable photoredox catalysis. *Angew Chem Int Ed* 54:12868–12884. doi:[10.1002/anie.201501788](https://doi.org/10.1002/anie.201501788)

433. Wang X, Blechert S, Antonietti M (2012) Polymeric graphitic carbon nitride for heterogeneous photocatalysis. *ACS Catal* 2:1596–1606. doi:[10.1021/cs300240x](https://doi.org/10.1021/cs300240x)
434. Zhu J, Xiao P, Li H, Carabineiro SA (2014) Graphitic carbon nitride: synthesis, properties, and applications in catalysis. *ACS Appl Mater Interfaces* 6:16449–16465. doi:[10.1021/am502925j](https://doi.org/10.1021/am502925j)
435. Liu J, Wang H, Antonietti M (2016) Graphitic carbon nitride “reloaded”: emerging applications beyond (photo)catalysis. *Chem Soc Rev* 45:2308–2326. doi:[10.1039/C5CS00767D](https://doi.org/10.1039/C5CS00767D)
436. Patnaik S, Martha S, Parida KM (2016) An overview of the structural, textural and morphological modulations of g-C₃N₄ towards photocatalytic hydrogen production. *RSC Adv* 6:46929–46951. doi:[10.1039/c5ra26702a](https://doi.org/10.1039/c5ra26702a)
437. Zhang G, Wang X (2013) A facile synthesis of covalent carbon nitride photocatalysts by Co-polymerization of urea and phenylurea for hydrogen evolution. *J Catal* 307:246–253. doi:[10.1016/j.jcat.2013.07.026](https://doi.org/10.1016/j.jcat.2013.07.026)
438. Chuang PK, Wu KH, Yeh TF, Teng H (2016) Extending the π -Conjugation of g-C₃N₄ by Incorporating Aromatic Carbon for Photocatalytic H₂ Evolution from Aqueous Solution. *ACS Sustainable Chem Eng* 4:5989–5997. doi:[10.1021/acssuschemeng.6b01266](https://doi.org/10.1021/acssuschemeng.6b01266)
439. Fan X, Zhang L, Cheng R et al (2015) Construction of graphitic C₃N₄-based intramolecular donor – acceptor conjugated copolymers for photocatalytic hydrogen evolution. *ACS Catal* 5:5008–5015. doi:[10.1021/acscatal.5b01155](https://doi.org/10.1021/acscatal.5b01155)
440. Cao S, Yu J (2014) g-C₃N₄-based photocatalysts for hydrogen generation. *J Phys Chem Lett* 5:2101–2107. doi:[10.1021/jz500546b](https://doi.org/10.1021/jz500546b)
441. Wang X, Maeda K, Chen X et al (2009) Polymer semiconductors for Artificial photosynthesis: hydrogen evolution by mesoporous graphitic carbon nitride with visible light. *J Am Chem Soc* 131:1680–1681. doi:[10.1021/ja809307s](https://doi.org/10.1021/ja809307s)
442. Zheng D, Zhang G, Hou Y, Wang X (2016) Layering MoS₂ on soft hollow g-C₃N₄ nanostructures for photocatalytic hydrogen evolution. *Appl Catal A* 521:2–8. doi:[10.1016/j.apcata.2015.10.037](https://doi.org/10.1016/j.apcata.2015.10.037)
443. Liang Q, Li Z, Yu X et al (2015) Macroscopic 3D porous graphitic carbon nitride monolith for enhanced photocatalytic hydrogen evolution. *Adv Mater* 27:4634–4639. doi:[10.1002/adma.201502057](https://doi.org/10.1002/adma.201502057)
444. He F, Chen G, Zhou Y et al (2015) The facile synthesis of mesoporous g-C₃N₄ with highly enhanced photocatalytic H₂ evolution performance. *Chem Commun* 51:16244–16246. doi:[10.1039/c5cc06713h](https://doi.org/10.1039/c5cc06713h)
445. Shen S, Zhao D, Chen J et al (2016) Enhanced photocatalytic hydrogen evolution over graphitic carbon nitride modified with Ti-activated mesoporous silica. *Appl Catal A* 521:111–117. doi:[10.1016/j.apcata.2015.11.004](https://doi.org/10.1016/j.apcata.2015.11.004)
446. Qiao S, Mitchell RW, Coulson B et al (2016) Pore confinement effects and stabilization of carbon nitride oligomers in macroporous silica for photocatalytic hydrogen production. *Carbon* 106:320–329. doi:[10.1016/j.carbon.2016.05.039](https://doi.org/10.1016/j.carbon.2016.05.039)
447. Chen X, Jun YS, Takanabe K et al (2009) Ordered mesoporous SBA-15 type graphitic carbon nitride: a semiconductor host structure for photocatalytic hydrogen evolution with visible light. *Chem Mater* 21:4093–4095. doi:[10.1021/cm902130z](https://doi.org/10.1021/cm902130z)
448. Xu L, Jin B, Zhang J et al (2016) Efficient hydrogen generation from formic acid using AgPd nanoparticles immobilized on carbon nitride-functionalized SBA-15. *RSC Adv* 6:46908–46914. doi:[10.1039/c6ra06071d](https://doi.org/10.1039/c6ra06071d)
449. Cheng R, Fan X, Wang M et al (2016) Facile construction of CuFe₂O₄/g-C₃N₄ photocatalyst for enhanced visible-light hydrogen evolution. *RSC Adv* 6:18990–18995. doi:[10.1039/c5ra27221a](https://doi.org/10.1039/c5ra27221a)
450. Tong J, Zhang L, Li F et al (2015) Rapid and high-yield production of g-C₃N₄ nanosheets via chemical exfoliation for photocatalytic H₂ evolution. *RSC Adv* 5:88149–88153. doi:[10.1039/c5ra16988g](https://doi.org/10.1039/c5ra16988g)

451. Han Q, Wang B, Gao J et al (2016) Atomically thin mesoporous nanomesh of graphitic C_3N_4 for high-efficiency photocatalytic hydrogen evolution. *ACS Nano* 10:2745–2751. doi:[10.1021/acsnano.5b07831](https://doi.org/10.1021/acsnano.5b07831)
452. Fan M, Song C, Chen T et al (2016) Visible-light-driven high photocatalytic activities of Cu/g- C_3N_4 photocatalysts for hydrogen production. *RSC Adv* 6:34633–34640. doi:[10.1039/c5ra27755h](https://doi.org/10.1039/c5ra27755h)
453. Bi L, Meng D, Bu Q et al (2016) Electron acceptor of Ni decorated porous carbon nitride applied in photocatalytic hydrogen production. *Phys Chem Chem Phys* 18:31534–31541. doi:[10.1039/c6cp05618k](https://doi.org/10.1039/c6cp05618k)
454. Xu L, Liu N, Hong B et al (2016) Nickel–platinum nanoparticles immobilized on graphitic carbon nitride as highly efficient catalyst for hydrogen release from hydrous hydrazine. *RSC Adv* 6:31687–31691. doi:[10.1039/c6ra01335j](https://doi.org/10.1039/c6ra01335j)
455. Ge L, Han C, Xiao X, Guo L (2013) Synthesis and characterization of composite visible light active photocatalysts MoS_2 -g- C_3N_4 with enhanced hydrogen evolution activity. *Inter J Hydrogen En* 38:6960–6969. doi:[10.1016/j.ijhydene.2013.04.006](https://doi.org/10.1016/j.ijhydene.2013.04.006)
456. Jin X, Fan X, Tian J et al (2016) MoS_2 quantum dot decorated g- C_3N_4 composite photocatalyst with enhanced hydrogen evolution performance. *RSC Adv* 6:52611–52619. doi:[10.1039/c6ra07060d](https://doi.org/10.1039/c6ra07060d)
457. Sun Q, Wang P, Yu H, Wang X (2016) In situ hydrothermal synthesis and enhanced photocatalytic H_2 -evolution performance of suspended rGO/g- C_3N_4 photocatalysts. *J Mol Catal A* 424:369–376. doi:[10.1016/j.molcata.2016.09.015](https://doi.org/10.1016/j.molcata.2016.09.015)
458. Suryawanshi A, Dhanasekaran P, Mhamane D et al (2012) Doubling of photocatalytic H_2 evolution from g- C_3N_4 via its nanocomposite formation with multiwall carbon nanotubes: electronic and morphological effects. *Inter J Hydrogen En* 37:9584–9589. doi:[10.1016/j.ijhydene.2012.03.123](https://doi.org/10.1016/j.ijhydene.2012.03.123)
459. Ge L, Han C (2012) Synthesis of MWNTs/g- C_3N_4 composite photocatalysts with efficient visible light photocatalytic hydrogen evolution activity. *Appl Catal B* 117–118:268–274. doi:[10.1016/j.apcatb.2012.01.021](https://doi.org/10.1016/j.apcatb.2012.01.021)
460. Wang N, Li J, Wu L et al (2016) MnO_2 and carbon nanotube co-modified C_3N_4 composite catalyst for enhanced water splitting activity under visible light irradiation. *Inter J Hydrogen En* 41:22743–22750. doi:[10.1016/j.ijhydene.2016.10.068](https://doi.org/10.1016/j.ijhydene.2016.10.068)
461. Gao LF, Wen T, Xu JY et al (2016) Iron-doped carbon nitride-type polymers as homogeneous organocatalysts for visible light-driven hydrogen evolution. *ACS Appl Mater Interfaces* 8:617–624. doi:[10.1021/acsami.5b09684](https://doi.org/10.1021/acsami.5b09684)
462. Min S, Lu G (2012) Enhanced electron transfer from the excited Eosin Y to mpg- C_3N_4 for highly efficient hydrogen evolution under 550 nm irradiation. *J Phys Chem C* 116:19644–19652. doi:[10.1021/jp304022f](https://doi.org/10.1021/jp304022f)
463. Zhang H, Li S, Lu R, Yu A (2015) Time-resolved study on xanthene dye-sensitized carbon nitride photocatalytic systems. *ACS Appl Mater Interfaces* 7:21868–21874. doi:[10.1021/acsami.5b06309](https://doi.org/10.1021/acsami.5b06309)
464. Mori K, Itoh T, Kakudo H et al (2015) Nickel-supported carbon nitride photo-catalyst combined with organic dye for visible-light-driven hydrogen evolution from water. *Phys Chem Chem Phys* 17:24086–24091. doi:[10.1039/c5cp04493f](https://doi.org/10.1039/c5cp04493f)
465. Cao SW, Yuan YP, Fang J et al (2013) In-situ growth of CdS quantum dots on g- C_3N_4 nanosheets for highly efficient photocatalytic hydrogen generation under visible light irradiation. *Inter J Hydrogen En* 38:1258–1266. doi:[10.1016/j.ijhydene.2012.10.116](https://doi.org/10.1016/j.ijhydene.2012.10.116)
466. Zhang Z, Zhang Y, Lu L et al (2017) Graphitic carbon nitride nanosheet for photo-catalytic hydrogen evolution: the impact of morphology and element composition. *Appl Surf Sci* 391:369–375. doi:[10.1016/j.apsusc.2016.05.174](https://doi.org/10.1016/j.apsusc.2016.05.174)
467. Yang S, Gong Y, Zhang J et al (2013) Exfoliated graphitic carbon nitride nanosheets as efficient catalysts for hydrogen evolution under visible light. *Adv Mater* 25:2452–2456. doi:[10.1002/adma.201204453](https://doi.org/10.1002/adma.201204453)

468. Xu J, Zhang L, Shi R, Zhu Y (2013) Chemical exfoliation of graphitic carbon nitride for efficient heterogeneous photocatalysis. *J Mater Chem A* 1:14766–14772. doi:[10.1039/C3TA13188B](https://doi.org/10.1039/C3TA13188B)
469. Bu X, Bu Y, Yang S et al (2016) Graphitic carbon nitride nanoribbon for enhanced visible-light photocatalytic H₂ production. *RSC Adv* 6:112210–112214. doi:[10.1039/c6ra23218c](https://doi.org/10.1039/c6ra23218c)
470. Schwinghammer K, Mesch MB, Duppel V (2014) Crystalline carbon nitride nanosheets for improved visible-light hydrogen evolution. *J Am Chem Soc* 136:1730–1733. doi:[10.1021/ja411321s](https://doi.org/10.1021/ja411321s)
471. Li L, Fang W, Zhang P et al (2016) Sulfur-doped covalent triazine-based frameworks for enhanced photocatalytic hydrogen evolution from water under visible light. *J Mater Chem A* 4:12402–12406. doi:[10.1039/c6ta04711d](https://doi.org/10.1039/c6ta04711d)
472. Lin L, Ou H, Zhang Y, Wang X (2016) Tri-s-triazine-based crystalline graphitic carbon nitrides for highly efficient hydrogen evolution photocatalysis. *ACS Catal* 6:3921–3931. doi:[10.1021/acscatal.6b00922](https://doi.org/10.1021/acscatal.6b00922)
473. Bhunia MK, Melissen S, Parida MR (2015) Dendritic tip-on polytriazine-based carbon nitride photocatalyst with high hydrogen evolution activity. *Chem Mater* 27:8237–8247. doi:[10.1021/acs.chemmater.5b02974](https://doi.org/10.1021/acs.chemmater.5b02974)
474. Liu H, Chen D, Wang Z et al (2017) Microwave-assisted molten-salt rapid synthesis of isotype triazine/heptazine based g-C₃N₄ heterojunctions with highly enhanced photocatalytic hydrogen evolution performance. *Appl Catal B* 203:300–313. doi:[10.1016/j.apcatb.2016.10.014](https://doi.org/10.1016/j.apcatb.2016.10.014)
475. Li Y, Xu H, Ouyang S, Ye J (2016) Metal–organic frameworks for photocatalysis. *Phys Chem Chem Phys* 18:7563–7572. doi:[10.1039/c5cp05885f](https://doi.org/10.1039/c5cp05885f)
476. So MC, Wiederrecht GP, Mondloch JE et al (2015) Metal–organic framework materials for light-harvesting and energy transfer. *Chem Commun* 51:3501–3510. doi:[10.1039/c4cc09596k](https://doi.org/10.1039/c4cc09596k)
477. Xiao JD, Shang Q, Xiong Y et al (2016) Boosting photocatalytic hydrogen production of a metal-organic framework decorated with platinum nanoparticles: the platinum location matters. *Angew Chem Int Ed* 55:9389–9393. doi:[10.1002/anie.201603990](https://doi.org/10.1002/anie.201603990)
478. Zhou JJ, Wang R, Liu XL et al (2015) In situ growth of CdS nanoparticles on UiO-66 metal-organic framework octahedrons for enhanced photocatalytic hydrogen production under visible light irradiation. *Appl Surf Sci* 346:278–283. doi:[10.1016/j.apsusc.2015.03.210](https://doi.org/10.1016/j.apsusc.2015.03.210)
479. Lin R, Shen L, Ren Z et al (2014) Enhanced photocatalytic hydrogen production activity via dual modification of MOF and reduced graphene oxide on CdS. *Chem Commun* 50:8533–8535. doi:[10.1039/c4cc01776e](https://doi.org/10.1039/c4cc01776e)
480. He J, Wang J, Chen Y et al (2014) A dye-sensitized Pt@UiO-66(Zr) metal–organic framework for visible-light photocatalytic hydrogen production. *Chem Commun* 50:7063–7066. doi:[10.1039/c4cc01086h](https://doi.org/10.1039/c4cc01086h)
481. Su Y, Zhang Z, Liu H, Wang Y (2017) Cd_{0.2}Zn_{0.8}S@UiO-66-NH₂ nanocomposites as efficient and stable visible-light-driven photocatalyst for H₂ evolution and CO₂ reduction. *Appl Catal B* 200:448–457. doi:[10.1016/j.apcatb.2016.07.032](https://doi.org/10.1016/j.apcatb.2016.07.032)
482. Sasan K, Lin Q, Mao CY, Feng P (2014) Incorporation of iron hydrogenase active sites into a highly stable metal–organic framework for photocatalytic hydrogen generation. *Chem Commun* 50:10390–10393. doi:[10.1039/c4cc03946g](https://doi.org/10.1039/c4cc03946g)
483. Ragon F, Campo B, Yang Q et al (2015) Acid-functionalized UiO-66(Zr) MOFs and their evolution after intra-framework cross-linking: structural features and sorption properties. *J Mater Chem A* 3:3294–3309. doi:[10.1039/C4TA03992K](https://doi.org/10.1039/C4TA03992K)
484. Wang D, Song Y, Cai J et al (2016) Effective photo-reduction to deposit Pt nanoparticles on MIL-100(Fe) for visible-light-induced hydrogen evolution. *New J Chem* 40:9170–9175. doi:[10.1039/c6nj01989g](https://doi.org/10.1039/c6nj01989g)

485. Vaddipalli SR, Sanivarapu SR, Vengatesan S (2016) Heterostructured Au NPs/CdS/LaBTC MOFs photoanode for efficient photoelectrochemical water split-ting: stability enhancement via CdSe QDs to 2D-CdS nanosheets transformation. *ACS Appl Mater Interfaces* 8:23049–23059. doi:[10.1021/acsami.6b06851](https://doi.org/10.1021/acsami.6b06851)
486. Sun X, Yu Q, Zhang F et al (2016) A dye-like ligand-based metal—organic framework for efficient photocatalytic hydrogen production from aqueous solution. *Catal Sci Technol* 6:3840–3844. doi:[10.1039/c5cy01716e](https://doi.org/10.1039/c5cy01716e)
487. Dong XY, Zhang M, Pei RB et al (2016) A crystalline copper(II) coordination polymer for the efficient visible-light-driven generation of hydrogen. *Angew Chem Int Ed* 55:2073–2077. doi:[10.1002/anie.201509744](https://doi.org/10.1002/anie.201509744)
488. Xu JY, Zhai XP, Gao LF et al (2016) In situ preparation of a MOF-derived magnetic carbonaceous catalyst for visible-light-driven hydrogen evolution. *RSC Adv* 6:2011–2018. doi:[10.1039/c5ra23838b](https://doi.org/10.1039/c5ra23838b)
489. Nellist MR, Laskowski FAL, Lin F, Mills TJ, Boettcher SW (2016) Semiconductor-electrocatalyst interfaces: theory, experiment, and applications in photoelectrochemical water splitting. *Acc Chem Res* 49:733–740. doi:[10.1021/acs.accounts.6b00001](https://doi.org/10.1021/acs.accounts.6b00001)
490. Orlandi M, Dalle Carbonare N, Caramori S, Bignozzi CA, Berardi S, Mazzi A, El Koura Z, Bazzanella N, Patel N, Miotello A (2016) Porous versus compact nanosized Fe(III)-based water oxidation catalyst for photoanodes functionalization. *ACS Appl Mater Interfaces* 8:20003–20011. doi:[10.1021/acsami.6b05135](https://doi.org/10.1021/acsami.6b05135)
491. Ronconi F, Syrgiannis Z, Bonasera A, Prato M, Argazzi R, Caramori S, Cristino V, Bignozzi CA (2015) Modification of nanocrystalline WO₃ with a dicationic perylene bisimide: applications to molecular level solar water splitting. *J Am Chem Soc* 137:4630–4633. doi:[10.1021/jacs.5b01519](https://doi.org/10.1021/jacs.5b01519)
492. Wang J, Li B, Chen J et al (2012) Enhanced photocatalytic H₂-production activity of Cd_xZn_{1-x}S nanocrystals by surface loading MS (M = Ni Co, Cu) species. *Appl Surf Sci* 259:118–123. doi:[10.1016/j.apsusc.2012.07.003](https://doi.org/10.1016/j.apsusc.2012.07.003)
493. Zong X, Yan H, Wu G et al (2008) Enhancement of photocatalytic H₂ evolution on CdS by loading MoS₂ as cocatalyst under visible light irradiation. *J Am Chem Soc* 130:7176–7177. doi:[10.1021/ja8007825](https://doi.org/10.1021/ja8007825)
494. Ji J, Guo L, Li Q et al (2015) A bifunctional catalyst for hydrogen evolution reaction: the interactive influences between CdS and MoS₂ on photoelectro-chemical activity. *Inter J Hydrogen En* 40:3813–3821. doi:[10.1016/j.ijhydene.2015.01.075](https://doi.org/10.1016/j.ijhydene.2015.01.075)
495. Jia T, Kolpin A, Ma C et al (2014) A graphene dispersed CdS–MoS₂ nanocrystal ensemble for cooperative photocatalytic hydrogen production from water. *Chem Commun* 50:1185–1188. doi:[10.1039/C3CC47301E](https://doi.org/10.1039/C3CC47301E)
496. Lu Y, Wang D, Yang P et al (2014) Coupling Zn_xCd_{1-x}S nanoparticles with graphene-like MoS₂: superior interfacial contact, low overpotential and enhanced photocatalytic activity under visible-light irradiation. *Catal Sci Technol* 4:2650–2657. doi:[10.1039/C4CY00331D](https://doi.org/10.1039/C4CY00331D)
497. Zhu B, Lin B, Zhou Y et al (2014) Enhanced photocatalytic H₂ evolution on ZnS loaded with graphene and MoS₂ nanosheets as cocatalysts. *J Mater Chem A* 2:3819–3827. doi:[10.1039/C3TA14819J](https://doi.org/10.1039/C3TA14819J)
498. Zhao H, Dong Y, Jiang P et al (2015) In situ light-assisted preparation of MoS₂ on graphitic C₃N₄ nanosheets for enhanced photocatalytic H₂ production from water. *J Mater Chem A* 3:7375–7381. doi:[10.1039/C5TA00402K](https://doi.org/10.1039/C5TA00402K)
499. Laursen AB, Kegnaes S, Dahl S, Chorkendorff I (2012) Molybdenum sulfides—efficient and viable materials for electro- and photoelectrocatalytic hydrogen evolution. *Environ Sci* 5:5577–5591. doi:[10.1039/C2EE02618J](https://doi.org/10.1039/C2EE02618J)
500. Liu M, Li F, Sun Z et al (2014) Noble-metal-free photocatalysts MoS₂–graphene/CdS mixed nanoparticles/nanorods morphology with high visible light efficiency for H₂ evolution. *Chem Commun* 50:11004–11007. doi:[10.1039/C4CC04653F](https://doi.org/10.1039/C4CC04653F)
501. Redman DW, Kim HJ, Stevenson KJ, Rose MJ (2016) Photo-assisted electrodeposition of MoS_x from ionic liquids on organic-functionalized silicon photoelectrodes for H₂ generation. *J Mater Chem A* 4:7027–7035. doi:[10.1039/C5TA09684G](https://doi.org/10.1039/C5TA09684G)

502. Kumar DP, Hong S, Reddy DA, Kim TK (2016) Noble metal-free ultrathin MoS₂ nanosheet-decorated CdS nanorods as an efficient photocatalyst for spectacular hydrogen evolution under solar light irradiation. *J Mater Chem A* 4:18551–18558. doi:[10.1039/c6ta08628d](https://doi.org/10.1039/c6ta08628d)
503. Du P, Zhu Y, Zhng J et al (2016) Metallic 1T phase MoS₂ nanosheets as a highly efficient co-catalyst for the photocatalytic hydrogen evolution of CdS nanorods. *RSC Adv* 6:74394–74399. doi:[10.1039/c6ra10170d](https://doi.org/10.1039/c6ra10170d)
504. Sasikala R, Gaikwad AP, Jayakumar OD et al (2015) Nanohybrid MoS₂-PANI-CdS photocatalyst for hydrogen evolution from water. *Colloids Surf A* 481:485–492. doi:[10.1016/j.colsurfa.2015.06.027](https://doi.org/10.1016/j.colsurfa.2015.06.027)
505. Du H, Xie X, Zhu Q et al (2015) Metallic MoO₂ cocatalyst significantly enhances visible-light photocatalytic hydrogen production over MoO₂/Zn_{0.5}Cd_{0.5}S hetero-junction. *Nanoscale* 7:5752–5759. doi:[10.1039/C4NR06949H](https://doi.org/10.1039/C4NR06949H)
506. Ma B, Liu Y, Li J et al (2016) Mo₂N: An efficient non-noble metal cocatalyst on CdS for enhanced photocatalytic H₂ evolution under visible light irradiation. *Inter J Hydrogen En* 41:22009–22016. doi:[10.1016/j.ijhydene.2016.08.133](https://doi.org/10.1016/j.ijhydene.2016.08.133)
507. Khan Z, Khannam M, Vinothkumar N et al (2012) Hierarchical 3D NiO–CdS heteroarchitecture for efficient visible light photocatalytic hydrogen generation. *J Mater Chem* 22:12090–12095. doi:[10.1039/C2JM31148H](https://doi.org/10.1039/C2JM31148H)
508. Lin CY, Lai YH, Mersch D, Reisner E (2012) Cu₂O/NiO_x nanocomposite as an inexpensive photocathode in photoelectrochemical water splitting. *Chem Sci* 3:3482–3487. doi:[10.1039/C2SC20874A](https://doi.org/10.1039/C2SC20874A)
509. Bi G, Wen J, Li X et al (2016) Efficient visible-light photocatalytic H₂ evolution over metal-free g-C₃N₄ co-modified with robust acetylene black and Ni(OH)₂ as dual co-catalysts. *RSC Adv* 6:31497–31506. doi:[10.1039/c6ra03118h](https://doi.org/10.1039/c6ra03118h)
510. Yuan YP, Cao SW, Yin LS et al (2013) NiS₂ Co-catalyst decoration on CdLa₂S₄ nanocrystals for efficient photocatalytic hydrogen generation under visible light irradiation. *Inter J Hydrogen En* 38:7218–7223. doi:[10.1016/j.ijhydene.2013.03.169](https://doi.org/10.1016/j.ijhydene.2013.03.169)
511. Parida KM, Biswal N, Das DP, Martha S (2010) Visible light response photocatalytic water splitting over CdS-pillared zirconium–titanium phosphate (ZTP). *Inter J Hydrogen En* 35:5262–5269. doi:[10.1016/j.ijhydene.2010.03.017](https://doi.org/10.1016/j.ijhydene.2010.03.017)
512. Sun Z, Chen H, Zhang L et al (2016) Enhanced photocatalytic H₂ production on cadmium sulfide photocatalysts using nickel nitride as a novel cocatalyst. *J Mater Chem A* 4:13289–13295. doi:[10.1039/c6ta04696g](https://doi.org/10.1039/c6ta04696g)
513. Cao S, Chen Y, Wang CJ et al (2014) Highly efficient photocatalytic hydrogen evolution by nickel phosphide nanoparticles from aqueous solution. *Chem Commun* 50:10427–10429. doi:[10.1039/C4CC05026F](https://doi.org/10.1039/C4CC05026F)
514. Yang JS, Ham DJ, Lakshminarasimhan N et al (2008) Role of platinum-like tungsten carbide as cocatalyst of CdS photocatalyst for hydrogen production under visible light irradiation. *Appl Catal A* 346:149–154. doi:[10.1016/j.apcata.2008.05.020](https://doi.org/10.1016/j.apcata.2008.05.020)
515. Yan Z, Wu H, Han A et al (2014) Noble metal-free cobalt oxide (CoO_x) nano-particles loaded on titanium dioxide/cadmium sulfide composite for enhanced photocatalytic hydrogen production from water. *Inter J Hydrogen En* 39:13353–13360. doi:[10.1016/j.ijhydene.2014.04.121](https://doi.org/10.1016/j.ijhydene.2014.04.121)
516. Yuan J, Wen J, Gao Q et al (2015) Amorphous Co₃O₄ modified CdS nanorods with enhanced visible-light photocatalytic H₂-production activity. *Dalton Trans* 44:1680–1689. doi:[10.1039/C4DT03197K](https://doi.org/10.1039/C4DT03197K)
517. Cao S, Chen Y, Hou CC et al (2015) Cobalt phosphide as a highly active non-precious metal cocatalyst for photocatalytic hydrogen production under visible light irradiation. *J Mater Chem A* 3:6096–6101. doi:[10.1039/C4TA07149B](https://doi.org/10.1039/C4TA07149B)
518. Yuan YJ, Ye ZJ, Lu HW et al (2016) Constructing anatase TiO₂ nanosheets with exposed (001) facets/layered MoS₂ two-dimensional nanojunctions for enhanced solar hydrogen generation. *ACS Catal* 6:532–541. doi:[10.1021/acscatal.5b02036](https://doi.org/10.1021/acscatal.5b02036)

519. Cao S, Chen Y, Kang L et al (2015) Enhanced photocatalytic H₂ evolution by immobilizing CdS nanocrystals on ultrathin Co_{0.85}Se/RGO—PEI nanosheets. *J Mater Chem A* 3:18711–18717. doi:[10.1039/c5ta04910e](https://doi.org/10.1039/c5ta04910e)
520. Zhang L, Jiang T, Li S et al (2013) Enhancement of photocatalytic H₂ evolution on Zn_{0.8}Cd_{0.2}S loaded with CuS as cocatalyst and its photogenerated charge transfer properties. *Dalton Trans* 42:12998–13003. doi:[10.1039/C3DT51256H](https://doi.org/10.1039/C3DT51256H)
521. Zhang L, Liu YN, Zhou M, Yan J (2013) Improving photocatalytic hydrogen evolution over CuO/Al₂O₃ by platinum-depositing and CuS-loading. *Appl Surf Sci* 282:531–537. doi:[10.1016/j.apsusc.2013.06.006](https://doi.org/10.1016/j.apsusc.2013.06.006)
522. Wang X, Liu M, Chen Q et al (2013) Synthesis of CdS/CNTs photocatalysts and study of hydrogen production by photocatalytic water splitting. *Inter J Hydrogen En* 38:13091–13096. doi:[10.1016/j.ijhydene.2013.03.016](https://doi.org/10.1016/j.ijhydene.2013.03.016)
523. Zhang J, Qiao SZ, Qi L, Yu J (2013) Fabrication of NiS modified CdS nanorod p–n junction photocatalysts with enhanced visible-light photocatalytic H₂-production activity. *Phys Chem Chem Phys* 15:12088–12094. doi:[10.1039/C3CP50734C](https://doi.org/10.1039/C3CP50734C)
524. Li N, Zhou B, Guo P et al (2013) Fabrication of noble-metal-free Cd_{0.5}Zn_{0.5}S/NiS hybrid photocatalyst for efficient solar hydrogen evolution. *Inter J Hydrogen En* 38:11268–11277. doi:[10.1016/j.ijhydene.2013.06.067](https://doi.org/10.1016/j.ijhydene.2013.06.067)
525. Li Y, Lin S, Peng S et al (2013) Modification of ZnS_{1-x-0.5y}O_x(OH)_y-ZnO photocatalyst with NiS for enhanced visible-light-driven hydrogen generation from seawater. *Inter J. Hydrogen En* 38:15976–15984. doi:[10.1016/j.ijhydene.2013.09.149](https://doi.org/10.1016/j.ijhydene.2013.09.149)
526. Zhu Y, Xu Y, Hou Y et al (2014) Cobalt sulfide modified graphitic carbon nitride semiconductor for solar hydrogen production. *Inter J Hydrogen En* 39:11873–11879. doi:[10.1016/j.ijhydene.2014.06.025](https://doi.org/10.1016/j.ijhydene.2014.06.025)
527. Chen Y, Qin Z (2016) General applicability of nanocrystalline Ni₂P as a noble-metal-free cocatalyst to boost photocatalytic hydrogen generation. *Catal Sci Technol* 6:8212–8221. doi:[10.1039/c6cy01653g](https://doi.org/10.1039/c6cy01653g)
528. Yasomane JP, Bandara J (2008) Multi-electron storage of photoenergy using Cu₂O–TiO₂ thin film photocatalyst. *Solar En Mater Solar Cells* 92:348–352. doi:[10.1016/j.solmat.2007.09.016](https://doi.org/10.1016/j.solmat.2007.09.016)
529. Jian JX, Ye C, Wang XZ et al (2016) Comparison of H₂ photogeneration by [FeFe]-hydrogenase mimics with CdSe QDs and Ru(bpy)₃Cl₂ in aqueous solution. *Energy Environ Sci* 9:2083–2089. doi:[10.1039/c6ee00629a](https://doi.org/10.1039/c6ee00629a)
530. Wen F, Li C (2013) Hybrid artificial photosynthetic systems comprising semiconductors as light harvesters and biomimetic complexes as molecular cocatalysts. *Acc Chem Res* 4:2355–2364. doi:[10.1021/ar300224u](https://doi.org/10.1021/ar300224u)
531. Yeh TF, Cihlar J, Chang CY et al (2013) Roles of graphene oxide in photocatalytic water splitting. *Mater Today* 16:78–84. doi:[10.1016/j.mattod.2013.03.006](https://doi.org/10.1016/j.mattod.2013.03.006)
532. Yang Y, Liu E, Dai H et al (2014) Photocatalytic activity of Ag-TiO₂-graphene ternary nanocomposites and application in hydrogen evolution by water splitting. *Inter J Hydrogen En* 39:7664–7671. doi:[10.1016/j.ijhydene.2013.09.109](https://doi.org/10.1016/j.ijhydene.2013.09.109)
533. Fang Z, Wang Y, Song J et al (2013) Immobilizing CdS quantum dots and dendritic Pt nanocrystals on thiolated graphene nanosheets toward highly efficient photocatalytic H₂ evolution. *Nanoscale* 5:9830–9838. doi:[10.1039/c3nr03043a](https://doi.org/10.1039/c3nr03043a)
534. Xiang Q, Yu J, Jaroniec M (2011) Enhanced photocatalytic H₂-production activity of graphene-modified titania nanosheets. *Nanoscale* 3:3670–3678. doi:[10.1039/C1NR10610D](https://doi.org/10.1039/C1NR10610D)
535. Hong Y, Shi P, Wang P, Yao W (2015) Improved photocatalytic activity of CdS/reduced graphene oxide (RGO) for H₂ evolution by strengthening the connection between CdS and RGO sheets. *Inter J Hydrogen En* 40:7045–7051. doi:[10.1016/j.ijhydene.2015.04.005](https://doi.org/10.1016/j.ijhydene.2015.04.005)
536. Yu X, Du R, Li B et al (2016) Biomolecule-assisted self-assembly of CdS/MoS₂/graphene hollow spheres as high-efficiency photocatalysts for hydrogen evolution without noble metals. *Appl Catal B* 182:504–512. doi:[10.1016/j.apcatb.2015.09.003](https://doi.org/10.1016/j.apcatb.2015.09.003)

537. Xu H, Li X, Kang S et al (2014) Noble metal-free cuprous oxide/reduced graphene oxide for enhanced photocatalytic hydrogen evolution from water reduction. *Inter J Hydrogen En* 39:11578–11582. doi:[10.1016/j.ijhydene.2014.05.156](https://doi.org/10.1016/j.ijhydene.2014.05.156)
538. Ding J, Yan W, Sun S et al (2014) Fabrication of graphene/CaIn₂O₄ composites with enhanced photocatalytic activity from water under visible light irradiation. *Inter J Hydrogen En* 39:119–126. doi:[10.1016/j.ijhydene.2013.10.077](https://doi.org/10.1016/j.ijhydene.2013.10.077)
539. Pan B, Wang Y, Liang Y et al (2014) Nanocomposite of BiPO₄ and reduced graphene oxide as an efficient photocatalyst for hydrogen evolution. *Inter J Hydrogen En* 39:13527–13533. doi:[10.1016/j.ijhydene.2014.02.031](https://doi.org/10.1016/j.ijhydene.2014.02.031)
540. Sun Z, Guo J, Zhu S et al (2014) A high-performance Bi₂WO₆–graphene photocatalyst for visible light-induced H₂ and O₂ generation. *Nanoscale* 6:2186–2193. doi:[10.1039/c3nr05249d](https://doi.org/10.1039/c3nr05249d)
541. Hong Z, Li X, Kang S et al (2014) Enhanced photocatalytic activity and stability of the reduced graphene oxide loaded potassium niobate microspheres for hydrogen production from water reduction. *Inter J Hydrogen En* 39:12515–12523. doi:[10.1016/j.ijhydene.2014.06.075](https://doi.org/10.1016/j.ijhydene.2014.06.075)
542. Alexander BD, Kulesza PJ, Rutkowska I et al (2008) Metal oxide photoanodes for solar hydrogen production. *J Mater Chem* 18:2298–2303. doi:[10.1039/B718644D](https://doi.org/10.1039/B718644D)
543. Kudo A, Kato H, Tsuji I (2004) Strategies for the development of visible-light-driven photocatalysts for water splitting. *Chem Lett* 33:1534–1539. doi:[10.1246/cl.2004.1534](https://doi.org/10.1246/cl.2004.1534)
544. Sayama K, Mukasa K, Abe R et al (2002) A new photocatalytic water splitting system under visible light irradiation mimicking a Z-scheme mechanism in photosynthesis. *J Photochem Photobiol A* 148:71–77. doi:[10.1016/S1010-6030\(02\)00070-9](https://doi.org/10.1016/S1010-6030(02)00070-9)
545. Sayama K, Mukasa K, Abe R et al (2001) Stoichiometric water splitting into H₂ and O₂ using a mixture of two different photocatalysts and an IO₃[−]/I[−] shuttle redox mediator under visible light irradiation. *Chem. Commun* 2416–2417. doi:[10.1039/B107673F](https://doi.org/10.1039/B107673F)
546. Schürch D, Currao A, Sarkar S et al (2002) The silver chloride photoanode in photoelectrochemical water splitting. *J Phys Chem B* 106:12764–12775. doi:[10.1021/jp0265081](https://doi.org/10.1021/jp0265081)
547. Abe R, Sayama K, Sugihara H (2005) Development of new photocatalytic water splitting into H₂ and O₂ using two different semiconductor photocatalysts and a shuttle redox mediator IO₃[−]/I[−]. *J Phys Chem B* 109:16052–16061. doi:[10.1021/jp0528481](https://doi.org/10.1021/jp0528481)
548. Abe R, Takata T, Sugihara H, Domen K (2005) Photocatalytic overall water splitting under visible light by TaON and WO₃ with an IO₃[−]/I[−] shuttle redox mediator. *Chem Commun* 3829–3831. doi:[10.1039/B505646B](https://doi.org/10.1039/B505646B)
549. Higashi M, Abe R, Takata T, Domen K (2009) Photocatalytic Overall Water Splitting under Visible Light Using ATaO₂N (A = Ca, Sr, Ba) and WO₃ in a IO₃[−]/I[−] Shuttle Redox Mediated System. *Chem Mater* 21:1543–1549. doi:[10.1021/cm803145n](https://doi.org/10.1021/cm803145n)
550. Higashi M, Abe R, Ishikawa A et al (2008) Z-scheme overall water splitting on modified-TaON photocatalysts under visible light ($\lambda < 500$ nm). *Chem Lett* 37:138–139
551. Abe R, Shinmei K, Koumura N et al (2013) Visible-light-induced water splitting based on two-step photoexcitation between dye-sensitized layered niobate and tungsten oxide photocatalysts in the presence of a triiodide/iodide shuttle redox mediator. *J Am Chem Soc* 135:16872–16884. doi:[10.1021/ja4048637](https://doi.org/10.1021/ja4048637)
552. Jia Q, Iwase A, Kudo A (2014) BiVO₄–Ru/SrTiO₃: Rh composite Z-scheme photo-catalyst for solar water splitting. *Chem Sci* 5:1513–1519. doi:[10.1039/C3SC52810C](https://doi.org/10.1039/C3SC52810C)
553. Maeda K, Lu D, Domen K (2013) Solar-driven Z-scheme water splitting using modified BaZrO₃–BaTaO₂N solid solutions as photocatalysts. *ACS Catal* 3:1026–1033. doi:[10.1021/cs400156m](https://doi.org/10.1021/cs400156m)
554. Kato H, Hori M, Kōta R et al (2004) Construction of Z-scheme type heterogeneous photocatalysis systems for water splitting into H₂ and O₂ under visible light irradiation. *Chem Lett* 33:1348–1349. doi:[10.1246/cl.2004.1348](https://doi.org/10.1246/cl.2004.1348)

555. Kato H, Sasaki Y, Iwase A, Kudo A (2007) Role of iron ion electron mediator on photocatalytic overall water splitting under visible light irradiation using Z-scheme systems. *Bull Chem Soc Jpn* 80:2457–2464. doi:[10.1246/bcsj.80.2457](https://doi.org/10.1246/bcsj.80.2457)
556. Bae SW, Ji SM, Hong SJ et al (2009) Photocatalytic overall water splitting with dual-bed system under visible light irradiation. *Inter J Hydrogen En* 34:3243–3249. doi:[10.1016/j.ijhydene.2009.02.022](https://doi.org/10.1016/j.ijhydene.2009.02.022)
557. Pan Z, Hisatomi T, Wang Q et al (2016) Photocatalyst sheets composed of particulate $\text{LaMg}_{1/3}\text{Ta}_{2/3}\text{O}_2\text{N}$ and Mo-Doped BiVO_4 for Z-scheme water splitting under visible light. *ACS Catal* 6:7188–7196. doi:[10.1021/acscatal.6b01561](https://doi.org/10.1021/acscatal.6b01561)
558. Iwase A, Ng YH, Ishiguro Y et al (2011) Reduced graphene oxide as a solid-state electron mediator in Z-scheme photocatalytic water splitting under visible light. *J Am Chem Soc* 133:11054–11057. doi:[10.1021/ja203296z](https://doi.org/10.1021/ja203296z)
559. Paulose M, Mor GK, Varghese OK et al (2006) Visible light photoelectrochemical and water-photoelectrolysis properties of titania nanotube arrays. *J Photochem Photobiol A* 178:8–15. doi:[10.1016/j.jphotochem.2005.06.013](https://doi.org/10.1016/j.jphotochem.2005.06.013)
560. Khan MA, Akhtar MS, Woo SI, Yang OB (2008) Enhanced photoresponse under visible light in Pt ionized TiO_2 nanotube for the photocatalytic splitting of water. *Catal Commun* 10:1–5. doi:[10.1016/j.catcom.2008.01.018](https://doi.org/10.1016/j.catcom.2008.01.018)
561. Zou Z, Ye J, Arakawa H (2002) Surface characterization of nanoparticles of $\text{NiO}_x/\text{In}_{0.9}\text{Ni}_{0.1}\text{TaO}_4$: effects on photocatalytic activity. *J Phys Chem B* 106:13098–13101. doi:[10.1021/jp0216225](https://doi.org/10.1021/jp0216225)
562. Jang JS, Kim HG, Reddy VR et al (2005) Photocatalytic water splitting over iron oxide nanoparticles intercalated in $\text{HTiNb}(\text{Ta})\text{O}_5$ layered compounds. *J Catal* 231:213–222. doi:[10.1016/j.jcat.2005.01.026](https://doi.org/10.1016/j.jcat.2005.01.026)
563. Wu G, Chen A (2008) Direct growth of F-doped TiO_2 particulate thin films with high photocatalytic activity for environmental applications. *J Photochem Photobiol A* 195:47–53. doi:[10.1016/j.jphotochem.2007.09.005](https://doi.org/10.1016/j.jphotochem.2007.09.005)
564. Kitano M, Iyatani K, Tsujimaru K et al (2008) The effect of chemical etching by HF solution on the photocatalytic activity of visible light-responsive TiO_2 thin films for solar water splitting. *Topics Catal* 49:24–31. doi:[10.1007/s11244-008-9064-5](https://doi.org/10.1007/s11244-008-9064-5)
565. Maeda K, Takata T, Hara M et al (2005) $\text{GaN}:\text{ZnO}$ solid solution as a photocatalyst for visible-light-driven overall water splitting. *J Am Chem Soc* 127:8286–8287. doi:[10.1021/ja0518777](https://doi.org/10.1021/ja0518777)
566. Liu H, Yuan J, Shangguang W, Teraoka Y (2008) Visible-light-responding BiYWO_6 solid solution for stoichiometric photocatalytic water splitting. *J Phys Chem C* 112:8521–8523. doi:[10.1021/jp802537u](https://doi.org/10.1021/jp802537u)
567. Sayama K, Nomura A, Arai T, Sugita T et al (2006) Photoelectrochemical decomposition of water into H_2 and O_2 on porous BiVO_4 thin-film electrodes under visible light and significant effect of Ag ion treatment. *J Phys Chem B* 110:11352–11360. doi:[10.1021/jp057539+](https://doi.org/10.1021/jp057539+)
568. Bornoz P, Abdi FF, Tilley SD et al (2014) A bismuth vanadate-cuprous oxide tandem cell for overall solar water splitting. *J Phys Chem C* 118:16959–16966. doi:[10.1021/jp500441h](https://doi.org/10.1021/jp500441h)
569. Saremi-Yarahmadi S, Upul Wijayantha KG, Tahir AA, Vaidhyanathan B (2009) Nanostructured $\alpha\text{-Fe}_2\text{O}_3$ electrodes for solar driven water splitting: effect of doping agents on preparation and performance. *J Phys Chem C* 113:4768–4778. doi:[10.1021/jp808453z](https://doi.org/10.1021/jp808453z)
570. Saremi-Yarahmadi S, Tahir AA, Vaidhyanathan B, Upul Wijayantha KG (2009) Fabrication of nanostructured $\alpha\text{-Fe}_2\text{O}_3$ electrodes using ferrocene for solar hydrogen generation. *Mater Lett* 63:523–526. doi:[10.1016/j.matlet.2008.11.011](https://doi.org/10.1016/j.matlet.2008.11.011)
571. Youngblood WJ, Lee SHA, Kobayashi Y et al (2009) Photoassisted overall water splitting in a visible light-absorbing dye-sensitized photoelectrochemical cell. *J Am Chem Soc* 131:926–927. doi:[10.1021/ja809108y](https://doi.org/10.1021/ja809108y)
572. Zou Z, Ye J, Arakawa H (2003) Photocatalytic water splitting into H_2 and/or O_2 under UV and visible light irradiation with a semiconductor photocatalyst. *Inter J Hydrogen En* 28:663–669. doi:[10.1016/S0360-3199\(02\)00159-3](https://doi.org/10.1016/S0360-3199(02)00159-3)

573. Oshikiri M, Boero M, Ye J et al (2002) Electronic structures of promising photocatalysts InMO_4 ($M = \text{V}, \text{Nb}, \text{Ta}$) and BiVO_4 for water decomposition in the visible wavelength region. *J Chem Phys* 117:7313–7318
574. Zou Z, Ye J, Arakawa H (2001) Photophysical and photocatalytic properties of InMO_4 ($M = \text{Nb}^{5+}, \text{Ta}^{5+}$) under visible light irradiation. *Mater Res Bull* 36:1185–1193. doi:[10.1016/S0025-5408\(01\)00607-9](https://doi.org/10.1016/S0025-5408(01)00607-9)
575. Xu J, Pan C, Takata T, Domen K (2015) Photocatalytic overall water splitting on the perovskite-type transition metal oxynitride CaTaO_2N under visible light irradiation. *Chem Commun* 51:7191–7194. doi:[10.1039/C5CC01728A](https://doi.org/10.1039/C5CC01728A)
576. Li Y, Jiang S, Xiao J, Li Y (2014) Photocatalytic overall water splitting under visible light over an In-Ni-Ta-O-N solid solution without an additional cocatalyst. *Inter J Hydrogen En* 39:731–735. doi:[10.1016/j.ijhydene.2013.10.092](https://doi.org/10.1016/j.ijhydene.2013.10.092)
577. Liu H, Yuan J, Jiang Z et al (2011) Novel photocatalyst of V-based solid solutions for overall water splitting. *J Mater Chem* 21:16535–16543. doi:[10.1039/C1JM11809A](https://doi.org/10.1039/C1JM11809A)
578. Guo DZ, Zhang GM, Zhang ZX et al (2006) Visible-light-induced water-splitting in channels of carbon nanotubes. *J Phys Chem B* 110:1571–1575. doi:[10.1021/jp055929q](https://doi.org/10.1021/jp055929q)
579. Maeda K, Wang X, Nishihara Y et al (2009) photocatalytic activities of graphitic carbon nitride powder for water reduction and oxidation under visible light. *J Phys Chem C* 113:4940–4947. doi:[10.1021/jp809119m](https://doi.org/10.1021/jp809119m)
580. Zhao G, Huang X, Fina F et al (2015) Facile structure design based on C_3N_4 for mediator-free Z-scheme water splitting under visible light. *Catal Sci Technol* 5:3416–3422. doi:[10.1039/C5CY00379B](https://doi.org/10.1039/C5CY00379B)
581. Wu X, Zhao J, Guo S et al (2016) Carbon dot and BiVO_4 quantum dot composites for overall water splitting via a two-electron pathway. *Nanoscale* 8:17314–17321. doi:[10.1039/c6nr05864g](https://doi.org/10.1039/c6nr05864g)
582. Haussener S, Hu S, Xiang C, Weber AZ, Lewis NS (2013) Simulations of the irradiation and temperature dependence of the efficiency of tandem photoelectrochemical water-splitting systems. *Energy Environ Sci* 6:3605–3618. doi:[10.1039/C3EE41302K](https://doi.org/10.1039/C3EE41302K)

<http://www.springer.com/978-3-319-68878-7>

Solar Light Harvesting with Nanocrystalline
Semiconductors

Stroyuk, O.

2018, XXXI, 378 p. 168 illus., 149 illus. in color.,

Hardcover

ISBN: 978-3-319-68878-7